REPORT DOCUMENTATION PAGE

Form Approved
OMB No. 0704-0188

1. REPORT DATE *(DD-MM-YYYY)*	2. REPORT TYPE	3. DATES COVERED *(From - To)*
08-14-2008	Final Technical	Oct 2000 – Sep 2008

4. TITLE AND SUBTITLE
Scattering from Inclusions in Marine Sediments: SAX04 Data/Model Comparisons, submitted 14 July 2008 to *J. Oceanic Engr*., Special Issue on sediment acoustics/SAX04 data analysis

5a. CONTRACT NUMBER

5b. GRANT NUMBER
N00014-01-1-0087

5c. PROGRAM ELEMENT NUMBER

6. AUTHOR(S)
Ivakin, Anatoliy N.

5d. PROJECT NUMBER

5e. TASK NUMBER

5f. WORK UNIT NUMBER

7. PERFORMING ORGANIZATION NAME(S) AND ADDRESS(ES)
Applied Physics Laboratory
University of Washington
1013 NE 40th St.
Seattle, WA 98105-6698

8. PERFORMING ORGANIZATION REPORT NUMBER

9. SPONSORING/MONITORING AGENCY NAME(S) AND ADDRESS(ES)
Office of Naval Research
875 North Randolph St.
Arlington, VA 22203-1995

10. SPONSOR/MONITOR'S ACRONYM(S)
APL-UW

11. SPONSORING/MONITORING AGENCY REPORT NUMBER

12. DISTRIBUTION AVAILABILITY STATEMENT
Approved for public release; distribution is unlimited

13. SUPPLEMENTARY NOTES

14. ABSTRACT
The role of discrete scatterers in marine sediments is evaluated based on acoustic and environmental measurements at the shallow water sediment acoustics experiment, SAX04, and shown to be significant. The sediment at SAX04 site was complicated and characterized as a mostly medium sand / mud mixture. Analysis of the sediment samples showed presence of a small volume portion of arger particles, such as coarse sand fraction and shell fragments, which were considered as inclusions, or sparsely distributed discrete scatterers, embedded in a homogeneous effective fluid with parameters corresponding to medium sand or mud sediment frame. This analysis provided also the size distributions for both types of inclusions, coarse sand particles and shells, which were used as inputs to a model of incoherent discrete scattering in the sediment. It is demonstrated that this approach in general is capable to provide a reasonable explanation of both frequency and angular dependencies of the SAX04 bottom backscattering strength, and discrete scattering from the sediment inclusions can be a significant mechanism of the SAX04 high frequency reverberation in a wide range of grazing angles (15 to 50 degrees) and frequencies (30 kHz to 500 kHz).

15. SUBJECT TERMS
backscattering strength, medium sand and mud sediments, shell fragments, coarse sand inclusions, particle size distribution

16. SECURITY CLASSIFICATION OF:			17. LIMITATION OF ABSTRACT	18. NUMBER OF PAGES	19a. NAME OF RESPONSIBLE PERSON
a. REPORT	b. ABSTRACT	c. THIS PAGE			Robert H. Headrick
U	U	U	UU	18	19b. TELEPHONE NUMBER (*Include area code*) 703-696-4135

Submitted by author to IEEE Journal of Ocean Engineering 14 Jul 2008

Scattering from Inclusions in Marine Sediments: SAX04 Data/Model Comparisons

Anatoliy N. Ivakin

***Abstract*—The role of discrete scatterers in marine sediments is evaluated based on acoustic and environmental measurements at the shallow water sediment acoustics experiment, SAX04, and shown to be significant. The sediment at SAX04 site was complicated and characterized as a mostly medium sand / mud mixture. Analysis of the sediment samples showed presence of a small volume portion of larger particles, such as coarse sand fraction and shell fragments, which were considered as inclusions, or sparsely distributed discrete scatterers, embedded in a homogeneous effective fluid with parameters corresponding to medium sand or mud sediment frame. This analysis provided also the size distributions for both types of inclusions, coarse sand particles and shells, which were used as inputs to a model of incoherent discrete scattering in the sediment. It is demonstrated that this approach in general is capable to provide a reasonable explanation of both frequency and angular dependencies of the SAX04 bottom backscattering strength, and discrete scattering from the sediment inclusions can be a significant mechanism of the SAX04 high frequency reverberation in a wide range of grazing angles (15 to 50 degrees) and frequencies (30 kHz to 500 kHz).**

***Index Terms*—Backscattering strength, medium sand and mud sediments, shell fragments, coarse sand inclusions, particle size distribution.**

I. Introduction

Testing various models and mechanisms of high frequency seabed scattering was one of primary goals of recent major shallow water experiments in sediment acoustics, SAX99 [Williams et al 2002] and SAX04 [Thorsos et al 2005]. The scattering mechanisms are related with different types of seabed irregularities: volume heterogeneity, continuous (smooth spatial fluctuations of the sediment acoustic parameters) and discrete (large particles in the sediment), roughness of the seabed interfaces, and volume-roughness interactions. Given different environmental conditions, frequencies and angles of scattering, relative contributions of these mechanisms can be also very different. For example, in the SAX99 situation, sediment rough surface scattering was demonstrated as a dominant mechanism at frequencies below 130 kHz and sub-critical grazing angles [Williams et al 2002].

Environmental conditions at SAX04 were quite different from those at SAX99 due to known weather events preceding and during the experiment, and, as a result, the SAX04 sediment was much more complicated and generally characterized as a complex mixture of mostly medium sand and mud [Richardson et al 2005, Williams et al 2008]. Acoustic backscattering from the sediments at SAX04 was also very different from SAX99. For example, the seabed roughness has been shown to be insignificant contributor to the sediment backscatter [Williams et al 2008]. It could be expected that other scattering mechanisms can be important in these complicated conditions. The objective of this paper is to evaluate, using a theoretical modeling approach, the role of discrete scattering mechanism for the SAX04 environment. This mechanism of scattering can be due to various discrete "inclusions" in the sediment, which can be defined as relatively large particles with the size larger than the mean grain size of the sediment, such as rocks, coarse sand and gravel particles, shells and shell fragments, shelled animals, etc. It is assumed that acoustic measurements of the seabed backscattering strength made at SAX04 [Williams et al 2008] along with environmental characterization of the sediment at this site and, particularly, analysis of the sediment inclusions [Ivakin 2008] can provide a necessary ground truth for such an evaluation. If this role is proved to be significant, this approach can be used to provide a physics-based model for analysis of bottom reverberation at SAX04 and other shallow water regions with similar conditions.

The SAX04 acoustic experiments were accompanied by extensive measurements of the sediment acoustic parameters, the density, sound speed and attenuation, and others [Richardson et al 2005]. These parameters are necessary inputs for description of sound propagation in the sediment, reflection from and transmission through the sediment interfaces. To describe the process of scattering in the sediment, another set of sediment parameters is required. In a companion paper [Ivakin 2008], we present results of granulometric analysis of the SAX04 sediment samples for particles of coarse fractions with the grain size (equivalent diameter) greater than 1 mm. These particles comprise only a small volume portion in the SAX04 medium sand / mud sediment, and can be considered as sparse discrete "inclusions" in the sediment. In this paper (Section II), a model of incoherent discrete scattering in the sediment is presented and discussed. The model considers inclusions as discrete scatterers embedded in a

sediment half-space with given effective fluid parameters, density, sound speed and attenuation. Acoustic scattering from the sediment inclusions is described in terms of the individual scattering functions of discrete targets and statistical distributions of their parameters (size, shape, orientation, material, etc). Parameters of these distributions (or at least possible limits of their values) can be obtained from an analysis of the sediment samples. In this paper (Section III), the results of analysis of the SAX04 sediment samples [Ivakin 2008] are used to provide the size distributions of the two types of inclusions, shell fragments and coarse sand particles, as the input parameters to the "inclusion scattering" model. In Section IV, this model is used to explain frequency-angular dependencies of seabed scattering strength measured at SAX04 experiment over a wide frequency range (30 kHz to 500 kHz) at grazing angles both above and below critical (about 30 degrees for medium sand). In Section V, some discrepancies in model/data comparisons and assumptions made in the model of scattering are discussed and possible future modifications of the model to eliminate these discrepancies and assumptions are outlined. Section VI gives the paper summary and conclusions.

II. Model of incoherent scattering

The "inclusion scattering" model is based on a theoretical approach described in [Ivakin 2000, 2004, 2005]. It assumes, in particular, that the inclusions are sparsely distributed in space and comprise only a small portion of the scattering volume. The sparse distribution of inclusions allows considering their positions as independent and mutually uncorrelated and, correspondingly, the incoherent summation of their scattered intensities. This approach is rather general and is often applied to various types of scatterers in the ocean, such as fish in water column, clouds of gas bubbles near the sea surface, naturally occurring plumes in the ocean, and others, see, e.g., [Medwin and Clay 1998, and Refs therein]. A similar approach has been widely used in acoustic sensing of suspended sediments [Sheng and Hay 1988, Thorne et al 1995, Thorne and Backingham 2004], which assumes that the particles are small and light enough so that they can be suspended in water above the seabed. This allows particularly estimating the particle sizes from multi-frequency acoustic backscatter at very high frequencies (about 1 MHz and higher) corresponding to suspended sediment grain sizes.

The case of non-suspended sediment (or large particles and correspondingly lower frequencies) is more complicated in the sense that such sediment is generally a densely packed granular medium, and a complex process of interactions between these large particles and surrounding smaller grains, presence of the sediment interfaces and related effects should be somehow taken into account. It seems reasonable however to assume that acoustic behavior of a large particle (or "inclusion") surrounded by a big number of small grains is similar to the case where this inclusion is submerged to an effective continuous medium with acoustic parameters corresponding to the surrounding sediment frame. The effective parameters of this frame and, correspondingly, sound propagation in the surrounding medium, where grains are much smaller than the wavelength, can be defined by various "effective medium" models, e.g., the "effective density fluid" model [Williams 2001]. The "inclusion scattering" model presented and discussed in this paper represents, in a way, represents a hybrid approach to discrete scattering in non-suspended sediments using advantages of both approaches, an "effective medium" approach, in part of description of propagation in the sediment, and the suspended particle approach, in part of description of local process of discrete scattering in the sediment.

An essential question in the case of non-suspended sediments remains when it is hard to distinguish the inclusions from surrounding granular sediment frame. In this case, the shape of the sediment grain size distribution becomes important and should be considered in more details. Usually, the sediment, as a granular medium, is being considered as having a rather narrow size distribution of particles and its mean grain size is assumed as a major parameter defining the sediment geotechnical and acoustic properties. For example, traditionally it defines the sediment type and related "word-based" characteristics (e.g., fine, medium, or coarse sand). This however has much less sense if the sediment has two or more "modes" with significantly different grain sizes, or has a wide range of sizes. In this case, standard granulometric description of the grain size distribution, even rather extended and involving other parameters in addition to the mean grain size, such as sorting, skewness, kurtosis, etc, see [Jackson and Richardson 2007], with respect to effect on the sediment scattering properties, is simply not relevant. From other hand, presence of a small volume portion of particles with the size much larger than in the main mode can contribute significantly to scattering properties of the sediment, although it does not affect the mean grain size of the sediment. A more accurate analysis of the sediment grain size distributions shows that they normally do have particles in a wide range of sizes larger than the mean grain size. Particles of this "tail" in the size distribution are usually sparse in space and satisfy the requirement for their total volume concentration to be small. Important is that they do not affect the value of the sediment mean grain size. Therefore, in the scattering model, these particles can be considered as inclusions submerged in an effective continuous medium with the effective acoustic parameters corresponding to this mean grain size. Important is that, in this case, the processes of propagation in this volume and local scattering by a single inclusion can be treated separately.

The incoherent scattering approach for inclusions in underwater sediments can be described as follows. Consider a sediment

volume with a number of discrete scatterers, or "inclusions". The intensity I_j of the field scattered by the *j*-th inclusion located in this volume is proportional to the intensity incident from water on the sediment surface, I_o. Note that it is not required here to specify the intensity of the field incident on an individual inclusion. At far enough distances r_o from the sediment surface, taking into account the spherical spread in water, the scattered intensity can be written as

$$I_j = \sigma_j I_o / {r_o}^2 \tag{1}$$

where σ_j is a factor that can be defined as the efficient target scattering cross-section for this inclusion. Regardless of complexity of the sediment structure, if inclusions are sparse enough and distributed randomly, their scattered intensities can be summed incoherently. This summation determines the seabed scattering coefficient (or the scattering cross section per unit seabed area, or, if expressed in dB, the seabed scattering strength)

$$m_s = \frac{{r_o}^2}{A I_o} \sum\nolimits_j I_j = \frac{1}{A} \sum\nolimits_j \sigma_j \tag{2}$$

where A is the horizontal cross section of the ensonified sediment volume. It can be assumed here that the scattering cross section of each inclusion essentially depends on its depth and size. Then summation in (2) can be performed using a number-size-depth distribution function

$$\psi_N(a,z) = \frac{\Delta N(a,z)}{A \Delta a \, \Delta z} \tag{3}$$

where ΔN is defined as the number of particles having the size and depth in small enough intervals, $a_j \in [a, a+\Delta a]$ and $z_j \in [z, z+\Delta z]$. Then summation in (2) can be replaced by integration and the seabed scattering coefficient at given frequency and directions of the incident and scattered waves can be written as follows

$$m_s(\vec{k}_s, \vec{k}_i) = \iint \psi_N(a,z)\, \sigma(\vec{k}_s, \vec{k}_i, a, z)\, da\, dz \tag{4}$$

where $\vec{k}_s$ and $\vec{k}_i$ are the wave vectors of the scattered and incident waves in water near the seabed. The expression (4) is rather general. It is assumed here only that all the particles with the same size and depth intervals belong to the same class and therefore their scattering intensities are averaged within this class, i.e., not only over these intervals, but also over their horizontal positions within the ensonified area and all other possible parameters, such as their material properties, orientation (for non-spherical particles), and others. Alternatively, the number of essential parameters of inclusions should be increased, which means that, e.g., the size parameter, a, should be understood as a vector, or a set of parameters, and the size distribution (3) and integration in (4) should be extended on these parameters as well.

The expression (4) can be used to introduce a generalized volume scattering coefficient of the medium, *m*, or the scattering cross section per unit sediment volume element located at given depth, as follows

$$m_s = \int m(z)\, dz \tag{5}$$

$$m(z) = \int \psi_N(a,z)\, \sigma(a,z)\, da \tag{6}$$

Using the size-depth distribution function, all practically important statistical characteristics of the sediment inclusions can be found. Then, using (4)-(6), the seabed scattering coefficient and the sediment volume scattering coefficient can be expressed through such parameters as the average cross section and average volume of the inclusions, their average volume concentration, the surface "coverage" parameter, and others (see Appendix I).

It is important to note that the individual scattering cross-section σ in the expressions above is defined rather generally. It is different from one in water or in the sediment unbounded (free) space, particularly, because it is affected not only by the

scattering process itself, but also by interactions with the sediment interfaces. For example, in the case of one interface (water-sediment), the interaction processes include transmission of the incident and scattered waves through the interface, their propagation and attenuation in the sediment, and possible multiple reflections between the interface and the target. All these processes are included to the individual scattering function as it is defined by expression (1), which can be used for direct measurements of this function. Such measurements, however, might be difficult for not large targets as their scattering amplitude can be too small compared to the level of background scattering from surrounding granular medium (this background can be rather strong at high frequencies [Ivakin and Sessarego 2007]). Other approaches can be related with computer simulations and theoretical modeling, which, using reasonably simplifying assumptions, can provide approximate solutions for this function.

In this paper, we consider the case of particles which are buried in the sediment and assume that all possible multiple reflections between the water-sediment interface and particle can be neglected. In this case, the process of scattering from the particle in the sediment can be described by a "free-field" scattering cross section $\sigma_o(\vec{k}_s, \vec{k}_i, a)$, i.e., by that in unbounded homogeneous sediment free space. The transmission through the water-sediment interface and propagation in the sediment, at given directions of incident and scattered waves, can be taken into account by a bistatic propagation factor, $T(\vec{k}_s, \vec{k}_i, z)$, so that

$$\sigma(\vec{k}_s, \vec{k}_i, a, z) = T(\vec{k}_s, \vec{k}_i, z)\ \sigma_o(\vec{k}_s, \vec{k}_i, a, z) \tag{7}$$

Correspondingly, Eq. (6) now becomes of the form

$$m(z) = T(z)\, m_o(z) \tag{8}$$

where m_o is the "free field" volume scattering coefficient of the sediment defined as follows

$$m_o(z) = \int \psi_N(a, z)\sigma_o(a, z)\, da \tag{9}$$

Assume now that particles are uniformly distributed through the layer of thickness h, so that $z_o < z < z_1 = z_o + h$. Then for the seabed scattering coefficient, using Eq.(5), one obtains

$$\begin{aligned} m_s &= m_o Z(z_o, z_1) \\ Z(z_1, z_2) &= \int_{z_o}^{z_1} T(z)\, dz \end{aligned} \tag{10}$$

Consider the case of the sediment inclusions embedded in a homogeneous fluid half-space. The propagation factor for this case is described in details in Appendix II. It is shown that this factor can be presented in an exponential form, see Eq. (35). Then for the bistatic seabed scattering coefficient, using Eq.(5), one obtains

$$m_s = T_o m_o \frac{\exp(-\kappa z_o) - \exp(-\kappa z_1)}{\kappa} \tag{11}$$

For the backward direction, assuming also that the top boundary of the scattering layer is close enough to the water-sediment interface, so that $\kappa z_o << 1$, Eq. (11) results in the following expression used for calculations later in this paper

$$m_s = \frac{|W_i|^4 m_o \sin\chi_t}{2\mu^2\beta}\left(1 - \exp(-2\beta h / \sin\chi_t)\right) \tag{12}$$

where μ is the sediment-to-water density ratio, W_i is the water-to-sediment transmission coefficient of the incident wave, β is the sound attenuation coefficient in the sediment, and χ_t is the grazing angle of the incident wave in the sediment (defined in Appendix II). This expression is similar to given previously in [Ivakin 2001] and generalizes the one for volume scattering from a half-space

$$m_s = \frac{|W_i|^4 m_o \sin\chi_t}{2\mu^2\beta} \qquad (13)$$

see, e.g., [Ivakin and Lysanov 1981, Ivakin 2000, and Jackson and Richardson 2007], to the case of a scattering layer of a finite thickness.

To define the sediment volume scattering coefficient, m_o, in according with Eq. (9), we need to specify the form of the size distribution of the particles and their individual scattering cross section. The size distribution for the SAX04 sediment discrete scatterers was measured [Ivakin 2008] and will be discussed in the following section. There were no measurements of the individual scattering from inclusions in the sediment, and there is no exact solution for non-spherical particles of irregular shape, which would be most relevant for natural sediment particles. In this paper, we will use an approximate "high-pass" expression for this function, given in Appendix III. Following other approaches used to define "high-pass" expressions, we assume that after average over random orientations of the particle, it can be approximated by that for spherical particle with the same equivalent radius (the radius of a sphere having the same volume). With this modification, the sediment particle size distribution as a function of the equivalent radius is required to provide inputs to the inclusion scattering model to provide comparison with the SAX04 acoustic backscatter data.

III. Some Results of Analysis of SAX04 Sediment Samples

In a companion paper [Ivakin 2008], we present detailed results of granulometric analysis of thirteen SAX04 sediment samples for particles of coarse fractions with equivalent diameter greater than 1 mm. The two visually different classes of grains in these fractions, coarse sand (mainly quartz particles) and shell fragments, were segregated from each other and analyzed separately. The size distributions of particles as functions of the equivalent diameter D, $D=2a$, were obtained and the results are shown in Fig. 1 for sand and shell particles in all the sediment samples. An important result of this analysis is that the size distributions of these two classes of particles closely follow the power law in all the range of sizes presented in these samples, 1mm < D < 4 mm for coarse sand particles, and 1mm < D < 20 mm for shell fragments. It is seen also that size distributions are much flatter for shells while decreasing steeply as the size increases for coarse sand particles, and this results in that shells become a dominating coarse fraction of the sediment for particles larger than certain "transition" size found here to be about 2 mm.

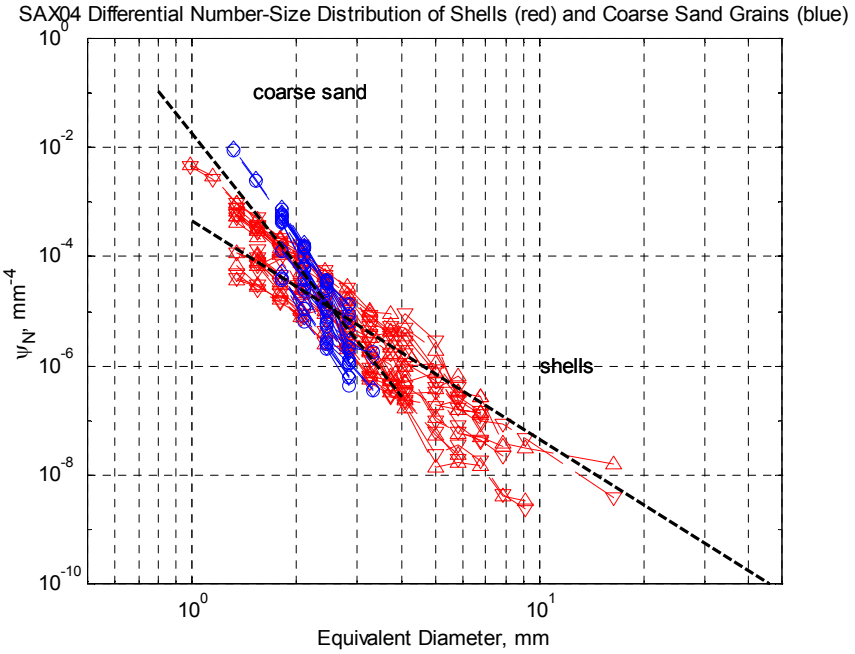

Fig. 1. Number-size distributions for the SAX04 sediment inclusions obtained from thirteen SAX04 sediment samples.

These results are used here in this paper to provide a set of input parameters for the seabed scattering model. First, however, it is important to notice that presented here size distributions, as usual in practice, result from an average over the sediment sample thickness and, therefore, are related with actual size-depth distributions through an integral relationship

$$\overline{\psi}_N(a) = H^{-1}\int \psi_N(a,z)\,dz \tag{14}$$

where H is the sediment sample thickness. Here, for the SAX04 samples, $H = 6$ cm. Correspondingly, there is a resolution uncertainty in defining the local volume concentration of the particles within the sediment sample. Also, one needs to assume if there are particles beyond the sediment sample. If particles are concentrated actually in a layer of thickness h, we use following assumptions to resolve this uncertainties

$$\begin{aligned}&\psi_N = (H/h)\overline{\psi}_N,\ h < H\\ &\psi_N = \overline{\psi}_N,\ h > H\end{aligned} \tag{15}$$

This means, in particular, that, if particles are concentrated in a thinner layer, $h < H$, then the volume concentration in this layer (see Appendix I) is larger than average in whole sample and can be defined as follows

$$C_v = (H/h)\overline{C}_v,\ \ \overline{C}_v = \int v(a)\overline{\psi}_N(a)\,da \tag{16}$$

For the "effective surface" concentration of the particles, if they are concentrated in a layer thinner than sample, there is no such uncertainty and it can be defined as follows

$$C_s = H\int s(a)\overline{\psi}_N(a)\,da \tag{17}$$

In following model/data comparisons, we use two models for the depth distribution of particles. First one corresponds to a half-space with uniformly distributed particles having the same volume concentration as the average. In the second model, the thickness of the scattering layer is taken to be smaller than for the sample, $h = 1.5$ cm, and therefore, $C_v = 4\overline{C}_v$.

To provide inputs for the theoretical model of scattering, we use power law approximations for the size distribution function of the form

$$\psi_N(a) \approx Ba_o^{-4}(a/a_o)^{-\gamma},\ \ a_1 < a < a_2, \tag{18}$$

where a_o being introduced as an intercept scale. This also makes a power law amplitude, B_o, dimensionless. Here we use a scale $a_o = 0.5$ mm. For shells and coarse sand particles, Eq.(18) is used with two different sets of parameters. In Fig.1, they are represented by two dashed lines. One line corresponds to coarse sand particles and was calculated with the following values of parameters: $B_o = 0.018,\ \gamma = 8,\ a_1 = 0.4$ mm, $a_2 = 2$ mm. Using Eqs. (16), (17), the particle volume concentration averaged over the sample volume and the effective surface concentration were estimated as well and obtained as follows $\overline{C}_v = 0.0058,\ C_s = 0.52$. Corresponding values for another dashed line provide inputs to the model of scattering for shells: $B = 0.00045,\ \gamma = 4,\ a_1 = 0.5$ mm, $a_2 = 45$ mm. These values give estimates for concentrations of shells: $\overline{C}_v = 0.0011,\ C_s = 0.021$, which are smaller than for coarse sand particles. In both cases, therefore, including the 4-times increase of volume concentration in the thinner layer (1.5 cm) model, we have $C_v << 1$, and the requirement for scatterers to be sparse enough is not violated. Also, in both cases, we have $C_s < 1$ that allows considering inclusions as a thin layer of particles. Based on these estimates, we can consider shells and coarse sand particles as two separate modes in the sediment grain size distribution, or as sparse inclusions of these two types, suspended in a homogeneous and uniform substrate of densely packed smaller particles (medium sand or mud).

IV. SAX04 DATA/MODEL COMPARISONS

The obtained sediment particle size distributions were used as inputs to the "inclusion scattering" model to provide comparison with the frequency-angular dependencies of acoustic backscattering from the seabed observed at the SAX04 site in wide ranges of frequency (30 to 500 kHz) and grazing angles (15 to 50 degrees) by [Williams et al 2008]. The first and main question to answer using this data/model comparisons in this paper is if the level of scattering corresponding to SAX04 sediment inclusions is comparable with the observed level at SAX04 and, therefore, if the inclusions can play a noticeable role in the SAX04 seabed scattering. Next question is if a simple model of scattering described in previous sections and based on a very simplified presentation of the complicated SAX04 environment is able to provide general features of the frequency-angular dependences. Another set of questions for discussion is which features of the observed dependencies do not appear in the model simulations, what can be the reason of the discrepancies, and which features of the SAX04 environment should be taken into account in future work to eliminate such discrepancies.

Examples of typical angular dependencies of the seabed backscattering strength, $10\log(m_s)$, are given in Fig. 2a for two frequencies, 70 and 400 kHz. It is seen that they are quite different. The angular dependence at the lower frequency shows a distinct "critical angle" effect for volume scattering, see, e.g., [Ivakin 1981, 2001, Jackson 2007], with the critical angle being around $30°$ which corresponds to a medium sand sediment. At the higher frequency, this effect is not pronounced or at least shifted to angles smaller than $20°$, where, at these frequencies, there were no measurements. Examples of frequency dependencies are shown in Fig. 2b for two fixed grazing angles, $\chi_w = 35°$ (above critical grazing angle) and $25°$ (below critical). It is seen that, first, that they are significantly different at medium frequencies, 70 to 130 kHz, and, secondly, for both angles, they have different slopes at low and high frequencies. A general idea of analysis in this paper is that such frequency dependencies of the scattering strength can be due to two different types (or modes) of inclusions in the SAX04 sediment, shells and coarse sand particles.

In the previous section of this paper, it was demonstrated that the size distributions of the two modes of inclusions have different slopes and this results in the shell mode being dominating at large sizes (greater than 2 mm) while the coarse sand mode dominating at smaller sizes. One can show (see Appendix IV) that the power law size distribution of inclusions results in the power law frequency dependence of the scattering strength. This is illustrated in Fig.3, where the normalized volume scattering strength (described in details in Appendix IV) is shown as a function of dimensionless frequency, ka_o, for different values of the power exponents γ, at fixed cut parameters, $a_o / a_1 = 2,\ a_o / a_2 = 0.02$. The following analysis shows that that the difference in frequency dependencies of the scattering strength at low and high frequency ranges can be due to two different types (or modes) of inclusions in the SAX04 sediment, shells dominating at lower frequencies, and coarse sand particles dominating at high frequency range. This explanation holds in both ranges of grazing angles, above and below $30°$.

First, calculations of the backscattering strength were made using Eq. (13) for scatterers uniformly distributed in a fluid sediment half-space. The density, sound speed and attenuation in water above the sediment were taken as follows: $\rho_w = 1.0$ g/cm^3, $c_w = 1.5$ km/s, $\delta = 0$. Correspondent parameters for the inclusions in the sediment were taken to be: $\rho_\alpha = 2.7$ g/cm^3, $c_\alpha = 5.7$ km/s, $\delta = 0$. Values of effective acoustic parameters of the sediment half-space in the model were taken to be: $\rho = 2.0$ g/cm^3, $c = 1.75$ km/s, $\delta = 0.006$, which is within reasonable uncertainty of environmental measurements at the SAX04 site. In Figs 4a and 4b, frequency and angular dependencies for the backscattering strength for the two modes of particles, shells and coarse sand (as inclusions in medium sand frame half-space), are presented by two solid lines correspondingly. The size distributions are taken for both cases as shown in Fig.1 by two dashed lines for shells and coarse sand particles and as specified in previous Section. The main result of this first data/model comparison is that the level of scattering by the SAX04 sediment inclusions is comparable with the observed level and, therefore, the inclusions indeed can play a noticeable role in the SAX04 seabed scattering. Moreover, this simple model provides a good explanation of both frequency and angular dependencies of the SAX04 backscatter at grazing angles starting from the critical angle (about $30°$) and above.

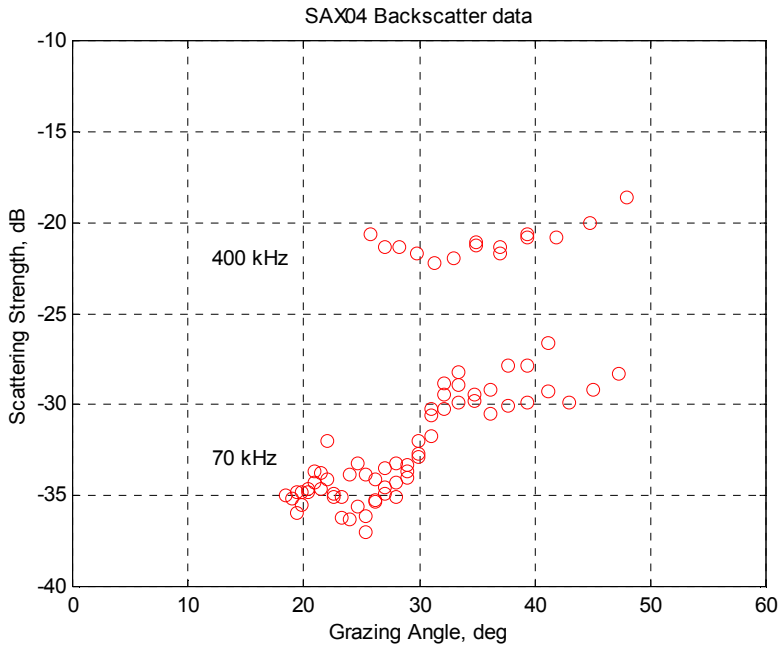

Fig. 2a.

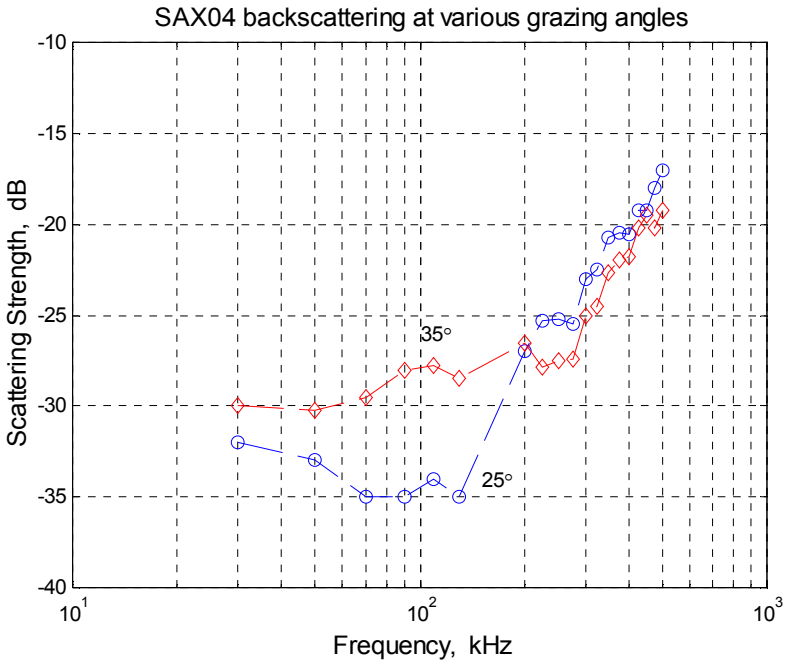

Fig. 2b.

Fig. 2. Angular and frequency dependences of the bottom backscattering strength measured at SAX04 by [Williams et al 2008].

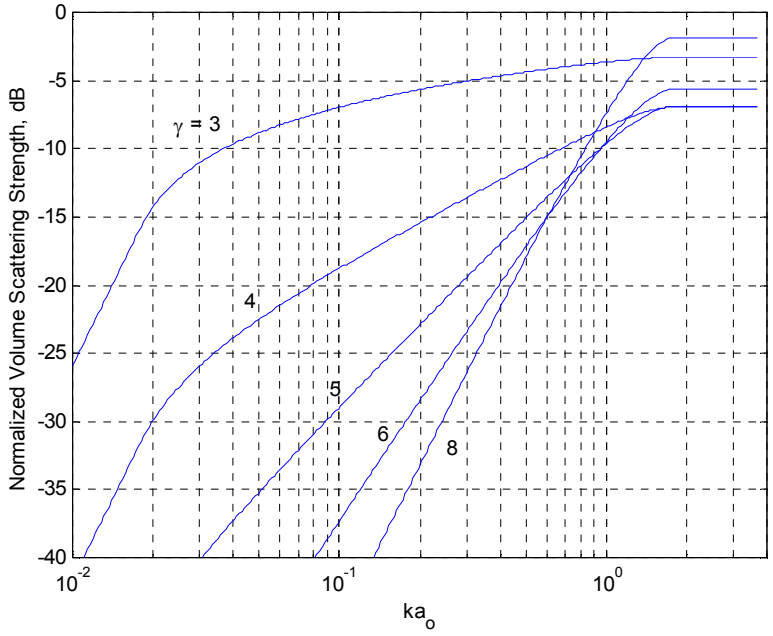

Fig. 3. The dependence of the normalized volume scattering coefficient M_o as a function of the dimensionless frequency ka_o for different values of the power exponents γ, see Appendix IV.

From Fig. 4b, it is easy to see however that there is a significant discrepancy of the observed and calculated angular dependencies at grazing angles below critical for both low and high frequencies. To understand the reason for this discrepancy, one should take into account that actually the SAX04 sediment was not purely medium sand, but rather a complex medium sand / mud mixture, with a thin (up to a few cm thick) mud layer covering the sand basement. A consistent consideration of the effects of the sediment layering is beyond the scope of this simple model and will be a subject of future work. However, some estimates can be done even without consideration of the sediment layering. At this stage, it can be enough to consider the stratification of scatterers only, that is to take into account a finite thickness of the scattering layer within a mud environment. Physics of such simplification is that in this case all possible reflections from the mud/sand interface are neglected. This, however, still can provide an approximate average level of scattering, but will neglect all possible interference patterns in frequency angular dependencies of the scattering strength usually appearing in the case of stratified sediments [Ivakin 1986 and 1998, Mourad and Jackson 1993].

For such rough estimates, calculations were made for the same model of "inclusion scattering", but using Eq. (12) for a thin scattering layer, instead of Eq. (13) for the scattering half-space, and using effective acoustic parameters of mud sediments, instead of those for medium sand. The scattering layer thickness was taken to be 1.5 cm, and parameters of the mud sediment were taken to be as follows: $\rho = 1.8$ g/cm^3, $c = 1.61$ km/s, $\delta = 0.006$. In Figs 5a and 5b, frequency and angular dependencies for the backscattering strength are presented by two dashed lines for two modes of particles, shells and coarse sand, correspondingly, and the size distributions were taken again for modes of inclusions as shown in Fig.1 by two dashed lines. Figure 5a shows that estimates of the scattering level for the SAX04 sediment inclusions are fitting well with the observed at grazing angles below $30°$. Figure 5b also shows a reasonable agreement, with the most significant discrepancy at low frequencies, 30 to 50 kHz. Generally, results shown in Fig.5 demonstrate that inclusions in the top sediment layer of mud can indeed be considered as a possible mechanism responsible for the enhanced level of scattering observed at the grazing angles below $30°$ in both low and high frequency range. This good fit in data/model comparison however is paid by an appearing inconsistency in the sediment model, where the mud inputs have to be used at small grazing angles, below $30°$, while medium sand inputs are used for the grazing angles above $30°$. This however gives a hint for a reasonable modification of the model to eliminate such inconsistency. It seems that a systematic consideration of the sediment stratification can be a natural next step in improving the model. This, along with other ways to improve the model of scattering, will be discussed in the next Section.

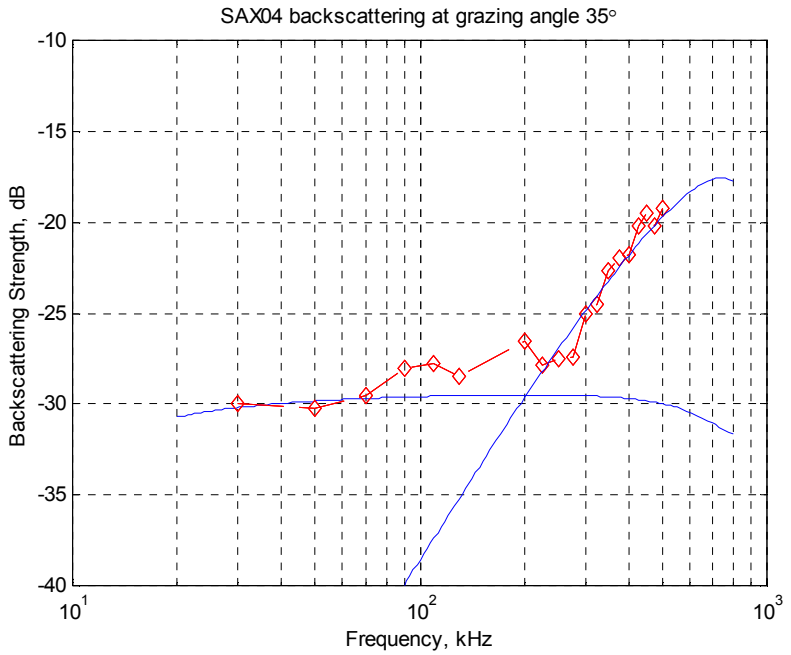

Fig. 4a.

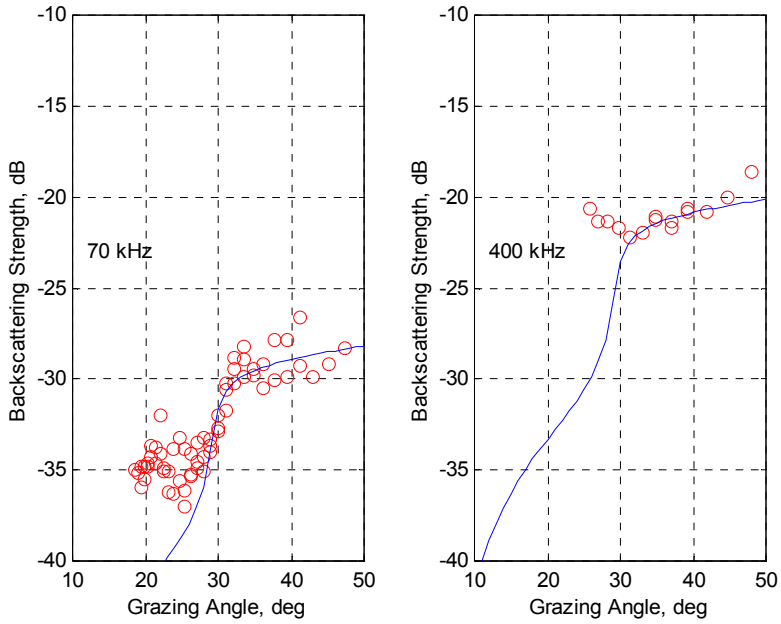

Fig. 4b.

Fig. 4. SAX04 data/model comparisons for frequency and angular dependencies of the bottom backscattering strength. The solid lines correspond to scattering from inclusions with the power law grain size distribution (see dashed lines in Fig. 1). It is assumed that inclusions are embedded to an effective fluid half-space with parameters corresponding to medium sand.

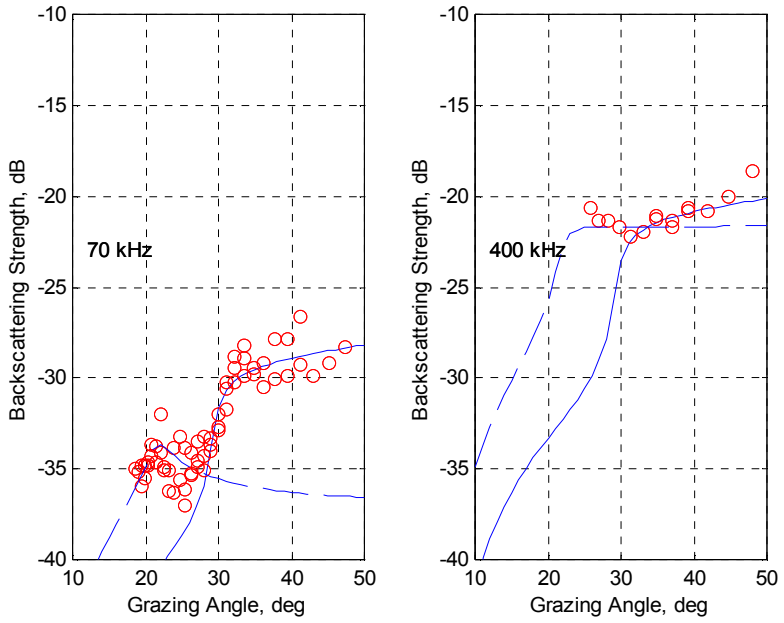

Fig. 5a.

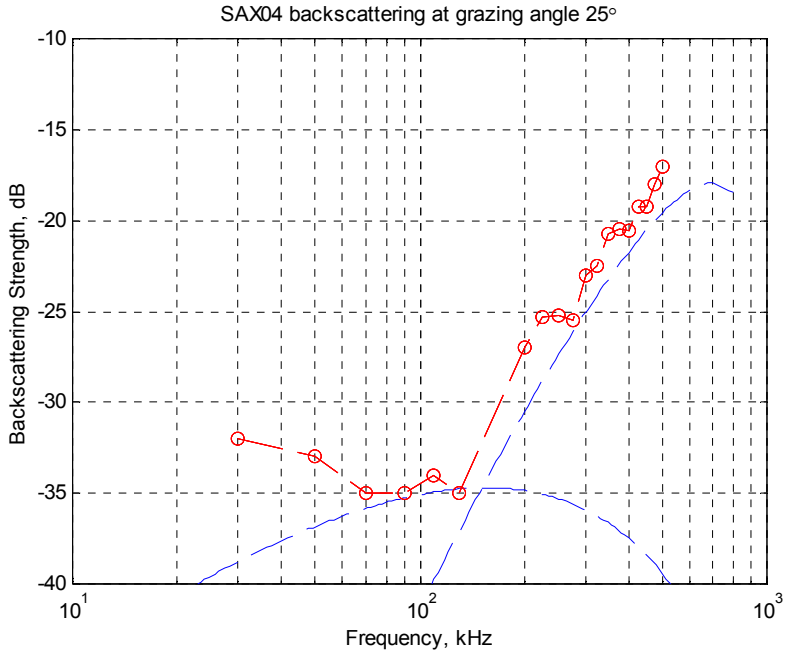

Fig. 5b.

Fig. 5. SAX04 data/model comparisons for angular and frequency dependencies of the bottom backscattering strength. The dashed lines correspond to the “inclusion scattering” model with the power law grain size distribution as was used for calculations in Fig.4 (shown here by solid lines as well for comparison). The difference is due to assumption that here inclusions are located in a thin top layer of the sediment and the sediment parameters correspond to mud.

V. DISCUSSION

The SAX04 data/model comparisons were made for the model of scattering using certain assumptions and simplifications, which can be responsible for some quantitative discrepancies and an inconsistency noticed in previous Section. In particular, the following assumptions can be important:

- Inclusions were considered as fully buried in the sediment assuming that contribution of particles located near the interface (including those partially buried) is insignificant;
- Individual scattering function was taken of a simplified form with low- and high-frequency limits as for equivalent fluid spheres assuming that for a non-spherical particle, upon average over their random orientation, it can be approximated by that for spherical one with the same equivalent radius;
- An incoherent summation of intensities scattered by different inclusions was assumed, neglecting possible effects of their correlations;
- Possible multiple scattering effects were neglected;
- The sediment surface was assumed flat, so that possible volume-roughness interactions were ignored;
- The sediment was considered as homogeneous fluid substrate, i.e., its stratification was not taken into account.

In order to eliminate these assumptions, corresponding modifications are required. For example, elimination of the first assumption is necessary to take into account scatterers located on the bottom surface or not buried completely but rather exposed in the water. In this case, analytical solutions are complicated, but can be analyzed numerically [Lim et al 1993 and Lim 1998, Fawcett 1996, Fawcett and Lim 2003, Zampolli et al 2008]. There is also a simpler semi-phenomenological approach, using ray considerations, that can be useful at high enough frequencies. In this case, the incident and scattered waves can be considered taking into account possible reflections on the water-sediment interface and corresponding bistatic channels of scattering [Williams et al 2001]. Although in the SAX04 conditions, exposed shells and other discrete scatterers on the sediment surface were not observed, such observations are common in many other shallow water regions. This can be especially important at higher frequencies and sub-critical grazing angles because of smaller sound penetration of the sediment and respectively decreased role of buried scatterers. Another correction should be made for scatterers buried near the water-sediment interface, so that their depth is smaller or comparable with their size. In this case, their individual scattering functions can be affected by possible multiple reflections between the interface and the particle. However, this effect can be neglected if the contrast of parameters at the water-sediment interface is small enough so that reflections are weak. Note also that these reflections can be substantially weakened by presence of a thin transition layer known to be usual near the water-sediment interface.

Elimination of the second assumption is particularly important for better description of the angular dependence of scattering which is known to be sensitive to the shape of the scatterers (the so-called aspect-effect) that is commonly used in remote sensing (see, e.g., [Ivakin 1981, 1985, 2001]). Third and forth assumptions can become too strong at higher frequencies (above 500 kHz), where the size of the most of the sediment particles in the medium sand sediment becomes comparable with the wavelength and, therefore, “inclusions” become not sparse. In this case corrections should be considered to take into account correlations of the particle positions, possible “collective” effects and effects of multiple scatter, see discussions in [Bunchuk and Ivakin 1989, Lyons 2005, Isimaru 1997]. Elimination of the fifth assumption would make it possible to give a consistent consideration of scattering at sub-critical grazing angles, taking into account, e.g., possible effects of the volume scattering enhancement due to better sound penetration into the sediment [Ivakin 1981, 2004, 2005].

The sixth assumption neglects possible strong effects of the sediment stratification or layering, gradient effects in the top transition layer, related effects of focusing, appearing new channels of scattering and their interference, etc. According to a results of the data/model comparisons presented in previous Section of this paper, the sediment stratification seems to be a natural candidate to focus in future work to better understand results of the SAX04 acoustic measurements. This corresponds also to real situation of the complex SAX04 sand/mud environment, appearing usually as a thin but distinctive mud layer covering a sand basement. The thickness of the mud layer varied from a few mm (forming a thin transition layer between water and sand) to about 5 cm (filling depressions in the sand rough surface [Richardson 2005, Thorsos 2005]). One of possible effects of the transition layer near the sediment surface is smoothing of an impedance contrast at the interface which can result in an additional enhancement of acoustic penetration and, therefore, enhances volume scattering. It is known that the sediment stratification can make a significant impact on the seabed scattering properties, see [Ivakin 1986 and 1998, Mourad and Jackson 1993], where it was shown, for example, that at high frequencies and small grazing angles, because of the smaller sound penetration to the sediment, only its near surface properties are important (and the SAX04 sediment therefore can be considered as having parameters of mud). At low enough frequencies and larger grazing angles, the thin top layer parameters become unimportant (and the SAX04 sediment can be treated as a medium sand half-space). In this paper, we consider only these two limit cases, leaving a more consistent consideration of the sediment stratification effects to a future work.

VI. SUMMARY AND CONCLUSIONS

In this paper, an "inclusion scattering" model is presented and used for analysis of backscattering data obtained during the SAX04 sediment acoustics experiment. The model considers discrete scatterers larger than mean grain size as inclusions embedded in a sediment half-space with given effective fluid parameters, density, sound speed and attenuation. Acoustic scattering from the sediment inclusions is described in terms of the individual scattering functions of discrete targets. It was assumed that the scattering function for non-spherical particles upon average over their random orientation can be approximated by that for spherical one with the same equivalent radius (same volume). With this modification, the sediment particle size distributions as function of the equivalent radius are required to provide input parameters to this model. They were obtained from granulometric measurements for coarse fractions of the SAX04 sediment particles with the grain size larger than 1 mm. These particles comprise only a small volume portion of the sediment and therefore do not affect the mean grain size. However, they can contribute significantly to the seabed acoustical properties affected by processes of discrete scattering in the sediment.

Generally, the results of data/model comparison demonstrate that scattering from the sediment inclusions, such as shell fragments and coarse sand particles, can be a significant or even a dominant mechanism of the SAX04 seabed scattering in a wide frequency range, 30 kHz to 500 kHz, and in a wide range of grazing angles, 15 to 50 degrees. A possible impact on improving existing algorithms for geoacoustic characterization of the sediments is that this work has demonstrated that the sediment grain size distribution "tails", corresponding to particles with sizes greater than the mean grain size, or the sediment inclusions, are critical characteristics and important factors affecting seabed scattering properties. This can be used, for example, to upgrade existing grain-size based algorithms for predicting bottom reverberation [Jackson and Richardson 2007, Briggs et al 1989 and 2002].

The analysis has shown however that, although the current version of the model is able to provide reasonable estimates for interpretation of SAX04 scattering data, some quantitative discrepancy in model/data comparisons appear. This can be due to using certain assumptions made in the model of scattering. It is clear now that the model needs some additional modifications to improve understanding of the role of the discrete scattering mechanism in the sound-bottom interactions, and, therefore, enhance its capabilities for potential acoustic data predictions and inversions. For example, taking into account the sediment stratification might be an important step in improving the model. This and other modifications can be interesting subjects for future work.

ACKNOWLEDGMENT

This research was conducted in collaboration with colleagues at the APL-UW and NRL and their contribution is gratefully acknowledged. Dr. M. Richardson of NRL arranged the sediment samples collection by APL and NRL divers. Dr. K. Williams of APL provided results of his acoustic measurements at SAX04 used for data/model comparisons in this paper. This work was supported by the U.S. Office of Navel Research.

APPENDIX I

STATISTICAL CHARACTERISTICS

Using the size-depth distribution function, all practically important statistical characteristics of the sediment inclusions can be found. For example, from the definition of this function (3), the total number of inclusions in the given sediment volume (or in the sediment sample) is

$$N = A\iint \psi_N(a,z)\,da\,dz \tag{19}$$

Normally, the scattering volume depends on the directivity, frequency and duration of the signal. The number of scatterers in this volume (or in the "resolution cell") plays a critical role in statistics of scattering [Abraham 2003, Abraham and Lyons 2004]. In particular, it is required for definition of the probability density function

$$\varphi_N(a,z) = (A/N)\psi_N(a,z) \tag{20}$$

using which the average of an arbitrary function appearing in the problem, $< u >$, over the particles size and depth can be defined as follows

$$< u >= \int u(a,z)\,\varphi_N(a,z)\,da\,dz \tag{21}$$

Consider a dimensionless volume concentration of particles at a given depth

$$C_v(z) = \int v(a,z)\psi_N(a,z)\,da \tag{22}$$

Here $v(a,z)$ is the volume of the particle having the size a and located at the depth z. This dependence generally can be different for particles with different shape. To establish such a relationship, one can introduce the equivalent radius of the particle, i.e., the radius of the sphere with the same volume. The equation (22) is important for controlling the requirement of not interpenetrating of particles, for which at any depth an inequality $C_v(z) < 1$ should hold. Also, comparing (22) with (6), the volume scattering coefficient in an arbitrarily thin layer of sediments can be defined as follows

$$m = C_v < \sigma > / < v > \tag{23}$$

For the average volume concentration of the inclusions in the sediment sample, assuming that the sample has a vertical size H, one obtains

$$\overline{C}_v = H^{-1}\int C_v(z)\,dz = \frac{N < v >}{AH} \tag{24}$$

If the sediment sample is thin enough, it can be more convenient to introduce a dimensionless "coverage" parameter, or an "effective surface" concentration of the particles in this sample

$$C_s = \iint \psi_N(a,z)\,s(a,z)\,da\,dz = \frac{N < s >}{A} \tag{25}$$

Here $s(a,z)$ is an "effective" cross-section of the particle, which defines a geometric projection of the particle onto a certain surface in the sediment. It can be a sediment interface, or a certain plane defined in the problem, e.g., oriented normally with respect to direction of sound scattering. This dependence, however, can be different for non-spherical particles with different orientation. A way to specify such a relationship can be averaging over possible orientations and defining an equivalent radius of the average projection. The equation (25) can be also important in the case where a monolayer of particles is considered. In this case, an inequality $C_s < 1$ should hold.

Using (19)-(21), it is easy to see that the scattering coefficient in (4) can be obtained from the equation

$$m_s = C_N \langle \sigma \rangle \tag{26}$$

where the factor C_N can be defined by any of the following expressions

$$C_N = \frac{N}{A} = \frac{C_s}{\langle s \rangle} = \frac{\overline{C}_v H}{\langle v \rangle} \tag{27}$$

and the choice of a particular expression depends on convenience for a specific scattering problem. Consider, e.g., the case where scatterers are distributed within a layer in a free-space. In a particular case of spherical particles with the radius a large in comparison with the wavelength, the individual scattering function can be approximated by its geometric acoustics expression $\sigma = a^2 R^2 / 4$, where R is the reflection coefficient for the material of the sphere (see Appendix III). Then from (27) with $s = \pi a^2$ one obtains a known expression, see, e.g., [Bunchuk 1989, Stanton 2000] $m_s = C_s R^2 / (4\pi)$, where however, the coverage parameter, if it is more convenient, can be replaced by the average volume concentration as follows $C_s = \overline{C}_v H \langle s \rangle / \langle v \rangle$.

APPENDIX II

PROPAGATION FACTOR

If scatterers are buried in the sediment, the incident and scattered waves in water are related with those in the sediment through corresponding transmission coefficients, W_i and W_S, and plane wave propagation/attenuation factors. Such approach is widely used in models of volume scattering in sediments [Ivakin 1981, 2000, 2001, 2004, Jackson 2007] and in detection of buried objects in the seabed [Hovem 1998]. Then the individual scattering cross-section can be presented in the form (7) with the bistatic propagation factor T defined as follows

$$T = \left|T_i T_s\right|^2 \mu^{-2} \tag{28}$$

$$T_{i,s} = W_{i,s} \exp(ik_w P_{i,s} z) \tag{29}$$

$$W_{i,s} = 2\mu \sin\chi_{i,s} / (\mu \sin\chi_{i,s} + P_{i,s}) \tag{30}$$

$$P_{i,s} = (n^2 - \cos^2\chi_{i,s})^{1/2} \tag{31}$$

Here $\mu = \rho / \rho_w$ is the sediment to water density ratio, $n = c_w / c = n_o(1 + i\delta)$ is the sediment complex refraction index, or the water to sediment sound speed ratio, $\chi_{i,s}$ are grazing angles of the incident and scattered waves near the seabed, k_w is the sound wave number in water, and $W_{i,s}$ is the water-to-sediment transmission coefficient in the direction of the incident and scattered wave (with corresponding subscript index).

Propagation of the incident and scattered waves in the sediment are controlled by the function $P_{i,s} = P(\chi_{i,s})$. One can show that

$$P = (n^2 - \cos^2\chi)^{1/2} = n_o(q + i\delta / q) \tag{32}$$

$$q = q(\chi) = \frac{1}{\sqrt{2}}\sqrt{\eta + \sqrt{\eta^2 + \delta^2}}\,,\ \eta = 1 - \frac{\cos^2\chi}{n_o^2} - \delta^2 \tag{33}$$

The real part of equation (32) represents in fact a generalized Snell's law for the practically important case where the refraction index is complex, corresponding to absorbing (lossy) sediments. It defines a relationship between directions of propagation of plane waves in an ideal (lossless) water and lossy sediment, i.e., directions of the normal to the phase fronts of the incident and transmitted (refracted) plane waves, and can be presented in the form

$$\sin\chi_t = q(\chi_i) = \frac{1}{n_o}\mathrm{Re}(P_i) \tag{34}$$

Correspondingly, the imagery part of Eq.(32), through the Eq. (29), describe exponential attenuation of the refracted wave along this direction and, at the same time, gives a uniform description of the amplitude of both refracted and evanescent waves in the sediment including their smooth mutual transformation near the critical grazing angle where $\chi_i \approx \chi_c$, $\cos\chi_c = n_o$. In particular, at the critical grazing angle, $q(\chi_c) = \sqrt{\delta}$, and at small subcritical grazing angles, at $\chi_i << \chi_c$, $q \approx \delta / \sqrt{1 - n_o^2}$.

Using Eqs. (28), (32) and (34), the propagation factor becomes of the form

$$T(z) = T_o e^{-\kappa z} \tag{35}$$

where $T_o = |W_i W_s|^2 \mu^{-2}$, $\kappa = \beta(1/\sin\chi_{ti} + 1/\sin\chi_{ts})$, and $\beta = 2\delta k_w n_o$ is the sound attenuation coefficient in the sediment.

APPENDIX III

INDIVIDUAL SCATTERING FUNCTION

Examples of exact expression for the individual scattering cross section in the case of an elastic solid and fluid spheres can be found, e.g., in [Hickling 1962, Morse and Ingard 1968, Medwin and Clay 1998]. There is no exact solution for non-spherical particles of irregular shape. However, there are approximate solutions for low-frequency (Rayleigh scattering) and high-frequency (geometry acoustics) limits [Palmer 1996, Bass and Fuks 1979]. There are also wide frequency range approaches that can be numerically efficient in the case of smooth enough bodies [Reeder and Stanton 2004]. For many practical applications, there have been developed simple empirical formulae, so-called "high-pass" expressions, defined in such way that they satisfy known low-frequency (Rayleigh scattering) and high-frequency (geometry acoustics) limits and have a reasonable continuous behavior for the intermediate frequencies (see, e.g., [Sheng and Hay 1988, Stanton 1989, Thorne et al 1995, Thorne and Backingham 2004]). In this paper, for numerical illustrations, we will use a simplest of possible "high-pass" approximations for the scattering function in the form

$$\sigma_o(a) = a^2 F(ka), \tag{36}$$

$$F(x) = \begin{matrix} \alpha_o x^4, & x \le x_o = (\alpha_\infty/\alpha_o)^{1/4} \\ \alpha_\infty, & x \ge x_o \end{matrix} \tag{37}$$

where a is a "size"-parameter, α_o and α_∞ are dimensionless parameters defined by material of the particle and their orientation. Generally, the values of this parameters, as well as the meaning of the "size" of a non-spherical particle, should result from a statistical averaging over possible orientation of the particle. In this paper, following other "high-pass" approaches, we assume that, after average over random orientations, the parameters in (37) can be approximated by those for spherical particles with the same equivalent radius (the radius of a sphere having the same volume). As such, for illustration purposes of this paper, we will use parameters of a fluid sphere [Morse 1968, Medwin 1998, Stanton 1989].

$$\alpha_o = \frac{R_0^2}{4},\ \alpha_\infty = \frac{R^2}{4} \tag{38}$$

with parameters R_0 and R defined as follows

$$R_0 = \frac{2}{3}\left(1 - \frac{\rho c^2}{\rho_\alpha c_\alpha^2}\right) + \frac{\rho_\alpha - \rho}{\rho_\alpha + \rho/2},\ R = \frac{\rho_\alpha c_\alpha - \rho c}{\rho_\alpha c_\alpha + \rho c}. \tag{39}$$

where c_α and ρ_α are the sound speed and the density of the sphere (representing inclusions), c and ρ are the sound speed and the density of a surrounding fluid medium (representing sediment).

APPENDIX IV

SCATTERING FROM INCLUSIONS WITH POWER-LAW SIZE DISTRIBUTION

Consider the inclusion size distribution of the power law form (or, more accurately, "truncated" power law) given by Eq. (18). From Eqs (9) and (36), one obtains

$$M_o \equiv m_o a_o / B = a_o^{\gamma-3} \int_{a_1}^{a_2} a^{2-\gamma} F(ka)\, da \tag{40}$$

This function represents a normalized volume scattering coefficient of the sediment. Consider its frequency dependence using a "high-pass" approximation for the individual scattering function given by (37). For high frequencies, where $ka_1 \geq x_o \equiv (\alpha_\infty / \alpha_o)^{1/4}$, it can be presented in the form

$$M_o = \alpha_\infty J_{3-\gamma}\left(\frac{a_1}{a_o}, \frac{a_2}{a_o}\right) \tag{41}$$

where

$$J_\eta(x,y) \equiv \int_x^y t^{\eta-1}dt = \frac{y^\eta - x^\eta}{\eta},\ J_0(x,y) = \ln(y/x) \tag{42}$$

Note that in this case, it becomes frequency independent regardless the power exponent of the size distribution. For low frequencies, where $ka_2 \leq x_o$, we have

$$M_o = \alpha_o (ka_o)^4 J_{7-\gamma}\left(\frac{a_1}{a_o}, \frac{a_2}{a_o}\right) \tag{43}$$

In this case, it follows the Rayleigh forth power frequency dependence regardless the power exponent of the size distribution.

At intermediate frequencies, where $x_o / a_2 < k < x_o / a_1$, one obtains

$$M_o = \alpha_o (ka_o)^4 J_{7-\gamma}\left(\frac{a_1}{a_o}, \frac{x_o}{ka_o}\right) + \alpha_\infty J_{3-\gamma}\left(\frac{x_o}{ka_o}, \frac{a_2}{a_o}\right) \tag{44}$$

For power exponents in the range $3 < \gamma \leq 7$ and wide enough size distributions, so that $x_o / a_2 << k << x_o / a_1$,

$$M_o = (ka_o)^{\gamma-3} G(\gamma),\ G(\gamma) = \int_0^\infty x^{2-\gamma} F(x)dx \approx \frac{\alpha_\infty^{(7-\gamma)/4} \alpha_o^{(\gamma-3)/4}}{(7-\gamma)(\gamma-3)} \tag{45}$$

It is important to note that the integral in (45) has little sensitivity to a particular behavior of the individual scattering function *F* at intermediate *x=ka*, which makes the approximation (45) very robust and stable with respect to variations of the scatterer type, its shape, material, etc. Therefore, using a simple high-pass expression (37), for which the approximate equality in (45) becomes exact, seems to be reasonable and won't affect the result significantly. If more realistic individual scattering functions are used, the reasonable accuracy of the approximate equality in (45) will still hold. All the material parameters of the inclusion are included in the factors α_o and α_∞. To define these parameters, for illustration purposes, Eqs. (38) and (39), corresponding to a fluid sphere case, are used in this paper. The result, the dependence of the normalized volume scattering coefficient M_o as a function of the dimensionless frequency ka_o for different values of the power exponents γ is shown in Fig.3. Another general result is important to emphasize here. According to (45), in the case of the wide power law size distribution of inclusions, and for the intermediate frequency range, the frequency dependence of the volume scattering coefficient is very sensitive with respect to parameters of the size distribution. In particular, it also obeys power law and its power exponent is linearly related to the one for the size distribution. This can be an important, particularly, for remote acoustic sensing of the sediment.

REFERENCES

[1] D.A. Abraham (2003), "Signal excess in K-distributed reverberation", *IEEE J. Ocean. Eng.*, **28**(3), pp.526-536.
[2] D.A. Abraham and A.P. Lyons (2004), "Reverberation envelop statistics and their dependence on sonar bandwidth and scattering patch size", *IEEE J. Ocean. Eng.*, **29**(1), pp.126-137.
[3] F.G. Bass and I.M. Fuks (1979), *Wave Scattering from Statistically Rough Surfaces*, Pergamon, Oxford.

[4] K.B. Briggs, P. Fleischner, W.H. Jahn, R.I. Ray, W.B. Sawyer and M.D. Richardson (1989), "Investigation of High-Frequency Acoustic Backscattering Model Parameters: Environmental Data from the Arafura Sea", NORDA Report 197.
[5] K.B. Briggs, D.R. Jackson, and K.Y. Moravan (2002), "NRL-APL Grain Size Algorithm Upgrade", NRL, Stennis Space Center, MS. Report NRL/MR/7430-02-8274.
[6] A.V. Bunchuk and A.N. Ivakin (1989), "Energy characteristics of an echo signal from discrete scatterers on the ocean bottom", Soviet Physics-Acoustics, **35**(1), pp.5-11.
[7] J.A. Fawcett (1996), "Acoustic scattering from cylindrical objects embedded between two half-spaces", *J. Acoust. Soc. Am.,* **100**(5), pp.3053-3060.
[8] J.A. Fawcett and R. Lim (2003), "Evaluation of the integrals of target/seabed scattering using the method of complex images", *J. Acoust. Soc. Am.,* **114**(3), pp.1406-1415.
[9] R. Hickling (1962), "Analysis of echoes from a solid elastic sphere in water", *J. Acoust. Soc. Am.,* **34**(10), pp.1582-1592.
[10] A. Isimaru (1997), *Wave Propagation and Scattering in Random Media*, IEEE Press, NY.
[11] A.N. Ivakin (1981), "Sound scattering by multi-scale bottom inhomogeneities", Oceanology, **21**(1), pp.26-27.
[12] A.N. Ivakin and Yu.P. Lysanov (1981), "Underwater sound scattering by volume inhomogeneities of a bottom medium bounded by a rough surface", Soviet Physics-Acoustics, **27**(5), pp.212-215.
[13] A.N. Ivakin and Yu. P. Lysanov (1985), "Determination of certain parameters of marine sediments from acoustic sensing data", Soviet Physics-Acoustics, **31**(6), pp.493-494.
[14] A.N. Ivakin (1986), "Sound scattering by random inhomogeneities of stratified ocean sediments", Soviet Physics-Acoustics, **32**, pp.492-496.
[15] A.N. Ivakin (1998), "Models of seafloor roughness and volume scattering", in, *Proc. OCEANS 1998,* vol.1, pp. 518-521.
[16] A.N. Ivakin (1998), "A unified approach to volume and roughness scattering", *J. Acoust. Soc. Am.,* **103**, pp.827-837.
[17] A.N. Ivakin (2000), "High frequency scattering from heterogeneous seabeds", in, *Proc. Fifth European Conference on Underwater Acoustics, ECUA2000,* (Lyon, France, 10-13 July 2000), vol.2, pp. 1241-1246.
[18] A.N. Ivakin (2001), "Models of scattering for remote acoustic sensing of the seafloor", in, *Proceedings of the Institute of Acoustics*, **23**: Part 2, pp. 268-275.
[19] A.N. Ivakin (2004), "Scattering from discrete inclusions in marine sediments", in *Proc. Seventh European Conference on Underwater Acoustics, ECUA2004*, (Delft, The Netherlands, D.G. Simons (Ed), 5-8 July 2004, vol.1, pp. 625-630.
[20] A.N. Ivakin (2005), "High frequency scattering from sandy sediments: roughness vs discrete inclusions", in, *Boundary Influences in High Frequency Shallow Water Acoustics*, N.G. Pace and P. Blondel (Eds), University of Bath, UK, pp.185-192.
[21] A.N. Ivakin and J.-P. Sessarego (2007), "High frequency broad band scattering from water-saturated granular sediments: Scaling effects", *J. Acoust. Soc. Am,.* **122**(5), pp.EL165-171.
[22] A.N. Ivakin (2008), "Inclusions in marine sediments: Size and shape distributions of coarse sand and shell fractions in SAX04 sediment", *J.Oceanic Engr.,* **??**, ??-??, to be submitted in current issue.
[23] D.R. Jackson and M.D. Richardson (2007), *High Frequency Seafloor Acoustics*, Springer Science, NY.
[24] R. Lim, J.L. Lopes, R.H. Hackman, and D.G. Todoroff (1993), "Scattering by objects buried in underwater sediments: Theory ad experiment", *J. Acoust. Soc. Am.,* **93**(4), pp.1762-1783.
[25] R. Lim (1998), "Acoustic scattering by a partially buried three-dimensional elastic obstacle", *J. Acoust. Soc. Am.,* **104**(2), pp.769-782.
[26] A.P. Lyons (2005), The potential impact of shell fragment distributions on high-frequency seafloor backscatter", *IEEE J. Ocean. Eng.*, **30**, pp.843-851.
[27] H. Medwin and C.S. Clay (1998), *Fundamentals of Acoustical Oceanography*, Academic Press, Boston.
[28] P.M. Morse and K.U. Ingard (1968), *Theoretical Acoustics*, McGraw-Hill, NY.
[29] P.D. Mourad and D.R. Jackson (1993), "A model/data comparison for low frequency bottom backscatter", *J. Acoust. Soc. Am.,* **94**, pp.344-358.
[30] D.R. Palmer (1996), "Rayleigh scattering from nonspherical particles", *J. Acoust. Soc. Am.,* **99**(4), pp.1901-1912.
[31] D.B. Reeder and T.K. Stanton (2004), "Acoustic scattering by axisymmetric finite-length bodies: An extension of a two-dimensional conformal mapping method", *J. Acoust. Soc. Am.,* **116**(2), pp.729-746.
[32] M.D. Richardson, K.B. Briggs, A.H. Reed, W.C. Vaughan, M.A. Zimmer, L.D. Bibee and R.I Ray (2005), "Characterization of the environment during SAX04: Preliminary results", in, *Proc. Internat. Conf. "Underwater Acoustic Measurements: Technologies & Results"*, (Heraklion, Crete, Greece, 28th June – 1st July 2005).
[33] J. Sheng and A.E. Hay (1988), "An examination of the spherical scatterer approximation in aqueous suspensions of sand", *J. Acoust. Soc. Am.,* **83**(2), pp.598-610.
[34] T.K. Stanton (2000), "On acoustic scattering by a shell-covered seafloor", *J. Acoust. Soc. Am.,* **108**, pp.551-555.
[35] T.K. Stanton (1989), "Simple approximate formulas for backscattering of sound by spherical and elongated objects", *J. Acoust. Soc. Am.,* **86**(4), pp.1499-1510.
[36] P.D. Thorne, K.R. Waters and T.J. Brudner (1995), "Acoustic measurements of scattering by objects of irregular shape", *J. Acoust. Soc. Am.,* **97**(1), pp.242-251.
[37] P.D. Thorne and M.J. Buckingham (2004), "Measurements of scattering by suspensions of irregularly shaped sand particles and comparison with a single parameter modified sphere model", *J. Acoust. Soc. Am.,* **116**(5), pp.2876-2889.
[38] E.I. Thorsos, K.L. Williams, D. Tang and S.G. Kargl (2005), "SAX04 overview", in, *Boundary Influences in High Frequency Shallow Water Acoustics*, N.G. Pace and P. Blondel (Eds), University of Bath, UK, pp. 3-12.
[39] K.L. Williams (2001), "An effective density fluid model for acoustic propagation in sedments derived from Biot theory", *J. Acoust. Soc. Am,.* **110**, pp.2956-2963.
[40] K.L. Williams, D.R. Jackson, E.I. Thorsos, D. Tang and K.B. Briggs (2002), "Acoustic Backscattering Experiments in a Well Characterized Sand Sediment: Data/Model Comparisons Using Sediment Fluid and Biot Models", *J.Oceanic Engr.,* **27**, 376-387.
[41] K.L. Williams, M.D. Richardson, K.B. Briggs and D.R. Jackson (2001), "Scattering of high-frequency acoustic energy from discrete scatterers on the seafloor: Glass spheres and shells", in, *Proceedings of the Institute of Acoustics*, **23**: Part 2, pp. 369-374.
[42] K.L. Williams, E.I. Thorsos, D. Tang, D.R. Jackson and K.B. Briggs (2007), "Acoustic Backscattering from a Sand and a Sand/Mud Environment: Experiments and Data/Model Comparisons", *J.Oceanic Engr.,* **??**, ??-??, current issue.
[43] M. Zampolli, A. Tesei, G. Canepa, and O.A. Godin (2008), "Computing the far field scattered or radiated by objects inside layered fluid media using approximate Green's functions", *J. Acoust. Soc. Am.,* **123**(6), pp.4051-4058.

Other Technical Articles and Presentations
based on research funded by
Office of Naval Research Grant N00014-01-1-0087

A. Articles in refereed journals:

Sessarego, J.-P., A.N. Ivakin and D. Ferrand (2008), "Frequency Dependence of Phase Velocity, Group Velocity and Attenuation in Water-saturated Sand: Laboratory Experiments", *J.Oceanic Engr.*, **33**(4) (preprint).

Sessarego, J.-P., R. Guillermin and A.N. Ivakin (2008), "High Frequency Sound Reflection by Water-saturated Sediment Interfaces", *J.Oceanic Engr.*, **33**(4) (preprint).

Ivakin, A.N. and J.-P. Sessarego (2007), "High frequency broad band scattering from water-saturated granular sediments", *J. Acoust. Soc. Amer. Express Letters*, **122**(5), pp.EL165-EL171.

B. Proceedings of conferences

Ivakin, A.N. (2008), "Modeling of narrow-band normal-mode reverberation in shallow water", in, *International Symposium on Underwater Reverberation and Clutter*, P.L. Nielsen, C.H. Harrison, and J.-C. Le Gac (Eds), NATO Underwater Research Centre, Lerici, Italy, 9-12 September 2008, pp.55-62.

Ivakin, A.N. (2005), "High frequency scattering from sandy sediments: roughness vs discrete inclusions", in *Boundary Influences in High Frequency Shallow Water Acoustics*, N.G. Pace and P. Blondel (Eds), University of Bath, UK, 5-9 September 2005, pp.185-192.

Ivakin, A.N. (2004), "Scattering from discrete inclusions in marine sediments", in *Proc. Seventh European Conference on Underwater Acoustics (ECUA2004)*, Delft, The Netherlands, 5-8 July 2004, v1. pp.625-630.

Ivakin, A.N. and D.R. Jackson (2004), "Near-Bottom Bistatic Measurements Technique for Acoustic Classification of the Sediment and Buried Objects", in *Proc. The Application of Recent Advances in Underwater Detection and Survey Techniques to Underwater Archaeology*, Bodrum, Turkey, 3-7 May 2004, pp.183-190.

Frequency Dependence of Phase Speed, Group Speed, and Attenuation in Water-Saturated Sand: Laboratory Experiments

Jean-Pierre Sessarego, Anatoly N. Ivakin, and Didier Ferrand

Abstract—**Sound propagation in water-saturated sandy sediments was studied under controlled laboratory conditions in the 0.1–1.3-MHz frequency range. In the "low-frequency domain" (100–200 kHz), the results obtained were consistent with classical Biot theory, which predicts a positive phase-speed dispersion, but at higher frequencies ($f > 500$ kHz), a strong negative dispersion of the phase speed was observed, which is in apparent contradiction with the Biot theory predictions. In addition, the attenuation coefficient was found to increase nonlinearly with frequency from 0.5 to 1.3 MHz, whereas Biot theory predicted an almost linear increase of this coefficient. The unexpected behavior of the phase speed and the attenuation coefficient observed in these sandy sediments in the very high-frequency domain may be attributable to scattering by the sand particles, which becomes the predominant mechanism involved when the size of particles is comparable to the wavelength.**

Index Terms—**Attenuation, Biot model, dispersion, group speed, phase speed, sediment acoustics.**

I. Introduction

THE understanding of sound–seafloor interactions is a challenging issue that requires a thorough knowledge of the intrinsic properties of the sediments. In particular, the phase speed and the attenuation coefficient for the longitudinal waves in sandy sediments are parameters that need to be accurately determined because they are used as input data to most acoustic models for sea-bottom reflection and backscattering. These parameters have been measured in marine sand by many scientists during the last 20 years (see, e.g., [1]–[8]). The measurements have been performed under both laboratory and natural (at sea) conditions, but the frequency range studied has usually been relatively low (<300 kHz). At these low frequencies, sediment can be modeled as a porous medium, and corresponding theories (such as that developed by Biot and other related approaches, e.g., "effective density fluid model" developed by Williams [7]) effectively explain the main features of sound propagation in these media. One of the main assumptions adopted in "low-frequency effective medium" models is that the particle size in the medium is much smaller than the acoustic wavelength. At these low frequencies (<300 kHz), the p-wave in the sediment is known to show positive phase-speed dispersion. In this study, the negative dispersion of the phase speed was found to occur at higher frequencies (>500 kHz). This finding suggests that in the high-frequency domain, scattering by sand particles becomes the predominant mechanism responsible for the negative phase-speed dispersion.

Manuscript received September 28, 2006; revised April 7, 2008; accepted April 21, 2008.

Associate Editor: J. F. Lynch.

J.-P. Sessarego and D. Ferrand are with the The Laboratoire de Mécanique et d'Acoustique (LMA), Centre National de la Recherche Scientifique (CNRS), 13009 Marseille, France (e-mail: sessarego@lma.cnrs-mrs.fr; ferrand@lma.cnrs-mrs.fr).

A. N. Ivakin is with the Applied Physics Laboratory, University of Washington, Seattle, WA 98105 USA (e-mail: ivakin@apl.washington.edu).

Digital Object Identifier 10.1109/JOE.2008.927584

II. Preliminary Measurements

Before the acoustical experiments, preliminary measurements were carried out to determine the geotechnical parameters of the sand used in this study. These measurements were performed at The Laboratoire de Mécanique et d'Acoustique (LMA, Marseille, France) with a well-sorted sand having a mean grain diameter of 245 μm and a relatively narrow size distribution with $d(0.1) = 165$ μm and $d(0.9) = 364$ μm. The parameter $d(W)$ is defined such that W is the ratio of the volume (weight) of the grains with diameters less than $d(W)$ to the total volume of all the grains (dry weight of the sediment sample). To determine the wet density of the sediment, two different measurements were performed. First, the density was measured without any settling of the sediment and the value obtained was $\rho = 1977$ kg/m$^3 \pm 10$ kg/m^3. Second, the density was measured once the sediment had settled (after manual shaking). The value obtained in this case was $\rho = 2004$ kg/m$^3 \pm 10$ kg/m^3. The porosity, which is defined as the ratio of the sediment pore volume to its total volume was found to be $\beta = 0.365 \pm 0.02$. This result is consistent with many measurements on the porosity of sand with a similar granulometry.

The permeability and the tortuosity of the sediment were also measured at the LMA. Tortuosity was measured by placing electrical conductivity probes in a small box containing sand saturated with a saline solution (30‰). The ratio between the resistivity of the saline solution and the resistivity of the saturated sand gives the formation factor F, which appears in the equation $\alpha = F\beta$ relating the tortuosity α to the porosity β. The value of the tortuosity obtained with this technique was $\alpha = 1.31 \pm 0.13$. To measure the permeability, a similar method to that described by Darcy was used, which gave the following: $\kappa = 1.65\ 10^{-11}\text{m}^2 \pm 1.2\ 10^{-11}$. It can be seen here that the uncertainty is very high, but this is quite usual with such measurements; see, for example, [7] and [9].

To compute the phase speed and the attenuation of the longitudinal wave using the Biot model [10], [11], these experimental

TABLE I
PARAMETERS USED TO COMPUTE THE PHASE SPEED AND THE ATTENUATION WITH THE BIOT MODEL

	Input parameters for the Biot model
Bulk modulus of grains	$3.2\ 10^{10}$ Pa
Permeability of sediment	$*1.6510^{-11}$ m^2 +/-1.2 10^{-11}
Tortuosity of sediment	*1.31 +/-0.13
Porosity of sediment	*0.365+/-0.02
Viscosity of water	0.001 kg.m^{-1}.s^{-1}
Mass density of sand grains	2690 kg/m^3
Bulk modulus of water	$2.19\ 10^9$ Pa
Mass density of water	998 kg/m^3
Shear modulus of sediment frame Real part Imaginary part	 $2.92\ 10^7$Pa $-1.8\ 10^6$ Pa
Bulk modulus of sediment frame Real part Imaginary part	 $4.36\ 10^7$ Pa $-2.08\ 10^6$ Pa

The symbol (*) indicates the measured values.

TABLE II
CHARACTERISTICS OF THE "PANAMETRICS" TRANSDUCERS USED IN THE EXPERIMENTS

Central frequency and type of transducer	Frequency band with @-3dB	Diameter D	$2\lambda/D$	Far Field Distance $N=D^2/4\lambda$	Angular Beamwidth $2\theta_3$ @-3dB
250 kHz (V3536)	120 kHz	40 mm	0.3	6.5 cm	7.5°
500kHz (V301)	250 kHz	25 mm	0.24	5.2 cm	6°
1MHz (V302)	480 kHz	25 mm	0.12	10.5 cm	3°

data were introduced into the Biot equations and standard values available in the literature [7], [12] were used for the other model parameters, such as the grain density, the bulk and shear modulus of the sediment frame, the bulk modulus and mass density of the sand grains, and the viscosity and bulk modulus of water. All the parameters used as inputs in the Biot model are summarized in Table I.

In our acoustical measurements of the phase speed and the attenuation coefficient, we used wet and carefully degassed sand. Because the presence of small air bubbles in sands is known to considerably affect the results, the sand used in our experiments was immersed in fresh water for several months before the experiments and careful degassing operations were performed for several weeks. The acoustical measurements were then performed on the water-saturated sand mixture after pouring it into a rectangular box, making sure that the sand was never exposed to air.

To fully cover the wide frequency range chosen, three different "panametrics" transducers were used. Their characteristics (the bandwidth, the diameter of the piezoelectric ceramic, the far-field distance, and the beamwidth) are given in Table II. The frequency spectra of the transducers are shown in Figs. 1–3. It can be seen from these figures that each of the three transducers used covered a very broad frequency band. Their frequency spectra overlapped, and together, they covered the whole 0.1–1.5-MHz frequency range. It can be noted that the overlapping frequencies were used to check the consistency of the phase-speed, group-speed, and attenuation measurements obtained with the three transducers.

III. SOUND-SPEED MEASUREMENTS

Fig. 4 gives a schematic diagram of the experimental setup. This setup consisted of a rectangular PVC box***[AU: Please define PVC]*** ($l = 15$ cm, $L = 20$ cm, $H = 15$ cm) in which ten transducers (four working at 500 kHz, four at 1 MHz, and two at 250 kHz) were fixed so that they were perfectly aligned face to face in pairs. The acoustic method used to measure the distances between transducers as accurately as possible will be described below.

Based on the far-field distances given in Table II, it can be seen in Table III that far-field conditions were fully satisfied in the case of the two lower frequency sources, whereas they were only partly fulfilled in that of the 1-MHz source. This situation did not affect the phase-speed measurements. It could only introduce minor errors in the attenuation measurements, but the values measured at 1 MHz were so high that this effect was taken to be negligible.

Transmission experiments were carried out separately in fresh water and sand. The transmission in fresh water was used to measure the distance between the transducers. For this measurement, it was assumed that the phase speed can be exactly determined as long as the water temperature is known and also that sound absorption in fresh water can be neglected. It is worth noting here that the sound attenuation in fresh water

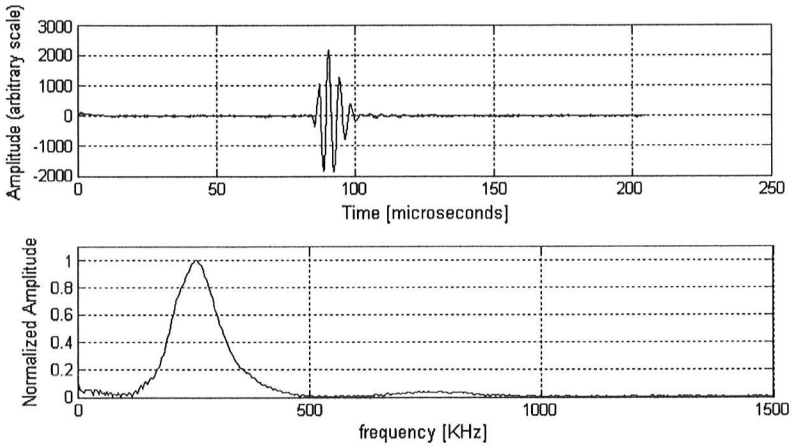

Fig. 1. Time response of the 250-kHz transducer and the corresponding spectrum.

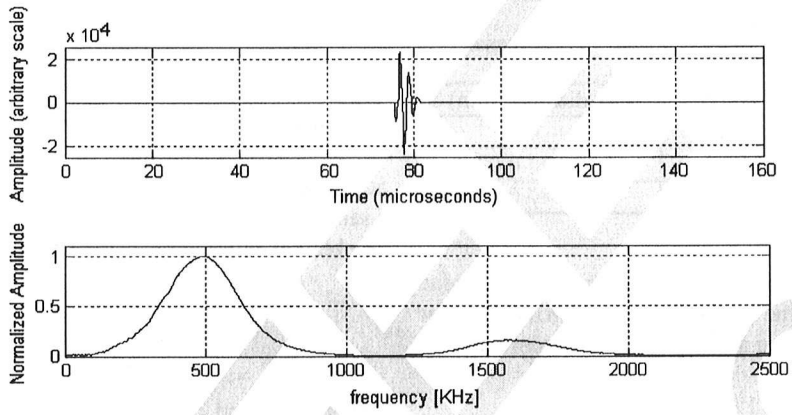

Fig. 2. Time response of the 500-kHz transducer and the corresponding spectrum.

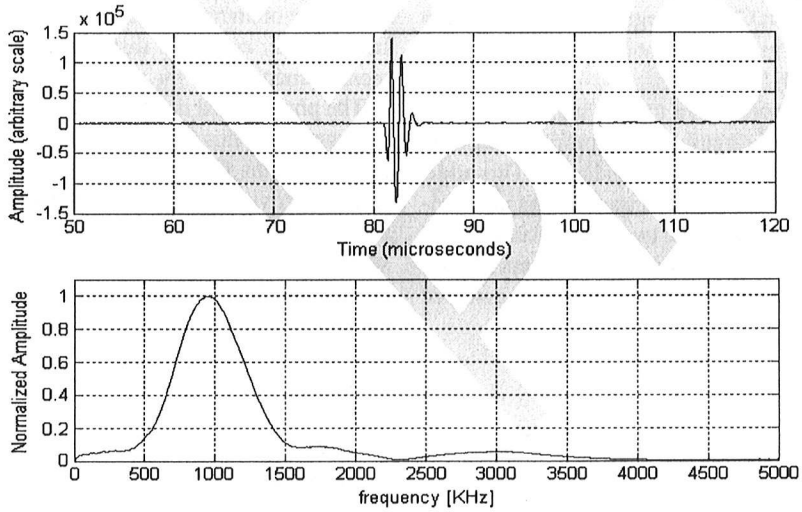

Fig. 3. Time response of the 1-MHz transducer and the corresponding spectrum.

is about 0.1 dB/m at 1 MHz, which is negligible compared with the sound attenuation in sediment (>100 dB/m at 1 MHz).

After immersing the PVC box in a large water tank, an acoustic method was used to measure the distances between the transducers. This method consisted first in measuring the delay between the transmitted and received short pulses in the transmitting mode. The distance d between the transducers was then calculated using the simple equation: $d = C_w\tau$, where τ is the delay between the transmitted impulse and received signal, and C_w is the sound speed in water. In the case of sound propagation in water, there is no dispersion and the beginning of the signal received can be measured with good accuracy, which

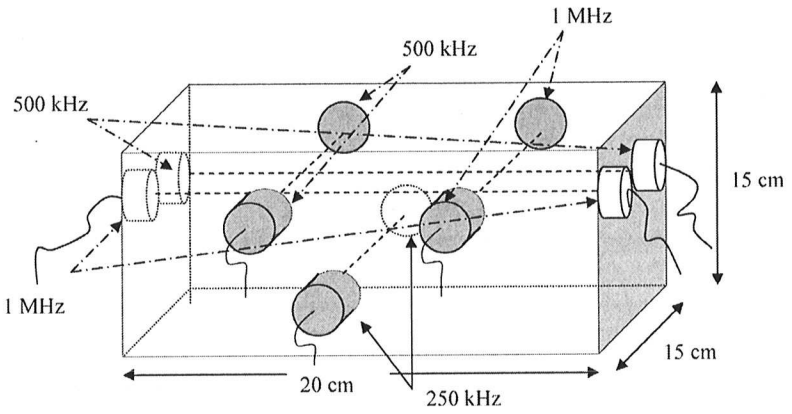

Fig. 4. Schematic diagram of the box equipped with transducers.

TABLE III
DISTANCES BETWEEN THE TRANSDUCERS DURING MEASUREMENTS

Transducers	Min distance (cm)	Max distance (cm)
250 kHz	12.78 +/- 0.02	-------
500 kHz	10.89 +/-0.02	15.88 +/-0.02
1 MHz	11.76 +/-0.02	15.88 +/-0.02

gives a satisfactory estimate of the propagation time. The value of C_w was obtained using the relation given by Grosso [14] for the sound speed in fresh water as a function of temperature

$$C_w(T) = 1402.388 + 5.03711T - 0.0580852T^2 + 3.342\ 10^{-4}T^3 - 1.478\ 10^{-6}T^4 + 3.15\ 10^{-9}T^5 \quad (1)$$

where T is the temperature in Celsius degrees. This relation is valid for $0° < T < 95°$. It gives the sound speed in the water with an uncertainty of ± 0.015 m/s.

Some minor corrections were made to take into account the transition time in the electrical circuit and the propagation time through the protection membrane of the transducers. This additional delay was measured by bringing the transducers into contact (using Panametrics gel between the two transducer faces to ensure perfect coupling). With each pair of transducers in contact, the delay τ_c was determined and used to correct the distance measurements as follows:

$$d = C_w(\tau - \tau_c). \quad (2)$$

Because the error in the time measurements was less than 0.15 μs, this method gives an acoustical estimate of the distance between the transducers with an accuracy of more than 0.2 mm. It is worth noting here that the overall accuracy of the phase-speed measurements in the sand was mainly limited by the lack of precision in the distance measurements [12]. The results obtained are summarized in Table III.

During the calibration process, the amplitudes $A_{w1}(f)$ and $A_{w2}(f)$ of the signals transmitted over distances d_1 and d_2 in water were also measured as a function of the frequency. When the calibration measurements in fresh water were completed, the PVC box was filled with water-saturated sand.

A. Phase-Speed Measurements

1) Broadband Measurements: In this wideband experiment, very short pulses were used in the transmission mode. The electric signals sent to the transducer were very short pulses of high voltage (>300 V) delivered by a "panametrics" pulser/receiver 5055PR. The corresponding acoustical signals were recorded on a sampling oscilloscope and transmitted to a PC for processing. To obtain the phase speed, the following relation was used [15]:

$$C_{ph}(\nu) = \frac{2\pi\nu d}{2\pi\nu\tau + \arg\left(\dfrac{\text{imag}\,(S_{\text{water}}(\nu))}{\text{imag}\,(S_{\text{sand}}(\nu))}\right)} \quad (3)$$

where S_{sand} and S_{water} are the Fourier transform of the signal received after propagating through sand and water, respectively, d is the distance between the transmitter and the receiver, and τ is the time of arrival of the signal, which has been defined above. In this case, only one distance was required for phase-speed measurements.

The phase speed is given in Fig. 5 as a function of frequency. The curves in this figure give the results of measurements obtained with the three wideband transducers. In the region where the curves overlap, reasonable agreement can be seen to exist between the data obtained with the three transducers. The phase-speed measurement error was about $+/-10$ m/s. The most important result obtained here is the noticeable decrease in the phase speed observed in the 0.5–1.3-MHz frequency range. In this experiment, the temperature of water was 20.9 °C giving a sound velocity ***[AU: sound speed?]*** of 1485 m/s.

2) Tone Bursts: It was then proposed to confirm the results obtained in the above wideband measurements using narrower band signals. For this purpose, another set of measurements were performed using tone bursts with various frequencies. By measuring the time of arrival of the signals transmitted in sand along two distances d_1 and d_2, the phase speed was obtained as a function of the frequency. In this case, the electrical signal delivered to the transducer was a sinusoidal wave train of 10, 15, or 20 periods depending on the frequency used. At "low frequencies" (<200 kHz), ten periods were used for the sinusoidal signal, while at "high frequencies" (>500 kHz), the number of periods was set at 20. The working frequency was increased in 20-kHz increments to cover the whole frequency range of interest. All

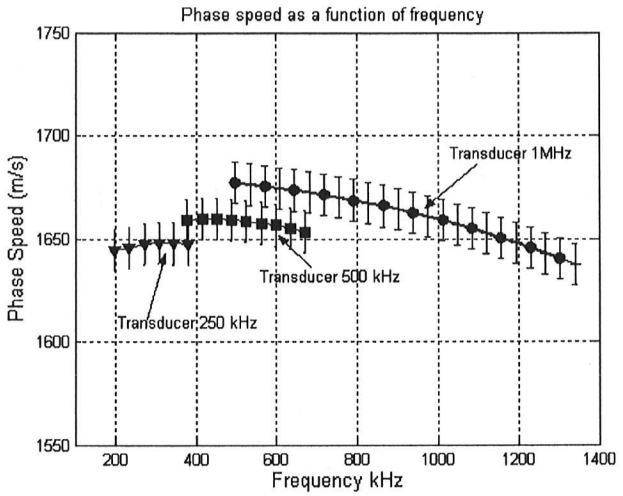

Fig. 5. Phase-speed measurements in sand.

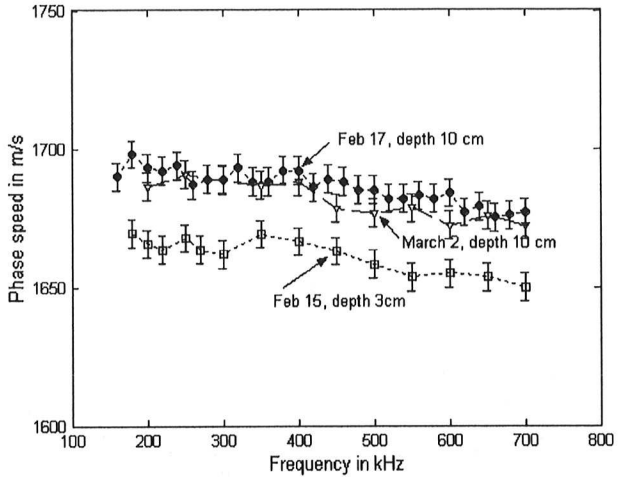

Fig. 6. Phase-speed measurements obtained at two different depths on different days (500-kHz panametrics transducer).

the signals transmitted over the two distances d_1 and d_2 were sent to an analog-to-digital converter before been recorded on a PC. To estimate the phase speed, the classical zero-crossing method of measurement was used and the sound speed was then obtained from the relation

$$C_{ph} = \frac{d_2 - d_1}{\tau_2 - \tau_1} \tag{4}$$

where τ_1 and τ_2 are the delays associated with a given number of zero crossings for distances d_1 and d_2. It was checked, for example, that with high-frequency signals, the tenth zero crossing was associated with a portion of the signal where the instantaneous frequency was constant. The velocity measurement ***[AU: Can "velocity" be changed to "speed" throughout?]***error obtained using this method was estimated to be approximately ± 5 m/s.

Curves giving the phase speed as a function of the frequency are shown in Fig. 6 in the 180–700–kHz frequency range. Measurements were performed on various days at various depths to determine whether the settlement of the sediment had any effects. The data given in Fig. 6 show that at the same transducer-embedding depth (10 cm), the results obtained before and after a period of two weeks were very similar (February 17 to March 2). It can also be seen that the phase speed measured at a depth of 3 cm was practically parallel to that obtained at a depth of 10 cm. This finding proves that the same dispersion law applied at two different depths. In addition, the phase speed at 3 cm below the sand–water interface was 20 m/s lower than that measured at a depth of 10 cm. This difference might be attributable to the fact that the near-surface sediment was more saturated by water than the deeper layer, and that there was probably a sound-speed gradient in the sand bottom. It was also checked that from February 15 to March 6, the temperature measured both in the water tank and in the sediment was constant and equal to 22 °C giving a sound speed of 1488.3 m/s in the water.

The results obtained with the 500- and 250-kHz transducers were compared in the same way (see Fig. 7). Although the measurements were performed on different days, the values obtained with the two transducers were consistent. Positive

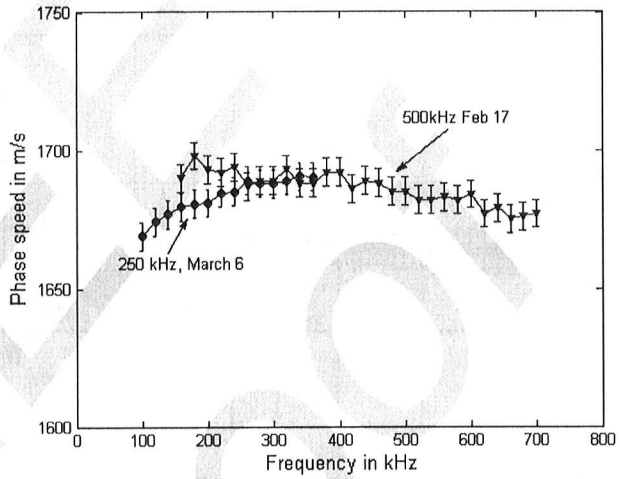

Fig. 7. Phase-speed measurements (250 and 500 kHz).

phase-speed dispersion can be observed in the low-frequency domain (100–300 kHz), which is in agreement with the Biot predictions, but at higher frequencies, negative phase-speed dispersion begins to occur.

To confirm the decrease in the phase speed observed here, another set of measurements were performed at higher frequencies (0.5–1.2 MHz). These measurements were carried out using long sinusoidal pulses (20 periods). The results are given in Fig. 8 and compared with those obtained with the 500-kHz transducer. Both curves show the occurrence of a similar decrease in the phase speed with the frequency. Some differences observed between the results obtained with the two different transducers (at the overlap frequencies) are within the range of uncertainty defined above. It is worth noting that the negative dispersion behavior of the phase speed at high frequencies (>400 kHz) was also observed by Moussatov *et al.* [16] in the case of sediments and glass beads of about the same sizes.

The measurements were performed with the transducers placed 3 cm below the water–sand interface; during these measurements, the temperature in both the water tank and the sand box was around 17.5 °C.

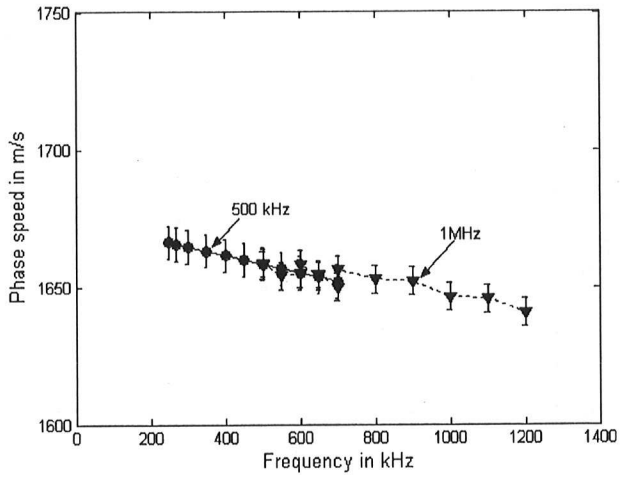

Fig. 8. Phase-speed measurements (500 and 1 MHz).

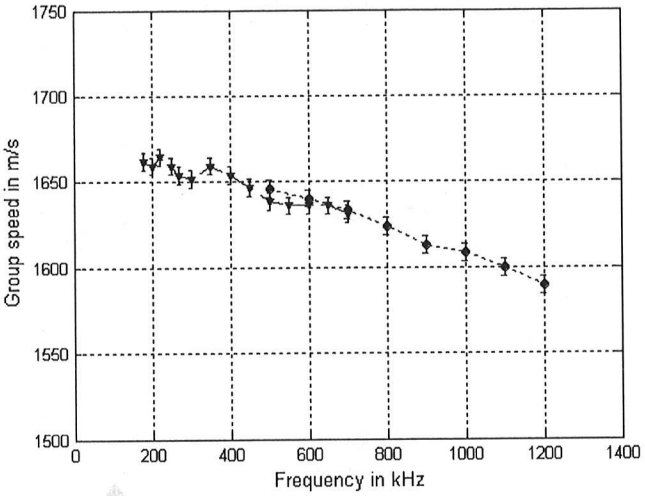

Fig. 10. Group speed as a function of the frequency.

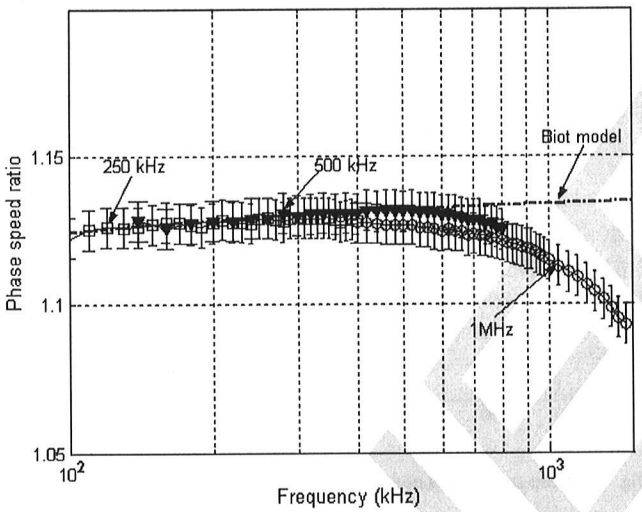

Fig. 9. Phase-speed measurements as a function of the frequency (comparison with Biot model [10], [11]).

To compare the experimental data with model predictions, it has often been proposed to normalize the sound speed in sediment with respect to the sound speed in water at the time of the measurements. The results obtained in the 0.1–1.5-MHz frequency range are given in Fig. 9. In this figure, the phase speed computed using the Biot model [10], [11] for water-saturated sand is given by the dashed line. The values of the parameters used with the Biot model are given in Table I.

The following comments can be made: At high frequencies (>500 kHz), the results of our experiments show that the phase speed no longer obeys the Biot model. The phase speed was found to decrease strongly as the frequency increased. This decrease was of the order of 40 m/s in the 0.5–1-MHz frequency range. This is in apparent contradiction with the Biot model predictions, but it can be noted that at these high frequencies, the size of the sand particles becomes comparable to that of the wavelength, and it is, therefore, not surprising that some scattering processes begin to occur.

B. Group-Speed Measurements

We also measured the group speed by making a correlation between the signals received in the sand at distances d_1 and d_2. The maximum value of the correlation function gives the time of arrival of the energy, from which the group speed can be calculated by using the relation

$$C_{gr} = \frac{d_2 - d_1}{\tau} \tag{5}$$

where τ is the delay obtained from the position of the maximum value of the correlation function. Fig. 10 gives the group speed as a function of frequency from 0.2 to 1.2 MHz. The group speed curve shows a strong dispersion, which is even more pronounced than in the case of the phase speed. The mean rate of decrease in the group speed was 60 m/s between frequencies of 0.4 and 1.2 MHz.

The phase speed and the group speed are shown in Fig. 11 on the same scale. It can be seen from this figure that the group speed was always lower than the phase speed. The higher the frequency, the greater is the difference between the two curves. This result can be explained using the classical relationship between the group speed and the phase speed

$$C_{gr} = C_{ph} + k\frac{dC_{ph}}{dk} \tag{6}$$

where k is the wave number.

IV. Attenuation Measurements

To measure the sound attenuation in the sediment, the same arrangement as that described above for measuring the phase speed was used. The amplitude of the wideband signals transmitted in both water and sand was measured. A Fourier transform was applied to the signals received to determine the amplitude spectrum in a very wide frequency range. The attenuation in the sediment was then determined as a function of the frequency from the ratio between the magnitude of the Fourier transforms obtained in the case of sediment and water. It was again assumed that there was no attenuation in fresh water (the

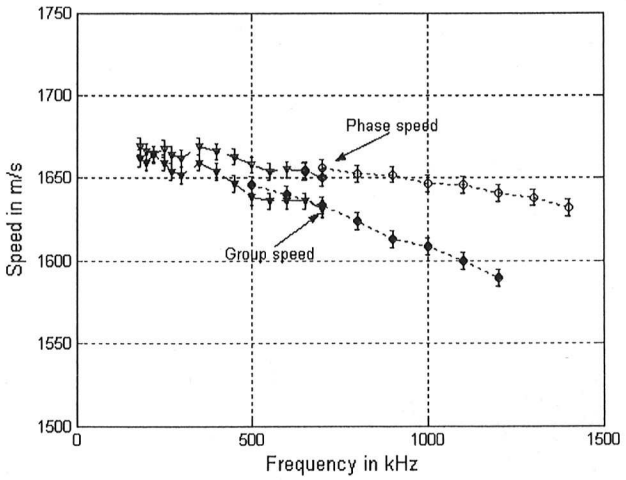

Fig. 11. Comparison between the phase speed and the group speed in the 0.2–1.2-MHz frequency band.

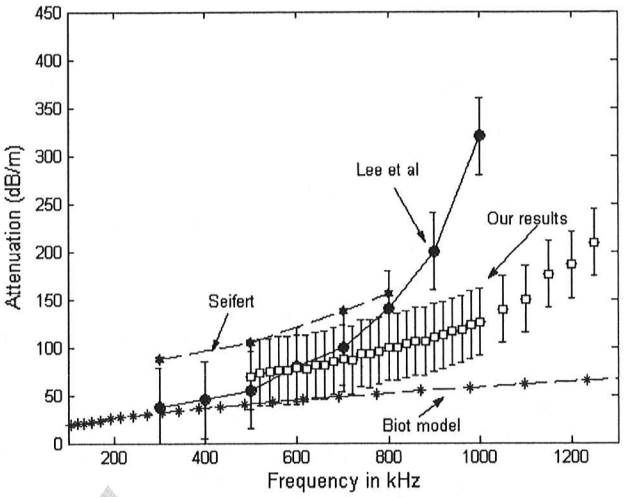

Fig. 12. Sound attenuation measurements versus frequency. Comparison with the Biot model computed in the case of fresh water and with data by Seifert [18] and Lee *et al.* [19]. (The stars correspond to the scattering attenuation obtained by Seifert and the circles to data by Lee *et al.*)

reference medium). This method was used previously by Buckingham [17]. The attenuation is given by the following relation:

$$\alpha(\nu) = 8.686 \frac{1}{d} \mathrm{Log}_{10} \left(\frac{N_w(\nu)}{N_s(\nu)} \right) \tag{7}$$

where

$$N_w(\nu) = \frac{A_{w1}(\nu)}{A_{w2}(\nu)}, \quad N_s(\nu) = \frac{A_{s1}(\nu)}{A_{s2}(\nu)}.$$

$A_{w1}(\nu)$, $A_{w2}(\nu)$, $A_{s1}(\nu)$, and $A_{s2}(\nu)$ are the amplitude spectra of the wideband signals received in water and sand at distances d_1 and d_2. The attenuation coefficient α is given in decibels per unit distance.

The results of the measurements obtained with the 1-MHz transducer are shown in Fig. 12. The maximum frequency used to calculate (7) was 1.3 MHz because at higher frequencies, no signals could be measured, because the attenuation was too strong. In this figure, each data point is the mean value of approximately 15 measurements and the error bars denote the standard deviations of these measurements.

The results of the attenuation obtained using the Biot model are also given in Fig. 12. As was to be expected, this model does not accurately describe the attenuation in the very high frequency range. We have also added some results obtained by Seifert *et al.* [18] on sand particles with a mean diameter of 230μm. Our measurements gave a lower attenuation, but the size distribution of the sand particles was not exactly the same in both studies. In addition, while correcting this manuscript, we received the paper by Lee *et al.* [19] and we have also added these authors' results to Fig. 12. The latter authors obtained similar results to those obtained here, but Lee *et al.* observed higher sound attenuation levels, probably because the mean particle diameter of the sand they used was 425 μm, which is much larger than that of our sand (245 μm). This difference suggests that the attenuation may depend not only on the frequency but also on the particle size. From all these results, it can be concluded that at high frequencies (>500 kHz), the attenuation coefficient increases nonlinearly with frequency (the attenuation seems to be proportional to f^2), which is probably due to both classical viscous losses (Biot theory) and scattering by sand particles. Ohkawa reached similar conclusions [20]. He mentioned that the scattering effect is the main process involved at frequencies above 200 kHz in sand with a mean particle diameter of 230 μm.

V. Conclusion

It can be concluded that although the Biot model can be used to predict the phase speed and the attenuation in the low-frequency domain in the case of a medium sand, this method is not appropriate for dealing with the high-frequency part of the spectrum (>500 kHz) where the sound scattering by sand particles becomes the main contribution. At the higher frequencies tested, a strong decrease in both phase speed and group speed and a strong increase in the attenuation were observed. Upon comparing our results with those of Lee *et al.* [19], it is suggested that the scattering by sand particles contributes to generating both attenuation and sound-speed "anomalies." These scattering effects can be very strong and can considerably affect sound reflection and backscattering by sediments.

Finally, it can be mentioned that for larger sand particles (coarse sand, for example) scattering can occur at lower frequencies and fall, in particular, to the frequency range of most high-resolution sonars used for sea-bottom imaging.

REFERENCES

[1] A. C. Kibblewhite, "Attenuation of sound in marine sediments: A review with emphasis on the new low frequency data," *J. Acoust. Soc. Amer.*, vol. 86, no. 2, pp. 716–738, 1989.

[2] D. J. Wingham, "The dispersion of sound in sediments," *J. Acoust. Soc. Amer.*, vol. 78, no. 5, pp. 1757–1760, 1985.

[3] L. D. Hampton, "Acoustic properties of sediments," *J. Acoust. Soc. Amer.*, vol. 42, no. 4, pp. 882–890, 1967.

[4] A. Maguer, E. Bovio, and W. L. J. Fox, "In situ estimation of sediment sound speed and critical angle," *J. Acoust. Soc. Amer.*, vol. 108, no. 3, pp. 987–996, 2000.

[5] R. D. Stoll, "Velocity dispersion in water-saturated granular sediment," *J. Acoust. Soc. Amer.*, vol. 111, no. 2, pp. 785–793, 2002.

[6] E. L. Hamilton and R. T. Bachman, "Sound velocity and related properties of marine sediments," *J. Acoust. Soc. Amer*, vol. 72, pp. 1891–1904, 1982.

[7] K. L. Williams, D. R. Jackson, E. I. Thorsos, D. Tang, and S. G. Schock, "Comparison of sound speed and attenuation measured in a sandy sediment to predictions based on the biot theory of porous media," *IEEE J. Ocean. Eng.*, vol. 27, no. 3, pp. 413–428, Jul. 2002.

[8] N. P. Chotiros and M. J. Isakson, "A broadband model of sandy ocean sediments: Biot-Stoll with contact squirt flow and shear drag," *J. Acoust. Soc. Amer.*, vol. 116, pp. 2011–2022, 2004.

[9] R. H. Bennett, M. H. Hulbert, C. Curry, H. P. Johnson, M. Hutnak, and K. J. Curry, "In situ permeameter probe for coastal marine sediments," *IEEE J. Ocean. Eng.*, vol. 27, no. 3, pp. 571–580, Jul. 2002.

[10] M. A. Biot, "Theory of propagation of elastic waves in a fluid-saturated porous solid. I. Low frequency range," *J. Acoust. Soc. Amer.*, vol. 28, no. 2, pp. 168–178, 1956.

[11] M. A. Biot, "Theory of propagation of elastic waves in a fluid-saturated porous solid. II. Higher frequency range," *J. Acoust. Soc. Amer.*, vol. 28, no. 2, pp. 179–191, 1956.

[12] A. H. Reed, K. B. Briggs, and D. L. Lavoie, "Porometric properties of sand from SAX99 derived from traditional measurements and image analysis/network modeling," *IEEE J. Ocean. Eng.*, vol. 27, no. 3, pp. 581–592, Jul. 2002.

[13] R. D. Stoll, "Acoustic waves in saturated sediments," in *Physics of Sound in Marine Sediments*, L. Hampton, Ed. New York: Plenum Press, 1974, pp. 19–40.

[14] V. A. Del Grosso and C. W. Mader, "Speed of sound in pure water," *J. Acoust. Soc. Amer.*, vol. 52, pp. 1442–1446, 1972.

[15] P. He, "Measurement of acoustic dispersion using both transmitted and reflected pulses," *J. Acoust. Soc. Amer.*, vol. 107, no. 2, pp. 801–807, 2000.

[16] ***[AU: Please spell out full name of the periodical and provide volume]*** A. Moussatov, L. Guillon, C. Ayrault, and B. Castagnede, "Experimental study of the dispersion of ultrasonic waves in sandy sediments," *C.R. Acad. Sci. Paris, II, b*, pp. 433–439, 1998.

[17] M. J. Buckingham and M. D. Richardson, "On tone-burst measurements of sound speed and attenuation in sandy marine sediments," *IEEE J. Ocean. Eng.*, vol. 27, no. 3, pp. 429–448, Jul. 2002.

[18] P. K. Seifert, B. Kaelin, and L. R. Johnson, "Effect on ultrasonic signals of viscous pore fluids in unconsolidated sand," *J. Acoust. Soc. Amer.*, vol. 106, no. 6, pp. 3089–3094, 1999.

[19] K. Lee, V. F. Humphrey, B.-N. Kim, and S. W. Yoon, "Frequency dependencies of phase velocity and attenuation coefficient in a water-saturated sandy sediment from 0.3 MHZ to 1.0 MHz," *J. Acoust. Soc. Amer.*, vol. 121, no. 5, pp. 2553–2558, 2007.

[20] K. Ohkawa, "Confirmation of the Biot theory for water-saturated sands at high frequencies and effects of scattering on the attenuation of sound waves (L)," *J. Acoust. Soc. Amer.*, vol. 119, no. 2, pp. 709–711, Feb. 2006.

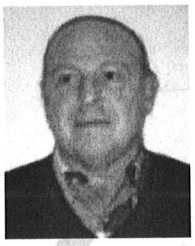

Jean-Pierre Sessarego received the Ph.D. degree ***[AU: In what field of study?]*** from the Université de Provence, Aix-Marseille I, France, in 1982.

He has been a Researcher at Centre National de la Recherche Scientifique (CNRS), Marseille, France. His primary focus was in shallow-water propagation and in scattering by elastic objects for target recognition. Currently, he is a Senior Scientist and Head of the Underwater Acoustic Group at the Laboratoire de Mécanique et d'Acoustique (LMA), CNRS, where he is now working on propagation through sediments. He is also Professor at the Ecole Centrale Marseille, France.

Dr. Sessarego is a member of the French Acoustical Society.

Anatoly N. Ivakin, photograph and biography not available at the time of publication.

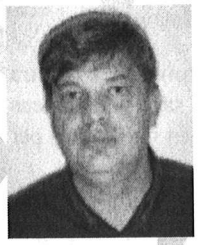

Didier Ferrand ***[AU: Please provide better quality photo]*** received the Supelec engineer degree in control and systems engineering in 1988. ***[AU: From what university; please provide city as well]***

From 1989 to 1991, he was Engineer at Aerospatiale Toulouse developing real-time control for the AIRBUS A320 braking system. In 1991, he moved to Centre National de la Recherche Scientifique (CNRS), Marseille, France, to develop telescope control systems (THEMIS, Very Large Telescope) and then HERSCHEL space telescope infrared interferometer scan electronics. In 2006, he joined the Underwater Acoustic Group at the Laboratoire de Mécanique et d'Acoustique (LMA), CNRS.

High-Frequency Sound Reflection by Water-Saturated Sediment Interfaces

Jean-Pierre Sessarego, R. Guillermin, and Anatoly N. Ivakin

***Abstract*—Sound reflection by water-saturated sands and glass beads with a flattened surface was studied under controlled laboratory conditions in a wide frequency range, from 200 kHz to 7 MHz. In the "low-frequency" domain and in the case of medium sand, the reflected sound level was found to be in good agreement with both classical sonar measurements and classical theories of reflection developed for fluid-porous media (this reflected level is practically independent of the frequency); as the frequency increases, a large decrease in the reflected level occurs, possibly due to incoherent scattering. In the very high-frequency regime (>3 MHz), the sound level measured was more than 20 dB below the classical level, and it remained constant at higher frequencies. Similar experiments were carried out with coarse sand to study the effect of grain size on the reflection loss. The same behavior with only a frequency shift was observed. These effects were confirmed by repeating the experiments with glass beads of two sizes. The anomalies observed in the reflected levels measured seem to be directly connected to the ratio between the grain size and the wavelength. One of the main conclusions reached in this study was that for very coarse sand and gravels, the effects of the granular structure of the bottom should not be neglected, even at the usual sonar frequencies.**

***Index Terms*—Granular media, reflection loss, scattering by grains, sediment acoustics, sound reflection.**

I. Introduction

MEASUREMENTS of sound reflection from sandy bottoms have been carried out for years in a relatively low-frequency regime (ranging between a few kilohertz to few hundreds of kilohertz) by many authors [1]–[3] and [4]. This interest in the low-frequency domain is mainly because most sonars work at relatively low frequencies (<300 kHz). Therefore, it has often been assumed that sound reflection is affected only by the surface roughness and, in the case of very low-frequency sonars, by volume inhomogeneities; the various models which have been developed up to now for acoustical backscattering, therefore, do not include scattering by sand grains because it is generally assumed that at these usual sonar frequencies, the grain size does not affect the sound reflection levels. The apparent lack of marine applications in the high-frequency domain may explain why very few sound reflection measurements have been carried out above 500 kHz. However, some interesting results have been obtained under laboratory conditions by Nolle [5] and Williams [6], and more recently, by Greenlaw *et al.* [7] and Ivakin *et al.* [8]–[10].

TABLE I
Statistical Characteristics of Sands and Glass Beads

	Medium Sand	Coarse Sand	Small Beads	Large Beads
Mean grain size	245 μm d(0.1)=165 μm d(0.9)=364 μm	1.50 mm d(0.1)=1.3 mm d(0.9)=2.6 mm	200 μm	3 mm

To better understand the complex mechanisms involved in sea bottom reflection, experiments were conducted at Laboratoire de Mécanique et d'Acoustique (LMA), Centre National de la Recherche Scientifique (CNRS, Marseille, France) with water-saturated sands and glass beads, where all the experimental parameters were perfectly controlled. The aim of this study was to measure the reflection loss as a function of the frequency over a very wide frequency range, from 200 kHz to 7 MHz, to see whether a transition zone between continuous and granular behavior could be detected in the reflection levels measured. Four wideband Panametrics transducers were used to cover this very wide frequency range.

II. The Experiment

Because the main goal of this study was to determine the reflection loss for different types of "sediments" as a function of the frequency, several experiments were performed on two types of sand (medium and coarse sand) and two types of glass beads (small and large beads). The granulometry of the sand and beads is given in Table I. In the case of medium sand, the size distribution of the particles was found to be Gaussian, and the mean diameter was 245 μm (Table I). This measurement was performed with a Mastersizer 2000. The results are given in Fig. 1.

In the case of coarse sand, the size distribution of a series of 244 particles was measured manually with a microscope. Fig. 2 is a photo of the particles analyzed: the ruler at the top of the figure gives a good idea of the particle sizes. As can be seen from the histogram, the size distribution was not exactly Gaussian, but the mean diameter of the particles was found to be 1.5 mm.

Reflection coefficient measurements were alternately performed on sand and beads of about the same mean size (Table I) to determine whether a monosize distribution of beads might explain the main features obtained with a Gaussian distribution of sand particles. The results of this comparison should be extremely useful for future modeling purposes.

Manuscript received March 30, 2007; revised December 18, 2007; accepted July 07, 2008.

Associate Editor: J. F. Lynch.

J.-P. Sessarego and R. Guillermin are with the Laboratoire de Mécanique et d'Acoustique (LMA), Centre National de la Recherche Scientifique (CNRS), 13009 Marseille, France (e-mail: sessarego@lma.cnrs-mrs.fr; guillermin@lma.cnrs-mrs.fr).

A. N. Ivakin is with the Applied Physics Laboratory, University of Washington, Seattle, WA 98105 USA (e-mail: ivakin@apl.washington.edu).

Digital Object Identifier 10.1109/JOE.2008.2002457

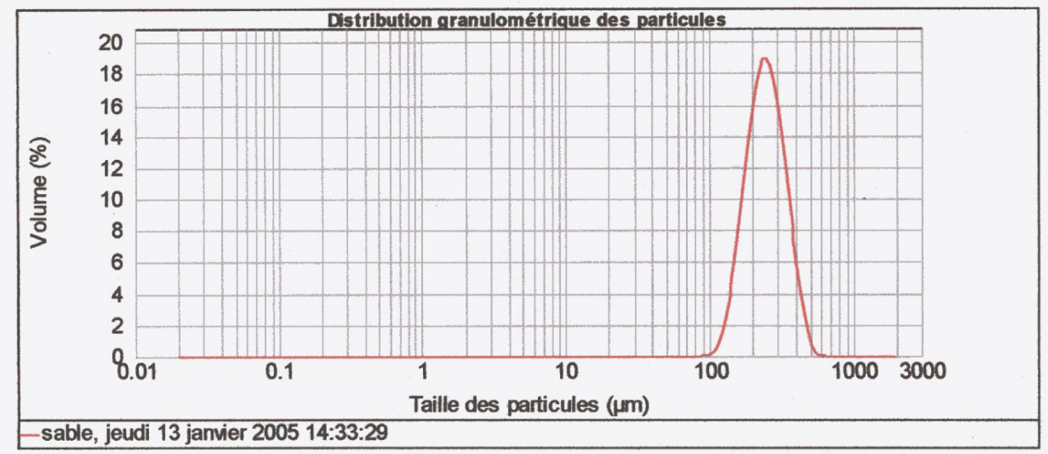

Fig. 1. Histogram of grain size in the case of medium sand (particle size is expressed in microns). ***[AU: Please provide new figure with English description]***

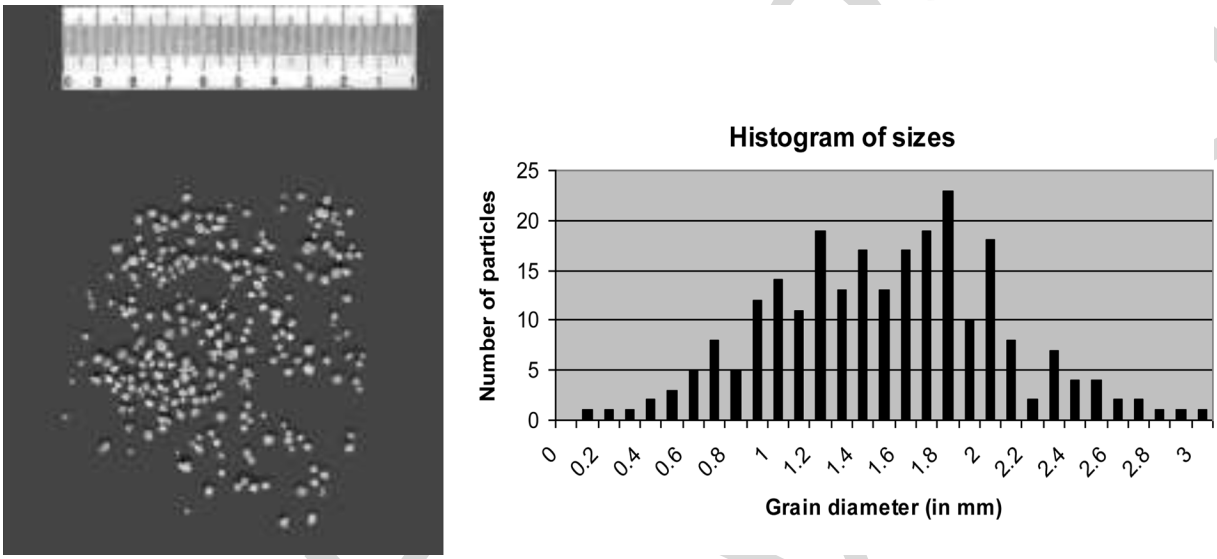

Fig. 2. Photograph of coarse sand particles and corresponding size distribution.

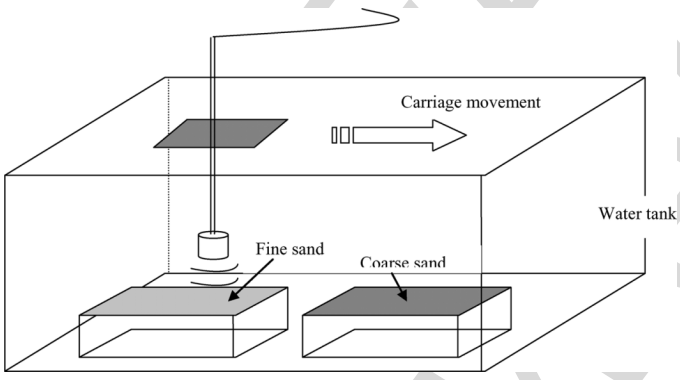

Fig. 3. Experimental arrangement.

In Table I, the parameter $\mathrm{d}(\mathrm{w})$ is defined so that w is the ratio between the volume (weight) of the grains with diameters less than $\mathrm{d}(\mathrm{w})$ and the total volume of all the grains (dry weight of the sediment sample).

Sand and glass beads were placed in four different plastic boxes of the same size: 24 cm $\times$ 18 cm $\times$ 10 cm. These boxes were then immersed in a water tank (2 m long, 1.2 m wide, and 1 m deep); see Fig. 3. The water had been in the tank for several months to make sure that it contained no bubbles. In addition, careful degassing operations were performed in both the sand and glass bead boxes to prevent the presence of bubbles in the medium. After these degassing operations, both the sand and bead surfaces were carefully flattened to remove any undesirable ripples on the water/sediment and water/bead interfaces. Any surface roughness could, therefore, be said to be due solely to the granular properties of the medium.

Four Panametrics transducers were used to cover the frequency range from 200 kHz to 7 MHz. These transducers were selected so that their spectra overlapped over a wide frequency band. This frequency overlapping was subsequently used to confirm the validity of the measurements by comparing the results obtained with various transducers. The physical characteristics of these transducers are given in Table II.

TABLE II
PHYSICAL CHARACTERISTICS OF THE PANAMETRICS TRANSDUCERS

Transducers	Bandwidth at -3 dB	Far-field distance	Beam width	Diameter D
T1 (250 kHz)	120 kHz	6.5 cm	7.5°	40 mm
T2 (500 kHz)	250 kHz	5.2 cm	6°	25 mm
T3 (2.25 MHz)	1 MHz	7 cm	2.5°	13 mm
T4 (5 MHz)	2 MHz	14 cm	1.2°	13 mm

This large frequency range was chosen so that with the various sands and beads, the dimensionless parameter ka would also cover a very large range, 10^{-1} to 40, where k is the wave number and a denotes the radius of the beads and the mean radius of the sand particles.

Before the beginning of the experiments, the transducers were calibrated using the air/water interface as a perfect reflector. The distance between transducer and air/water interface was about 25 cm in all the calibration experiments except for that in which the 2.25-MHz transducer was used, where for the sake of convenience, the distance was set at only 16 cm. It is important to stress that these distances were chosen to satisfy transducer far-field conditions (Table II).

As an example, Fig. 4 gives the time signal reflected by the air/water interface with transducers T1, T2, T3, and T4. This figure also gives the corresponding spectra, which show that the frequency bands of the various transducers overlapped considerably.

A. Experiments on Sand

The reflection coefficient of a sand bottom was measured at normal incidence and at the same distance as that chosen for the calibration at the air/water interface. In this case, we did not have to apply any divergence correction to the signal amplitude. The backscattered echoes were recorded with the transducers in various horizontal positions. These transducers were mounted on a carriage moved by stepping motors (Fig. 3). The increment chosen for the displacement was 0.5 cm, which was much smaller than the footprint of the beam on the sand bottom. The footprint size of the beam depends on the size of the transducer, the working frequency, and the distance from the transducer to the reflecting surface. In our experiments, the footprint diameter was about 2 cm with transducers T3 and T4 and about 7 cm with transducers T1 and T2. Examples of echograms are shown in Fig. 5 in the case of medium and coarse sand. In this experiment, the two boxes filled with medium and coarse sand were successively ensonified with transducers T1, T2, T3, and T4. The 115 traces shown in Fig. 5 correspond to a total transducer displacement of 57 cm. In the lower part of the figure, the signal reflected by the medium sand is shown, and in the upper part, the signal reflected by the coarse sand is shown. The effects of the walls of the boxes (ripples in the lower part of the figure) are also visible. These spurious echoes were due to the diffraction of the signal by the plastic edges of the boxes. This was checked by making simple ray travel time calculations. This effect was particularly pronounced with low-frequency transducers because of their large aperture. It can also be seen that with the medium sand at the lowest frequencies (transducers T1

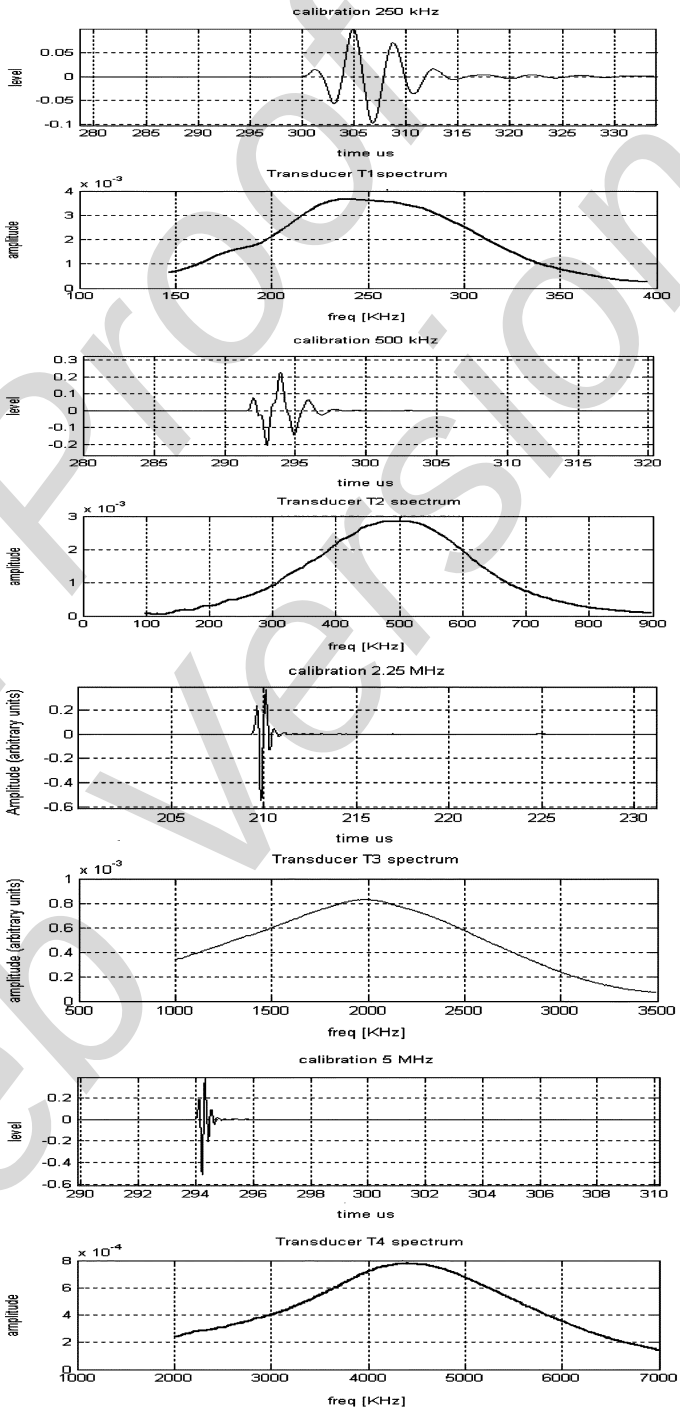

Fig. 4. Calibration signals and the corresponding spectra. Transducers T1, T2, T3, and T4.

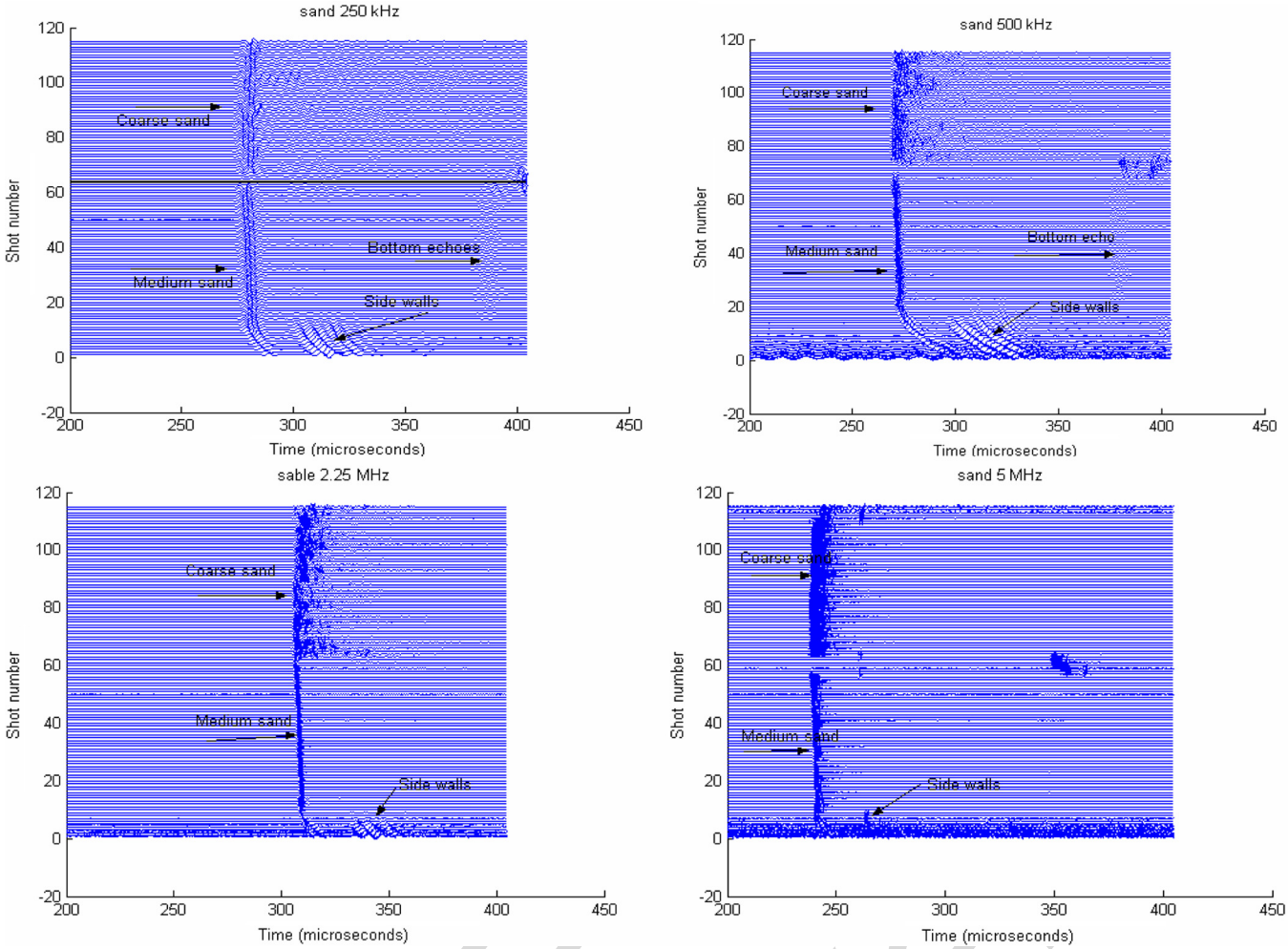

Fig. 5. Received echoes from medium and coarse sand. Transducers T1 (250 kHz), T2 (500 kHz), T3 (2.25 MHz), and T4 (5 MHz).

and T2), a very weak echo was reflected by the bottom of the plastic box (echoes labeled *bottom echo* in Fig. 5). At relatively low frequencies (<500 kHz), the attenuation of the signal by the sand was not sufficiently strong to absorb the energy of the transmitted signal over a distance of 10 cm, and a weak echo was reflected by the plastic structure of the box. All these undesirable echoes were eliminated in the data processing, using a suitable time windowing procedure. It can be noted that these spurious echoes were not visible in the case of the coarse sand because the signal had a highly scattered structure just after the first reflection. This complex structure is often called a coda in the seismic field. In our experiments, the coda was due to the multiple scattering by the grains. This process also began to appear in the case of medium sand at very high frequencies (Fig. 5).

To determine the reflection loss, we measured successively the total, coherent, and incoherent intensities defined as follows. If $p_i(t)$ is a time series of the signal reflected by the bottom when the transducer is in a position denoted by i, based on the definition of the total intensity $(I_{\rm t})$, coherent intensity $(I_{\rm coh})$, and incoherent intensity $(I_{\rm incoh})$, we can write

$$I_t = \left\langle |P_i(f)|^2 \right\rangle_i$$
$$I_{\rm coh} = \left| \langle P_i(f) \rangle_i \right|^2$$
$$I_{\rm incoh} = I_t - I_{\rm coh}.$$

To obtain the reflection loss corresponding to the total intensity, the following procedure was applied.

— Take the Fourier transform of the time signal $p_i(f) = TF\{p_i(t)\}$.
— Take the square root of the total averaged intensity $I_t(f)$.
— Compute the following ratio: square root of the total averaged intensity/absolute value of the Fourier transform of the calibration signal at the air/water interface. The result gives the reflection coefficient as a function of the frequency. The reflection loss is then obtained by taking the decimal logarithm of this expression.

To obtain the coherent part of the reflection coefficient, we used the coherent intensity instead of the total intensity. The incoherent part of the reflection coefficient was then obtained by calculating the difference between total and coherent intensities. The same procedure was successively applied with all the transducers. Both total and coherent intensities were obtained by averaging about 50 signals. A time window was applied to remove the signals affected by spurious echoes before the averaging process.

The reflection loss for this medium sand is given in Fig. 6, where also the contributions of the incoherent, coherent, and

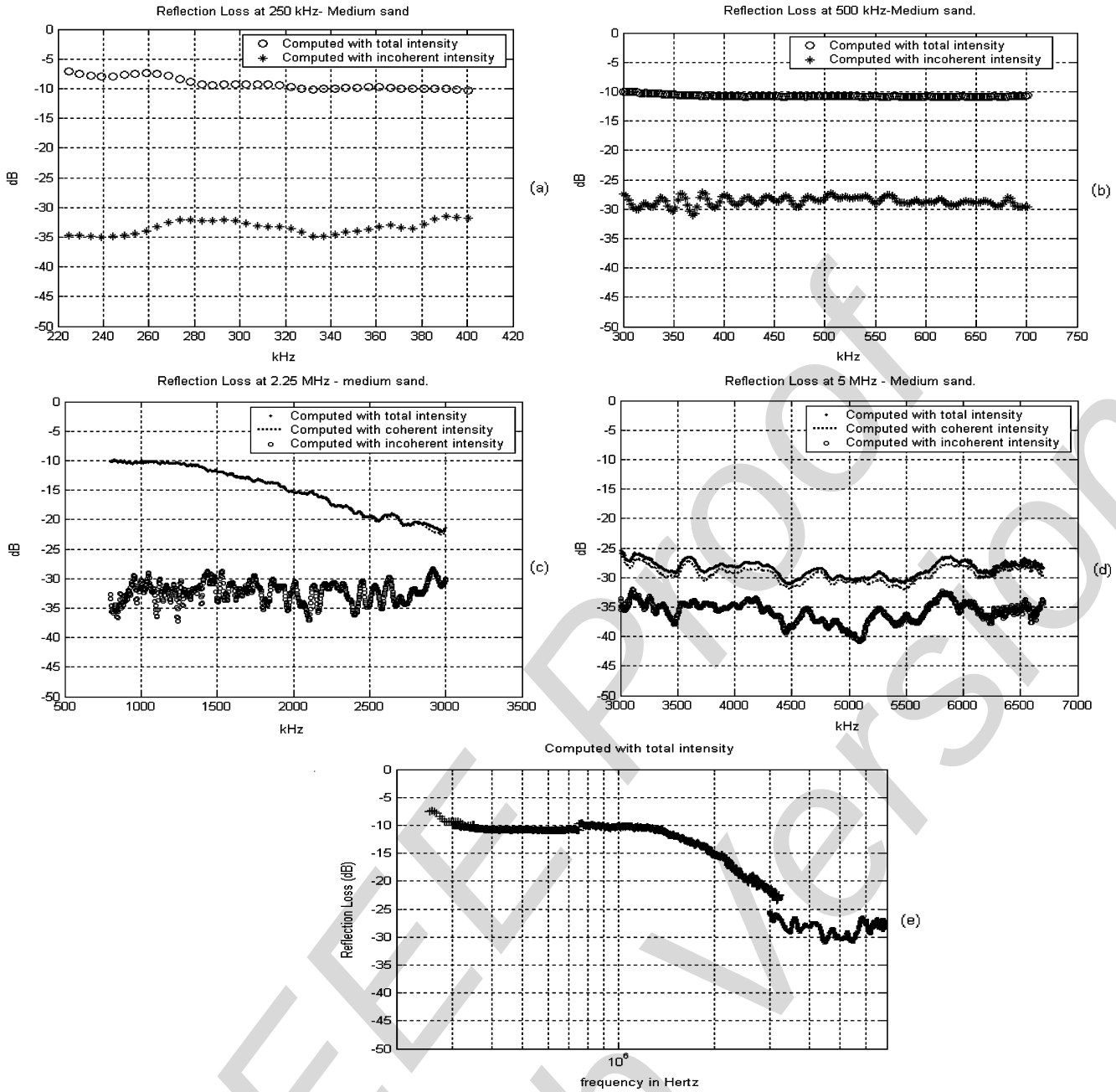

Fig. 6. Reflection losses in the case of medium sand at various frequencies. (a) Transducer T1. (b) Transducer T2. (c) Transducer T3. (d) Transducer T4. (e) All transducers.

total intensity are shown. From Fig. 6(a) and (b), it can be seen that the incoherent intensity level was very low (around -35 dB) in comparison with both total and coherent intensity levels; this means that the reflection was mainly coherent. In other words, no scattering was introduced by the granular structure of the interface, and the interface acted just like a perfectly flat, homogeneous interface.

Fig. 6(e) shows that at frequencies less than 1.4 MHz, the reflected level was constant and the amplitude was around -10 dB, which is in agreement with classical laboratory measurements on sand at these frequencies, as well as with the classical theory of reflection on a water/sand interface. At very high frequencies (>3 MHz) the level dropped to -30 dB, which corresponds to a loss of amplitude of 20 dB between the lowest frequency (<1 MHz) and the highest frequency (>3 MHz). This was certainly due to a complex scattering process introduced by the sand grains. Note that in this region of the spectrum, the wavelength began to be of the same order of magnitude as the mean particle size ($a/\lambda = 0.25$ at 3 MHz). Another important feature that can be observed here is the transition zone between the "low-frequency" and the "high-frequency" part of the spectrum. In this transition zone [Fig. 6(c)], the reflection loss can be seen to have decreased quasi-linearly with the frequency.

The particular point at which a break occurred in the slope corresponds to a frequency of 1.4 MHz (wavelength: 1 mm),

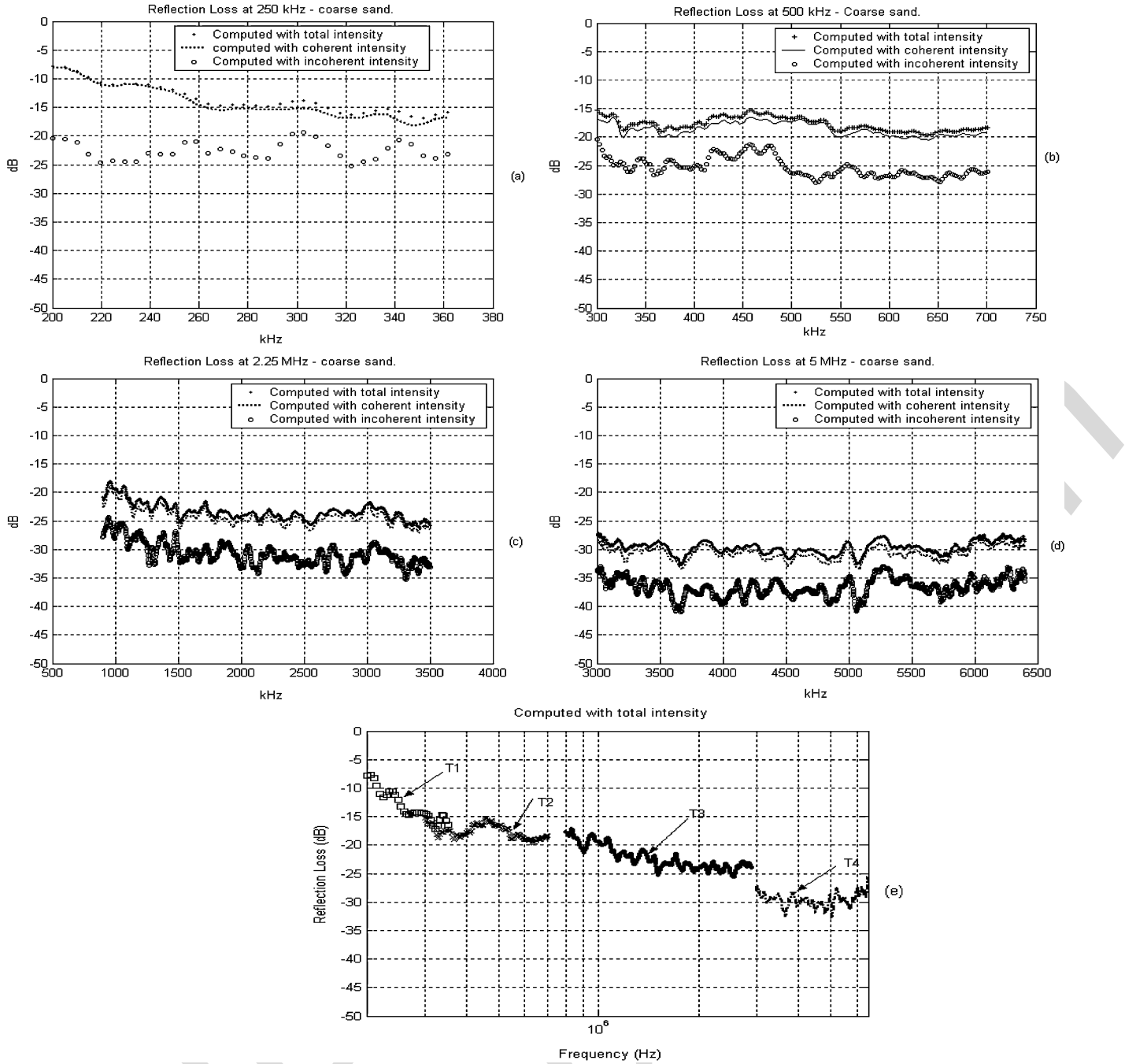

Fig. 7. Reflection losses in the case of coarse sand at various frequencies. (a) Transducer T1. (b) Transducer T2. (c) Transducer T3. (d) Transducer T4. (e) All transducers.

which corresponds to $ka \sim 0.76$ (where k is the wave number and a is the mean particle radius).

Similar measurements were performed with the coarse sand, the granulometry of which is given in Table I.

The reflection loss for this coarse sand is given in Fig. 7(a)–(d) in the case of transducers T1, T2, T3, and T4. Fig. 7(e) gives the overall result obtained in the frequency range from 200 kHz to 6 MHz.

It can be observed in Fig. 7(a) and (b) that the reflection loss occurring at low frequencies (250 kHz $< f <$ 500 kHz) and computed with total intensity was around -15 dB, which is 5 dB less than the level observed with medium sand. The incoherent intensity was also plotted in the same figure. It can be seen that this incoherent intensity was relatively high in comparison with the coherent part, which proves that some scattering process was certainly involved. When the frequency increases ($f > 3$ MHz), the level of the reflection loss seems to tend asymptotically to -30 dB. Note that this value is the same as that obtained with medium sand. Moreover, the breaking point seems to have shifted to the low-frequency region. It is difficult to determine the exact frequency corresponding to this point, but 200 kHz seems to be a reasonably accurate estimate. At this breaking point, the dimensionless parameter ka was about 0.65, which is very similar to the value obtained with medium

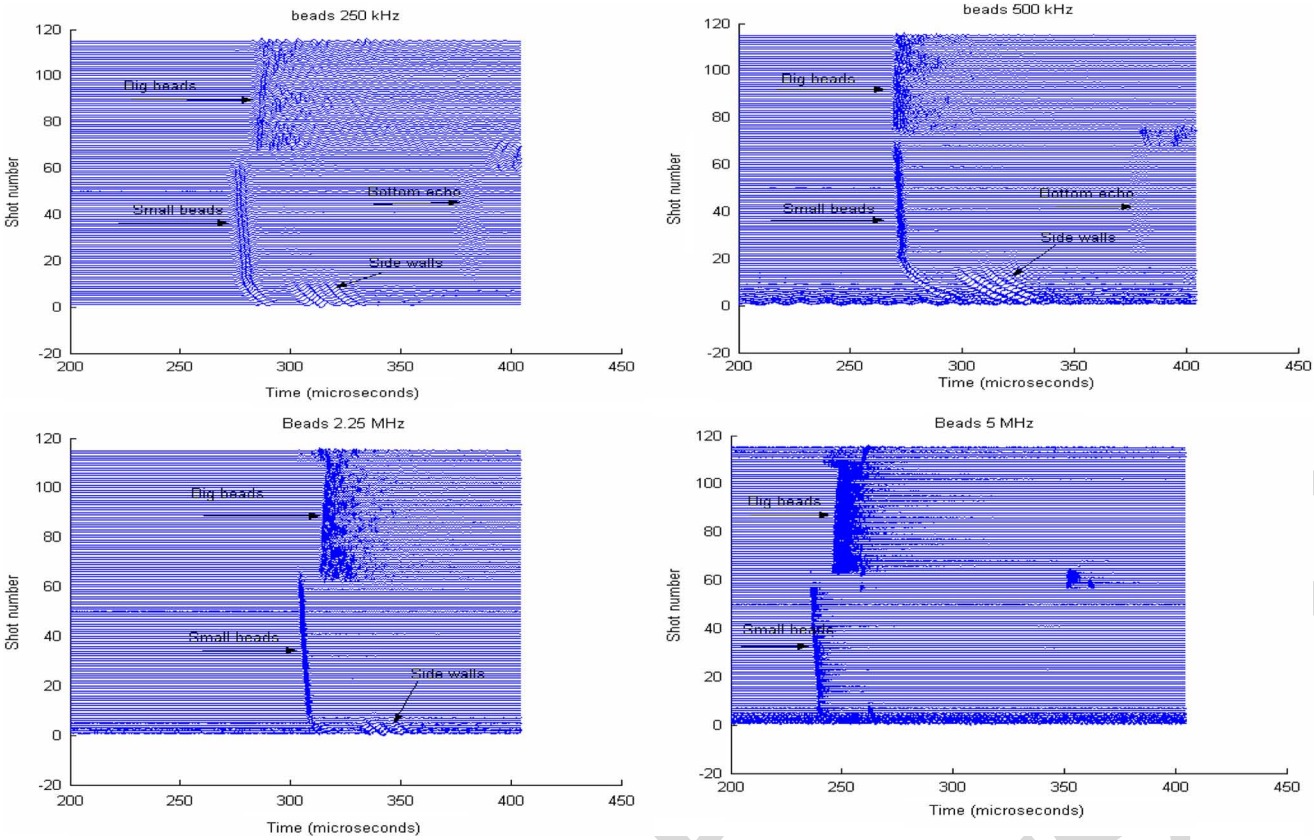

Fig. 8. Received echoes from small and large glass beads. Transducers T1 (250 kHz), T2 (500 kHz), T3 (2.25 MHz), and T4 (5 MHz).

sand. This finding seems to indicate that the main parameter governing the reflection loss is the dimensionless parameter $\boldsymbol{ka}$, which depends directly on the ratio between the particle size and the wavelength.

B. Experiments on Glass Beads

Similar experiments to those performed on the two types of sand were carried out with glass beads of two sizes. Fig. 8 gives the echogram obtained with transducers T1, T2, T3, and T4. As in the experiments with sand, the lower part of the image corresponds to the small beads and the upper part to the large beads. The edge effects (ripples) that can be observed here in the lower part of the image were again due to the scattering by the edges of the plastic box. It can also be seen in this case that the water/sediment interfaces were not perfectly horizontal, which resulted in the "bottom trace" being tilted. The slope of the bottom was calculated and found to be around 1.7° with small beads and less than $-1°$ with large beads. The main objective in preparing the sample was to obtain a perfectly flattened bottom (with no ripples), rather than obtaining a perfectly horizontal interface. An error of $+/-1.5°$ in the horizontality was taken to be acceptable. It was, therefore, necessary to shift the signals before carrying out any data processing to compensate for the time shift observed between signals due to the bottom slope. A weak echo generated by the bottom of the plastic boxes can also be observed at low frequencies (transducers T1 and T2). This weak echo was not visible with the large beads because the signals were strongly scattered just after the reflection by the interface (coda).

The reflection loss for small beads (200 μm) is given in Fig. 9. In this figure, as with the medium sand, we can see that the reflection level was around -10 dB and that this amplitude was practically constant over the whole frequency range from 200 kHz to 1.3 MHz. The incoherent reflection level was very low in comparison with the coherent one, which means that no strong scattering was generated by the interface. It can also be observed that the reflection levels computed with the total intensity and the coherent intensity were the same. This means that the reflection was mainly coherent. As the frequency increased, the reflection loss computed with the total intensity decreased to a value of -25 to -30 dB, as previously observed with medium sand.

Fig. 9(e) shows the reflection loss over the whole frequency range from 250 kHz to 7 MHz . Between 300 kHz and 1.3 MHz, the reflection loss remains constant before showing [Fig. 9(c)] a linear decrease as the frequency increases. It reaches a constant level again at very high frequencies, but other experiments are now required at higher frequencies to confirm this pattern.

The reflection loss for large beads showed different patterns, depending on the frequency of the ensonification. Fig. 10 shows the reflection loss obtained with transducers T1, T2, T3, and T4. The reflection behavior observed was actually more chaotic than with small beads, but the mean level seems to have been stabilized in the low-frequency part of the spectrum (250 kHz $< f <$ 500 kHz) at -15 dB, which is 5 dB lower than with the small

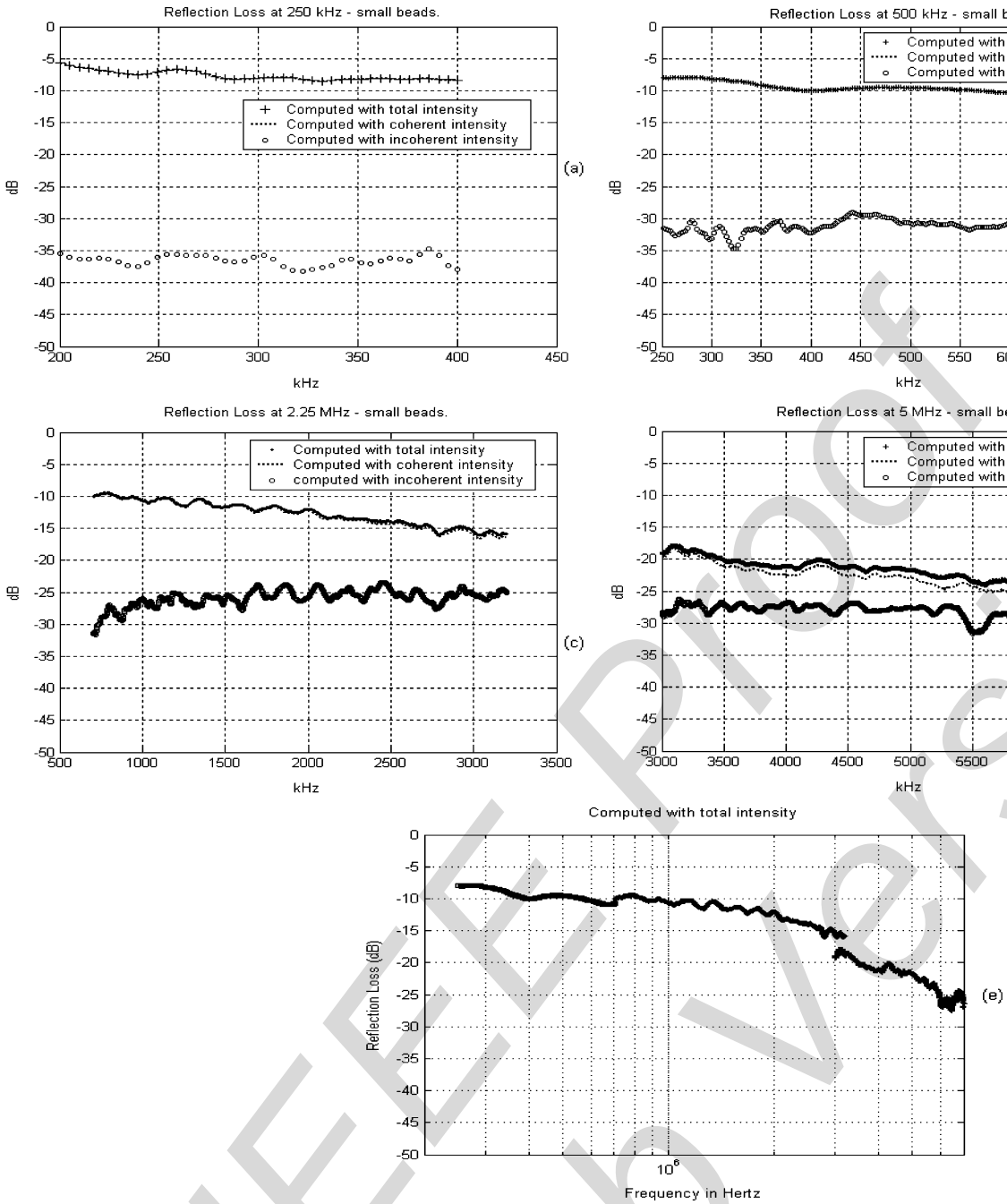

Fig. 9. Reflection loss in the case of small beads at various frequencies. (a) Transducer T1. (b) Transducer T2. (c) Transducer T3. (d) Transducer T4. (e) All transducers.

beads. In the high-frequency regime (1 MHz $< f <$ 3 MHz), the reflection loss subsequently decreased with the frequency before reaching (at $f >$ 3 MHz) a constant level (at around -30 dB).

In this case, at all the frequencies, the reflection loss was found to have a significantly large incoherent component.

If we compare now the reflection losses obtained with large beads and coarse sand, we can see some similarities (Fig. 11). This observation confirms that a monosize distribution of beads can be used to simulate the reflection loss in a complex system of sand particles. The level of the reflection loss at very high frequencies also seems to be independent of the particle size as well as being independent of the frequency.

If we now compare the reflection losses for both medium sand and small beads (Fig. 12), we can see that the two patterns were very similar in the low-frequency range. The only difference was the rate of decrease of the reflection loss as the frequency increased. This observation again confirms that small beads have a very similar pattern of behavior to that of sand, as long as the bead diameter is of the same order as the mean size of the sand particles. Further research is now required to explain why a difference in the amplitude of the reflection loss was observed in the transition zone, but it can already be assumed that in this fre-

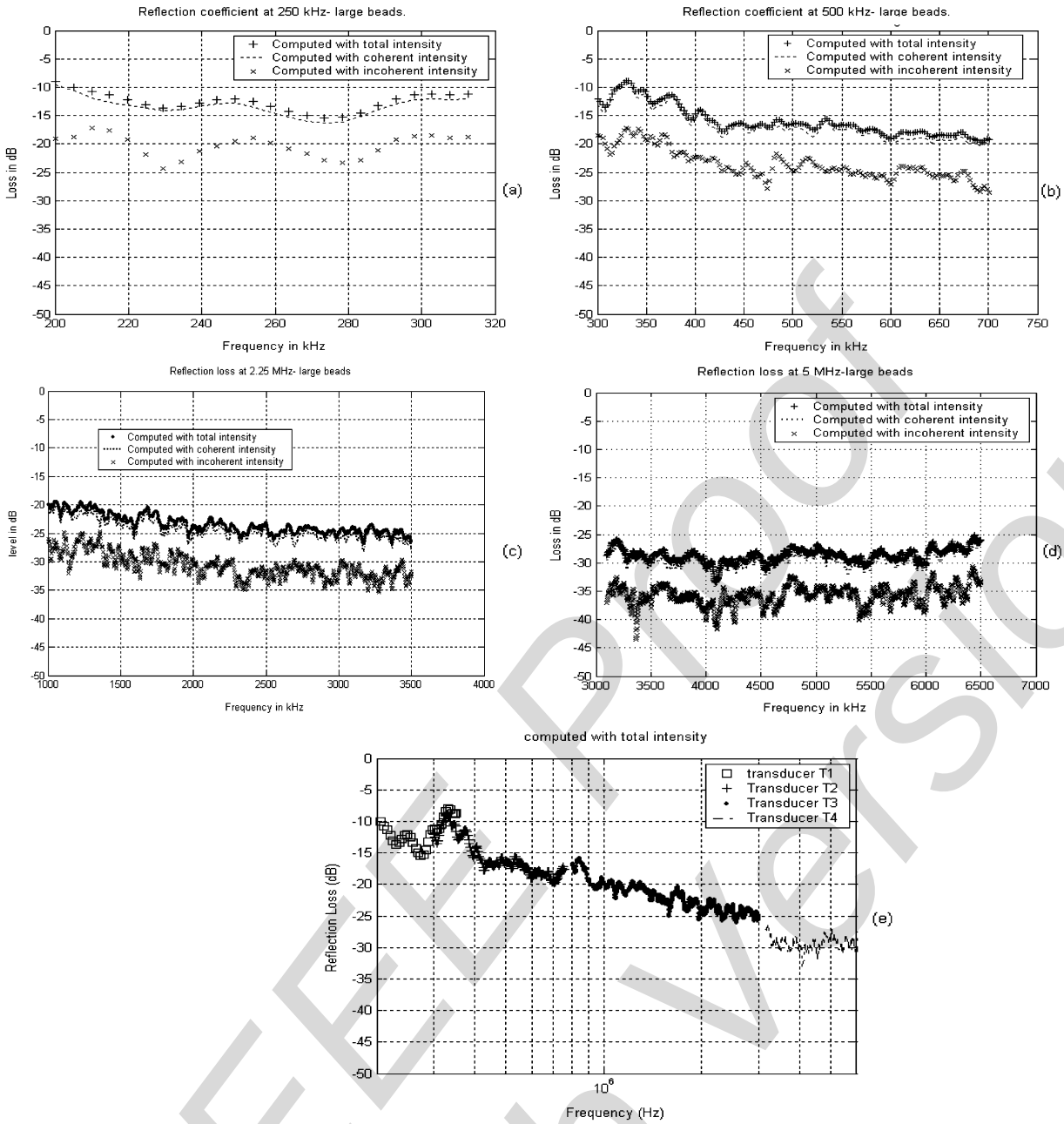

Fig. 10. Reflection loss in the case of large beads at various frequencies. (a) Transducer T1. (b) Transducer T2. (c) Transducer T3. (d) Transducer T4. (e) All transducers.

quency range, where large scattering effects occur, both the size and the shape of the grains have greatly affected the reflection loss.

Last, comparisons between small and large beads are made in Fig. 13 and between medium and coarse sand in Fig. 14. The two curves in these figures both point to the same conclusion. With medium sand and small beads, the reflection level decreased conspicuously in the high-frequency domain; it can, therefore, be concluded that in the case of medium sand at the usual sonar frequencies, the granular structure of the sediment does not play any role, whereas in the case of coarse sand, the decrease in the reflected level begins at the usual sonar frequencies. When working with systems operating at 300 kHz at sea on coarse sand bottom, the influence of the granular structure of the sediment cannot, therefore, be ignored.

III. Conclusion

The results of this study show that the sound reflected by a sand bottom depends strongly on the ratio between the wavelength and the particle size. This effect was also observed with a monosize distribution of glass particles. The main result obtained in this paper is that when the ka parameter is less than 1, the reflection loss is constant and the sand can be regarded as a continuous homogeneous medium. When the ka parameter is around 1, a strong decrease in this reflection loss occurs, which means that the medium behaves like a scattering medium.

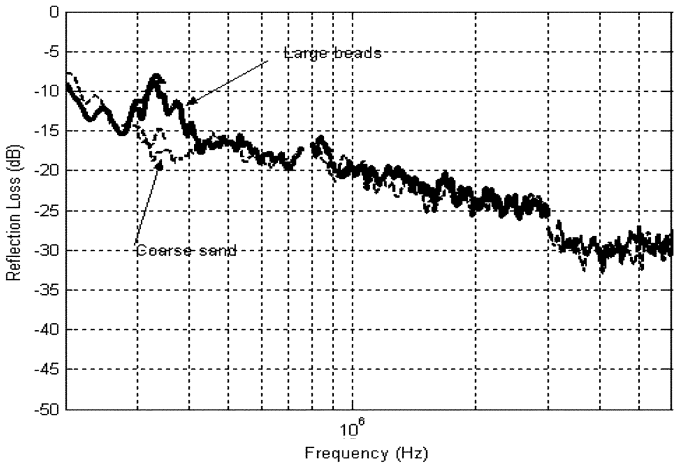

Fig. 11. Comparison between large beads and coarse sand.

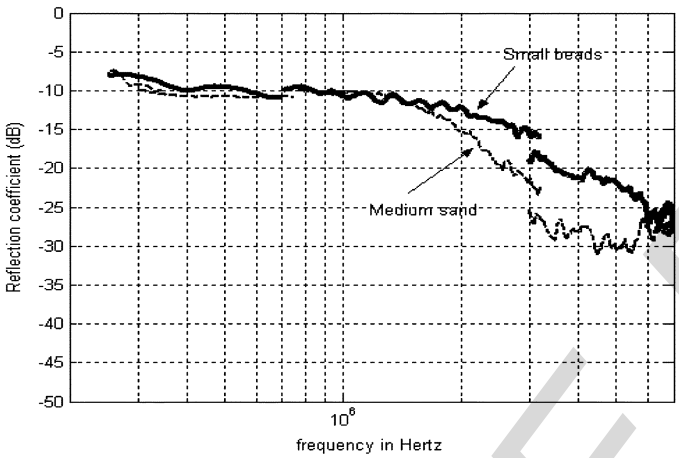

Fig. 12. Comparison between medium sand and small beads.

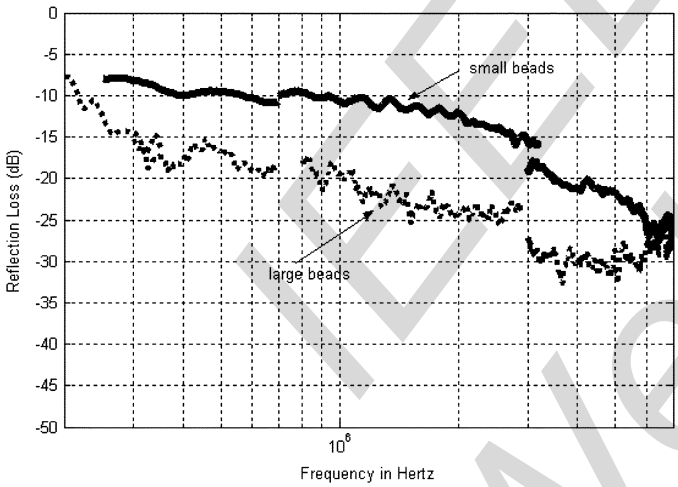

Fig. 13. Comparison between small and large beads.

This finding shows the role played by the size of particles in the process of reflection by granular media. Although we can explain at this stage why for medium sand and small glass beads the reflected level is frequency independent (this level depends mainly on the sound speed and the density contrast between water and sediment assumed to be a homogeneous medium), it is

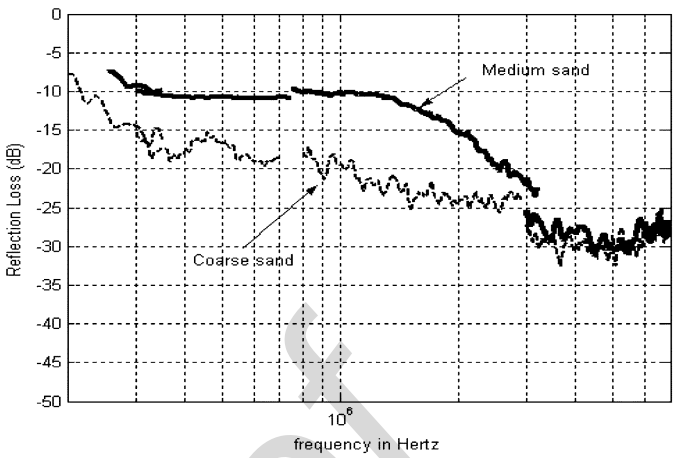

Fig. 14. Comparison between medium sand and coarse sand.

not yet possible to explain why the level dropped to around -30 dB when very high frequencies were used. This level of -30 dB was obtained with both medium and coarse sand, as well as with both small and large glass beads. These data, therefore, indicate that at very high frequencies, sand behaves mainly like a granular medium and that the transition between continuous to granular behavior is linearly dependent on the frequency.

ACKNOWLEDGMENT

The authors would like to thank D. Ferrand (Laboratoire de Mécanique et d'Acoustique (LMA), Centre National de la Recherche Scientifique (CNRS), Marseille, France) for his help with the data processing.

REFERENCES

[1] R. D. Stoll, "Reflection of acoustic waves at a water-sediment interface," *J. Acoust. Soc. Amer.*, vol. 70, no. 1, pp. 149–156, 1981.

[2] N. P. Chotiros, "Reflection and reverberation in normal incidence echo sounding," *J. Acoust. Soc. Amer.*, vol. 95, no. 5, pt. 1, pp. 2921–2929, 1994.

[3] C. M. McKinney and C. D. Anderson, "Measurement of backscattering of sound from the ocean bottom," *J. Acoust. Soc. Amer.*, vol. 36, no. 1, pp. 158–163, 1964.

[4] M. J. Isakson, S. McJunkin, E. Hood, and N. Chotiros, "A comparison of models for water-saturated sand by inversion of reflection loss measurements," *J. Acoust. Soc. Amer.*, vol. 111, no. 5, pp. 2330–2330, 2002.

[5] A. W. Nolle, "Acoustical properties of water filled sands," *J. Acoust. Soc. Amer.*, vol. 35, no. 9, pp. 1394–1408, 1963.

[6] K. L. Williams, R. H. Hackman, and D. H. Trivett, "High-frequency scattering from liquid/porous sediment interfaces," *J. Acoust. Soc. Amer.*, vol. 84, no. 2, pp. 760–770, 1988.

[7] C. F. Greenlaw, D. V. Holliday, and D. E. McGehee, "High frequency scattering from saturated sand sediments," *J. Acoust. Soc. Amer.*, vol. 115, no. 6, pp. 2818–2823, 2004.

[8] ***[AU: Please provide full page range]*** A. Ivakin, J.-P. Sessarego, and P. Sanchez, "Laboratory study of high frequency scattering from water-saturated sandy sediments," *J. Acoust. Soc. Amer.*, vol. 117, no. 4, pt. 2, p. 2433, Jun. 2005.

[9] ***[AU: Please provide page range]*** A. Ivakin, J.-P. Sessarego, and R. Guillermin, "Laboratory study of high frequency scattering from water-saturated granular sediments," in *Proc. 152nd ASA Meeting*, Honolulu, HI, Nov. 2006.

[10] ***[AU: Please provide volume]*** A. Ivakin and J.-P. Sessarego, "High frequency broad band scattering from water-saturated granular sediments: Scaling effects," *J. Acoust. Soc. Amer.*, pp. 165–171, 2007.

Jean-Pierre Sessarego received the Ph.D. degree in physics from the Université de Provence, Aix-Marseille I, France, in 1982.

He has been a Researcher at Centre National de la Recherche Scientifique (CNRS), Marseille, France. His primary focus was in shallow-water propagation and in scattering by elastic objects for target recognition. Currently, he is a Senior Scientist and Head of the Underwater Acoustic Group at the Laboratoire de Mécanique et d'Acoustique (LMA), CNRS, where he is now working on propagation through sediments. He is also Professor at the Ecole Centrale Marseille, France.

Dr. Sessarego is a member of the French Acoustical Society.

R. Guillermin ***[AU: Please provide photo and short bio]***

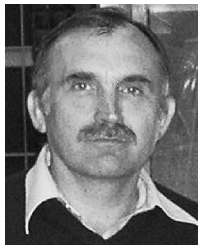

Anatoly N. Ivakin received the M.Sc. degree in physics from Moscow Institute of Physics and Technology, Moscow, Russia, in 1978 and the Ph.D. degree in physics and mathematics from Andreev Acoustics Institute, Moscow, Russia, in 1982.

He was a Researcher, and then, a Senior Scientist at Andreev Acoustics Institute, Moscow, Russia, where he worked in the field of ocean and seabed acoustics. Since 2001, he has been a Senior Physicist at the Applied Physics Laboratory, University of Washington, Seattle. His research interests include acoustics of marine sediments, propagation and scattering in heterogeneous and granular media, ocean reverberation and remote acoustic sensing.

Dr. Ivakin is a Fellow of the Acoustical Society of America.

High frequency broad band scattering from water-saturated granular sediments: Scaling effects

Anatoliy N. Ivakin
Applied Physics Laboratory, University of Washington, Seattle, Washington 98105
ivakin@apl.washington.edu

Jean-Pierre Sessarego
CNRS/LMA, 31 Chemin Joseph Aiguier, 13402, Marseille, Cedex 20, France
sessarego@lma.cnrs-mrs.fr

Abstract: Sound backscattering from water-saturated granular sediments at frequencies from 150 kHz to 8 MHz at oblique incidence was studied in controlled laboratory conditions. Two kinds of sediments, medium and coarse sands, were degassed, and their surface was flattened. In these conditions, the sediment granular structure can be considered as a controlling mechanism of backscattering. Comparison of frequency dependencies of backscatter for the two sediments with different mean grain size shows the existence of a persistent scaling effect that allows description of the backscattering strength as a function of one parameter, the mean grain size/wavelength ratio.

PACS numbers: 43.30.Ma [GD]
Date Received: June 3, 2007 **Date Accepted:** August 23, 2007

1. Introduction

Reported measurements of seabed scattering are largely confined to relatively low frequencies, up to 300 kHz (see, e.g., Jackson and Richardson[1] and references therein). Still higher frequencies, up to a few megahertz, are used in seafloor imagery (e.g., in pencil-beam sonars), particularly to observe dynamic processes at the seafloor. From the physics of sound-sediment interaction standpoint, however, interesting effects can be anticipated at these high frequencies as the wavelength can become comparable with the sediment typical grain sizes. Unfortunately, existing observations in this case are usually noncalibrated and, therefore, do not allow measurements of system independent scattering characteristics of the seabed, such as the bottom scattering strength. A recent exception is presented in Greenlaw *et al.*,[2] where the backscattering strength for sand sediments in shallow water was measured at frequencies from 265 kHz to 1.85 MHz. However, physical interpretation of results obtained in this work is quite ambiguous due to a significant uncertainty of the sediment parameters. As the authors noted,[2] the sediment surface was only relatively smooth and had, e.g., pockmarks created by fish foraging on the bottom fauna. A small but detectable sediment gas content was noticed as well. Therefore, acoustic observations could be affected by the small-scale roughness, the presence of gas bubbles in the sediment, and other mechanisms, e.g., those related to possible near-surface stratification of the sediment.[3,4]

Unfortunately such ambiguities are quite usual for experimental studies of sediment acoustics in shallow water where the dynamical complexity and unpredictability of environmental conditions can be so great that even very extensive time- and labor-consuming environmental measurements (such as those at the recent major sediment acoustics experiment, SAX04[5,6]) may not be enough to sufficiently reduce the uncertainty in interpretation of acoustic data. In this connection, conducting experiments in well-controlled laboratory conditions can become a valuable (but much less expensive) supplement to the experiments at sea. An impor-

tant advantage of laboratory studies of sediment scattering is that they make it possible to simplify the problem by reduction of the number of controlling parameters and allow observation of the effects of different scattering mechanisms separately. For example, the sediment can be degassed to eliminate effects of micro-bubbles, and its surface can be flattened to exclude contributions of the sediment roughness at scales greater than the grain size. This approach was used by Nolle *et al.*[7] in their study of acoustical properties of sand sediments at two frequencies, 500 kHz and 1050 kHz. Williams *et al.*[8] studied broadband backscattering from several types of the sediments in a wider frequency range, about 200 kHz to 2.5 MHz. Unfortunately, the bottom scattering strength was not obtained, as the measurements were still not calibrated.

In this paper (Sec. 2), we describe experiments conducted at the CNRS/LMA water tank facility on backscatter from sands over a wide frequency range, 150 kHz to 8 MHz. Note that existing methods for measuring the bottom scattering strength normally assume using narrow band signals (see, e.g., Jackson and Richardson,[1] Ch. G.2, pp. 497–502). To be applied to broadband transducers, significant modifications are required. One such modification is considered in Sec. 3 of this paper. It made possible, to our knowledge for the first time, measurement and analysis of the frequency dependence of the sediment backscattering strength over such a wide frequency range. The results are given in Sec. 4. The analysis assumes that, for the given conditions, only one mechanism of scattering can be dominating, which is due to the sediment granular structure, and that the controlling sediment parameter is the mean grain size. In this case a scaling effect is possible: Given grazing angle, the backscattering strength, which is system independent and depends only on frequency and sediment properties, can be presented as a unique function of only one parameter, the mean grain size/wavelength ratio. This effect is demonstrated and the scaling function is presented in Sec. 4 as well.

2. Experiments

Two kinds of water-saturated sediments with different grain sizes, moderately well sorted medium and coarse sands, were chosen for the study. Sediment properties such as the density, porosity, and grain size, were measured by nonacoustical methods. The medium sand had the mean grain diameter 0.245 mm, sediment/water density ratio 1.98, and porosity 36.5%. The coarse sand had the mean grain diameter 1.55 mm, sediment/water density ratio 2.02, and porosity 33%. Prior to the experiments, the two sediments were stored in containers filled with water treated with chlorine to exclude the presence of living organisms which might generate bubbles. The sediments were transferred in smaller containers (without exposure to air) to a large water tank (chlorine treated as well) where, in addition, they were sieved and agitated to eliminate remaining bubbles. After such preparations, the two sediments were placed in different plastic rectangular boxes of the same size with horizontal dimensions 17×23 cm and 9 cm in the vertical. The sediment surface was carefully flattened by scraping even with the box edges to eliminate roughness at scales larger than the sediment grains. Therefore, the necessary measures were taken to ensure that only the sediment granular structure be considered as a dominating mechanism (rather than large scale roughness and/or gas bubbles) controlling total scattering in and from the sediment.

Experiments on backscattering from the sediments were conducted using a typical monostatic geometry with the transducers acting as both source and receiver (see, e.g., Jackson and Richardson,[1] Fig. G3). Two broadband Parametrics transducers with nominal center frequencies 500 kHz and 5 MHz were used which, altogether, allowed covering continuously the wide frequency range of 150 kHz to 8 MHz. The transducers are circular pistons with radii 12.5 mm (500 kHz) and 6.5 mm (5 MHz). Their directivities are documented over all used frequencies and well described by the corresponding theoretical function $D=2J_1(ka \sin \vartheta)/(ka \sin \vartheta)$, where a is the piston radius, $k=2\pi/\lambda$ is the wave number in water, $J_1(\ldots)$ is the Bessel function of the first order, and ϑ is the angle between the direction of observation and the maximum response axis (MRA) of the transducer.

The position of the transducers was controlled by a system allowing their automatic vertical and horizontal translation with 0.1 mm accuracy and their rotation with 0.1° accuracy.

For calibration of each transducer, first the time series of the echo signal reflected from the water-air interface at normal incidence were measured and Fourier analyzed. Then, the transducer was rotated toward the sediment surface and set in a position with a fixed direction. Horizontal translations of the transducer (parallel to the sediment surface) were used to develop a statistically uniform ensemble of realizations for the echo signals. To provide the necessary statistics, a number of horizontal positions of the transducer was set automatically with a consecutive horizontal shift of 0.5 cm. At each position, time series of the echo signal scattered from the sediment (at a fixed incidence angle) were measured for a number of pings (up to 64) and coherently averaged to reduce possible effects of noise.

Fourier spectral analysis was performed on the echo signals with a flexible time-windowing. The windowing was used, first, to reduce the effects of reverberation from the sediment box walls and, second, to accommodate corresponding distances and the scattering areas of the sediment surface with the frequency dependent beam pattern of the transducer (as discussed below). The windowed echo frequency spectra, $F(f)$, were normalized by the spectra of the calibration signal, $F_0(f)$. These normalized spectra provided a data set for the statistical processing. Particularly, their second moments (the squared magnitudes averaged over realizations), were used to estimate the normalized scattered intensity

$$I_s(f)/I_0(f) = \langle |F(f)|^2 \rangle / |F_0(f)|^2, \tag{1}$$

and to obtain the frequency dependencies of the sediment backscattering coefficient, m_s, and its decibel equivalent, the scattering strength, $10 \log m_s$, as given in the next section.

3. Extracting scattering strength

The intensity of calibration and scattered signals in the frequency domain, I_o and I_s [see Eq. (1)], can be calculated from the corresponding signal time series taken in the observation time window. Specifically, the scattering intensity is defined as the squared magnitude of the Fourier transform of the scattered signal time series taken in the time window, $t \in [t_1, t_2]$, related to time-delays occurring in the process of scattering and defined by corresponding range-time inequality

$$ct_1 < r_i + r_s < ct_2, \tag{2}$$

with r_i and r_s being the distances from the source and receiver to the ensonified area (or, more accurately, the observation area) and c being the sound speed in water.

Consider the case of a monostatic geometry, where $r_i = r_s = r = ct/2$. The incidence angle (measured from the vertical), θ, is defined as follows: $\cos\theta = t_f/t$, $t \geqslant t_f = 2H/c$, where t_f is the arrival time in the vertical direction (fathometer return) and H is the vertical distance from the source to the sediment surface. For the angle window $\theta \in [\theta_1, \theta_2]$, taking into account that $\tan\theta d\theta = d \ln t$, we have $\theta_2 - \theta_1 \approx (t_2 - t_1)/t_w \tan\theta_w$ with $t_w = (t_1 + t_2)/2$ and $\theta_w = (\theta_2 + \theta_1)/2$ being centers of the corresponding time and angle windows.

The scattering cross section per unit area per unit solid angle (see, e.g., Ref. 1, p. 23) or, for brevity, the scattering coefficient, m_s, can be defined from the equation

$$I_s = I_o \frac{r_o^2}{r^4} A_{ef} m_s, \tag{3}$$

where I_o is the intensity at the distance $r_0 = ct_0$ in the direction of maximum directivity (on the transducer MRA) with t_0 being the arrival time of the calibration signal, and A_{ef} is an effective observed scattering surface obtained from the directivity D, defined with respect to the field amplitude, by integration over the observation area, defined by Eq. (2), as follows:

$$A_{ef} = \int_{A(t)} D^4 dA. \tag{4}$$

The integral (4) can be written using spherical variables (θ, φ), which are the incidence and azimuth angles of the incident wave. However, for directional sources not vertically oriented, it is more convenient to describe their directivity and analyze the integral (4) in angular coordinates measured not from vertical direction, but from the transducer MRA, i.e., from its depression incidence angle, θ_0. Consider new variables (not spherical), $\theta' = \theta - \theta_0$ and $\varphi' = \varphi \sin\theta$, which represent angular coordinates measured in two mutually orthogonal planes so that their intersection is the transducer MRA, where $\theta' = 0$ and $\varphi' = \varphi = 0$. One of these two planes is always vertical (the incidence plane). The second is an auxiliary one perpendicular to the incidence plane and referred to as the slant azimuth plane.

Using the new variables, the integral (4) can be written in the form

$$A_{\text{ef}} = \frac{r^2}{\cos\theta_w}\Omega_{\text{ef}}, \tag{5}$$

where Ω_{ef} is an effective solid angle of the observation area

$$\Omega_{\text{ef}} = \int_{\theta_1}^{\theta_2} d\theta \int_{-\pi\sin\theta}^{\pi\sin\theta} D^4(\theta - \theta_0, \varphi')d\varphi'. \tag{6}$$

Note that the integral (6) at high enough frequencies (and correspondingly narrow directivities) has a maximal value at $\theta_w = \theta_0$, where the observation angle window matches with the maximum of the transducer directivity.

Assume that the transducer has directivity with an axial symmetry, so that for the directivity factor we have $D^4(\theta', \varphi') = Q(\vartheta/\vartheta_o)$, where ϑ is the angle between the direction of observation and the transducer MRA, and ϑ_0 is a parameter defining the directivity angular width. Note that at $\vartheta_0 \ll \theta$, limits in the φ'-integral in Eq. (6) can be replaced by infinities, and integration can be performed using an approximation $\vartheta \approx (\theta'^2 + \varphi'^2)^{1/2}$. Then, in the matching case, $\theta_w = \theta_0$, we obtain

$$\Omega_{\text{ef}} \approx \vartheta_0^2 P\left(\frac{\theta_2 - \theta_1}{2\vartheta_0}\right), \quad P(\alpha) = \int_{-\alpha}^{\alpha} dx \int_{-\infty}^{\infty} Q(\sqrt{x^2 + y^2})dy. \tag{7}$$

The integral in Eq. (7) has two simple asymptotic approximations:

$$P \approx M_1\alpha, \quad \alpha \ll 1, \quad M_1 = \int_{-\infty}^{\infty} Q(s)ds,$$

$$P \approx M_2, \quad \alpha \gg 1, \quad M_2 = 2\pi\int_0^{\infty} sQ(s)ds. \tag{8}$$

A uniform approximation (for arbitrary α) can be sought in the form of a scaling expression

$$P(\alpha) \approx M_2 P_\eta(\alpha M_1/M_2), \quad P_\eta(x) = (1 + x^{-\eta})^{-1/\eta}, \quad \eta > 0. \tag{9}$$

At any value of η, this approximation has two correct asymptotes [Eq. (8)] for small and large α. This allows use of η as a free parameter that can be chosen so as to provide the best fit of the scaling function [Eq. (9)] to the integral (7) at intermediate α, taking into account a specific transducer directivity function $Q(s)$.

In our case of the circular piston transducers, we can assume that at high frequencies $\vartheta_0 \equiv (ka)^{-1} \ll 1$ and perform the integration in Eqs. (7) and (8) numerically with $Q(s) = (2J_1(s)/s)^4$. For the integrals in Eq. (8) we obtain $M_1 \approx 2.4$ and $M_2 \approx 5.8 \approx M_1^2$. The result for the integration in Eq. (7) is shown in Fig. 1 by the solid curve. The uniform scaling approximation given in Eq. (9) is shown for different η by dashed curves. It is seen that the best agreement is provided by $\eta \approx 4$. Therefore, the set of Eqs. (1), (3), (5), (7), and (9) provides a practical

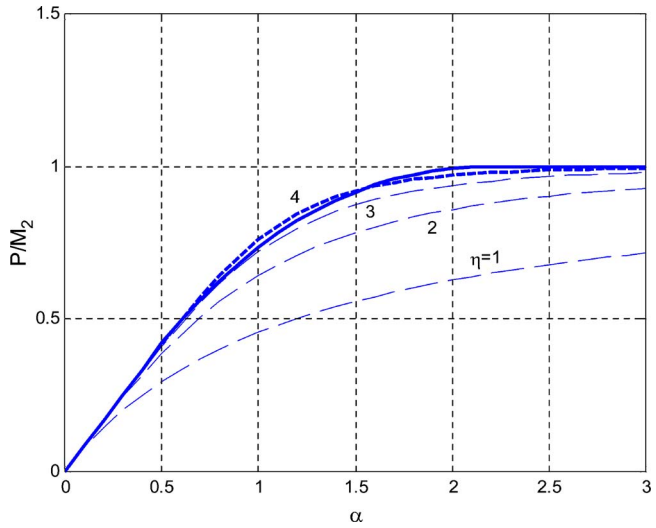

Fig. 1. (Color online) Choosing the parameter η for a scaling power law approximation (9): numerical integration for $P(\alpha)/M_2$ (solid curve) compared to the scaling function $P_\eta(\alpha M_1/M_2)$ for different η (dashed curves). The best fit is provided by $\eta \approx 4$.

algorithm for extracting the backscattering coefficient from analysis of the normalized scattered intensity in the frequency domain using time-windowing of the echo-signal.

4. Results

In Fig. 2, the frequency dependence of the backscattering strength is presented in a wide frequency range, 150 kHz to 8 MHz, for the two sediments, medium and coarse sand, at an incidence angle of 50° (grazing angle of 40°). It demonstrates, in particular, a noticeable difference in the scattering strength of the two sediments at frequencies below 2 MHz. For example, this

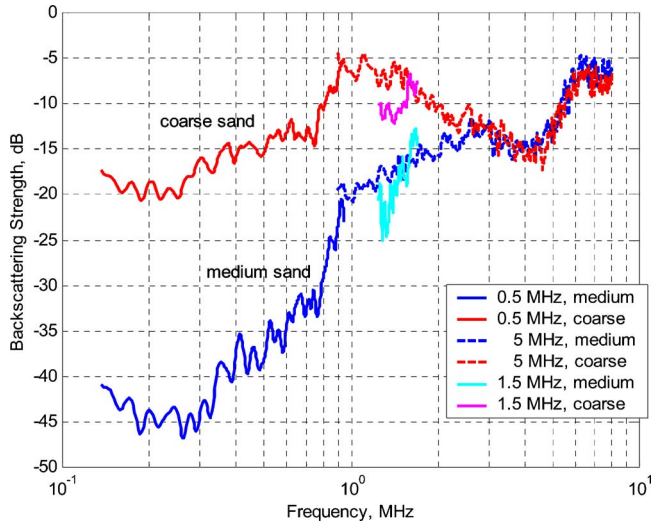

Fig. 2. (Color online) The backscattering strength at the incidence angle 50° obtained for medium and coarse sand using the broad band transducers with 500 kHz and 5 MHz nominal center frequencies. The center frequency of the 500 kHz transducer was nominal indeed, as the transducer had actually another, although weaker, maximum in its frequency spectrum, at 1.5 MHz, which was used to obtain additional scattering data.

difference at frequencies 400 kHz to 800 kHz is about 20 dB. It can mean practically important strong sensitivity of the scattering strength at these frequencies to the mean grain size of the sediment. Note also that at frequencies above 2.5 MHz the difference is small and, therefore, the scattering strength may have too little sensitivity to the grain size.

The ratio of the mean grain diameter to the acoustic wavelength in water, d/λ, varied, in our frequency range, from 0.024 to 1.3 for the medium sand, and from 0.15 to 8.3 for the coarse sand. Therefore, in the interval $0.15 < d/\lambda < 1.3$, we have two data sets for sediments with different mean grain size. This interval is especially interesting as it corresponds to a "transition frequency regime", where the acoustic properties of granular sediments can change dramatically. This change is due to transition from the "low frequency regime", where the ratio d/λ is very small and the continuum media assumptions are valid, to the "very high frequency regime", where this ratio is not small and the sediment must be considered as an essentially discrete granular medium. At these high frequencies, intrinsic (bulk) scattering due to the sediment granular structure becomes important. For example, the ratio d/λ becomes about 0.5 at frequencies around 3 MHz for the medium sand, and at 500 kHz for the coarse sand. Corresponding shift (for the sediments with different grain size) related to the "transition" effects and appearance of the new dominating scattering mechanism can be anticipated. In Fig. 2, such a scaling shift is clearly seen.

In Fig. 3, the scaling effect is demonstrated by plotting scattering data (same as in Fig. 2) versus the ratio d/λ. It is seen that the backscattering strength collapses to a function of only one parameter, at least over the interval $0.15 < d/\lambda < 1.3$, where both data sets are available. This confirms the assumption that, for the given conditions, only one mechanism of scattering is dominating, which is the intrinsic (bulk) scattering due to the sediment granular structure, and that the controlling sediment parameter is the mean grain size. In this case, the scattering strength must be a unique function of the ratio d/λ. This explains, e.g., that the two different grain-size cases match when shifted horizontally, but no shift in the vertical is needed (see Figs. 2 and 3). This is because the scattering strength is unique, system independent, and controlled only by the sediment parameters. This result is practically important, as it provides both prediction and inversion capabilities: if the scattering strength is measured at one frequency and one grain size, it can be predicted at others or inverted with respect to the grain sizes. Therefore, the scaling effects demonstrated here can potentially be used in acoustic sensing of marine sedi-

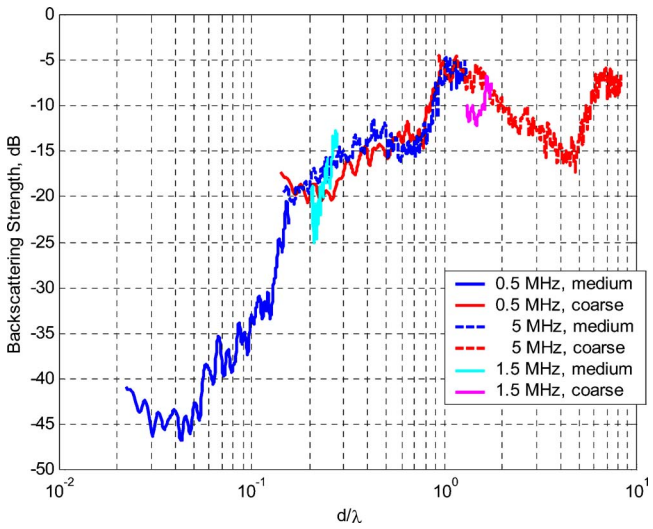

Fig. 3. (Color online) The same data as in Fig. 2, but plotted vs the sediment mean grain diameter ratio to the wavelength in water, d/λ.

ments to remotely estimate their mean grain size. Further analysis of these effects might be an interesting and promising subject of future theoretical and experimental studies.

Acknowledgments

This work was supported by the U.S. Office of Naval Research, and CNRS/LMA, France.

References and links

[1]D. R. Jackson and M. D. Richardson, *High Frequency Seafloor Acoustics* (Springer Science, New York, 2007).
[2]C. F. Greenlaw, D. V. Holliday, and D. E. McGehee, "High-frequency scattering from saturated sand sediments," J. Acoust. Soc. Am. **115**, 2818–2823 (2004).
[3]A. N. Ivakin, "High frequency scattering from sandy sediments: Roughness vs discrete inclusions," in *Boundary Influences in High Frequency Shallow Water Acoustics*, edited by N. G. Pace and P. Blondel, (University of Bath, UK, 2005), pp. 185–192.
[4]A. N. Ivakin, "Models of scattering for remote acoustic sensing of the seafloor," in *Proceedings of the Institute of Acoustics* (Bath University, Bath, UK, 2001), Vol. 23, Part 2, pp. 268–275.
[5]E. I. Thorsos, K. L. Williams, D. Tang, and S. G. Kargl, "SAX04 overview," in *Boundary Influences in High Frequency Shallow Water Acoustics*, edited by N. G. Pace and P. Blondel (University of Bath, UK, 2005), pp. 3–12.
[6]M. D. Richardson, K. B. Briggs, A. H. Reed, W. C. Vaughan, M. A. Zimmer, L. D. Bibee, and R. I. Ray, "Characterization of the environment during SAX04: Preliminary results," in *Proceedings of the International Conference on Underwater Acoustic Measurements: Technologies & Results*" (Heraklion, Crete, Greece, 28 June–1 July 2005).
[7]A. W. Nolle, W. A. Hoyer, J. F. Mifsud, W. R. Runyan, and M. B. Ward, "Acoustical properties of water-filled sands," J. Acoust. Soc. Am. **35**, 1394–1408 (1963).
[8]K. L. Williams, R. H. Hackman, and D. H. Trivett, "High-frequency scattering from liquid/porous sediment interfaces," J. Acoust. Soc. Am. **84**, 760–770 (1988).

International Symposium on Underwater Reverberation and Clutter

Proceedings of a Symposium held at
Villa Marigola, Lerici, Italy.
9-12 September 2008.

Published by the NATO Undersea Research Centre (NURC), 2008.

Proceedings printed by: İstanbul Ofset Basım Yayın A.Ş.

Illustration on front cover: Clutter statistics are an important indicator for target detection. This clutter map obtained in the Malta Plateau region of the Mediterranean Sea indicates the degree of non-Rayleighness of the reverberation as the ratio of the local standard deviation to the mean. Thus red areas are more target-like. Courtesy Mark Prior, NURC, 2006.

Illustration on back cover: Synthetic aperture sonar image of sand ripples and a shell-covered bank.

MODELING OF NARROW-BAND NORMAL-MODE REVERBERATION IN SHALLOW WATER

ANATOLIY N. IVAKIN

Applied Physics Laboratory, Univ. of Washington, 1013 NE 40th Street, Seattle WA 98105, USA
E-mail: ivakin@apl.washington.edu

A model of reverberation in a shallow-water waveguide caused by the volume heterogeneity and rough interfaces is proposed. Normal modes are used as a common approximation of the one-way propagation. Narrow-band approximation allows defining a scattering volume for each mode-to-mode channel of scattering at given time. Smoothing of inter-channel interference provides an estimate for the intensity of reverberation as an incoherent summation over different channels. Local scattering matrix elements quantify the energy exchange between modes. A simple relationship of the temporal dependence of the reverberation intensity with the scattering matrix, attenuation and group velocities of the normal modes is obtained. Possible effects of multiple scattering are discussed and, in particular, the effect of backscattering enhancement, which is not described by existing models of reverberation.

1 Introduction

Acoustic reverberation in the underwater waveguide is complicated particularly because of appearing different multiple paths of sound propagation and related multiple channels of local scattering. In shallow water conditions, there are additional complications caused by difficulties to resolve these multiple paths and channels. This is due to natural limitations on vertical apertures of acoustic systems, their instability in extremely dynamic shallow water conditions, spatial complexity of this environment, and other reasons. There are various approaches, in modeling of shallow water reverberation, to take into account these multiple paths and complicated conditions. They all assume, in various ways, a summation of signals arriving through the different paths. Normal modes and rays are commonly used to describe these signals and have their own advantages at different frequency ranges and in different environments. An approach based on incoherent summation of intensities results in various models of reverberation in terms of the energy flux integral. These models have an advantage of simplicity, but fail in some cases where the various coherence effects may be important.

In this paper, a general formulation of the reverberation problem is given, based on a unified approach to volume and roughness scattering [1,2], in Section 2. A narrow-band normal-mode reverberation model is described in Section 3. A simple relationship of the temporal dependence of the reverberation intensity with the scattering matrix, attenuation and group velocities of the normal modes is obtained. In Section 4, possible coherence and multiple scattering effects are discussed. An approach is described which generalizes a multiple-forward-single-backscatter (MFSB) approximation [3]. The

approach, in particular, allows modeling of the effect of backscattering enhancement in strongly inhomogeneous shallow water waveguide (which cannot be described by energy flux theory).

2 General formulation

A general formulation of the problem can be based on a unified approach to volume and roughness scattering in layered media described in [1,2]. Consider an inhomogeneous medium with parameters, mass density, $\tilde{\rho}(r)$, and compressibility, $\tilde{\kappa}(r)$, fluctuating in space relative to their unperturbed values, ρ and κ, which can be given functions of r and called also the reference parameters, or parameters of a reference medium [1]. Here $r = \{R, z\}$, $R = \{x, y\}$ denote three- and two-dimensional position vectors. For given frequency ω and spectrum $\tilde{U}(\omega)$ of a source of radiation located at position r', the spectral component of acoustic pressure will obey the Helmholtz equation

$$[\hat{L}(r) + \hat{\varepsilon}(r)]\tilde{P}(\omega, r, r') = \tilde{U}(\omega)\rho\delta(r, r') \tag{1}$$

$$\hat{L} = \rho\nabla(\rho^{-1}\nabla) + k^2 \tag{2}$$

$$\hat{\varepsilon} = \rho\omega^2(\tilde{\kappa} - \kappa) + \rho\nabla\left[\left(\tilde{\rho}^{-1} - \rho^{-1}\right)\nabla\right] \tag{3}$$

where $\hat{L}$ is the unperturbed Helmholtz operator, with $k = \omega / c$ and $c = (\kappa\rho)^{-1/2}$ being wave number and sound speed, and $\hat{\varepsilon}$ is the medium perturbation operator. Assume that a solution for the Green function of the reference medium, G, which obeys the equation

$$\hat{L}(r)G(\omega, r, r') = \rho\delta(r, r') \tag{4}$$

is known. Then the solution of the Eq. (1) can be expressed through the Green function using the equivalent to Eq. (1) integral equation of the form

$$\tilde{P}(\omega, r', r'') = \tilde{U}(\omega)G(\omega, r', r'') + \int\hat{\varepsilon}(r)G(\omega, r, r')\tilde{P}(\omega, r, r'')d^3r \tag{5}$$

with the first term being the field in the reference medium and the second one being the field perturbation. Then the first iteration gives the first-order perturbation field, or reverberation, as follows

$$\tilde{p}(\omega, r', r'') = -\tilde{U}(\omega)\int\hat{\varepsilon}(r)G(\omega, r, r')G(\omega, r, r'')d^3r \tag{6}$$

It is important to emphasize here that the mentioned above reference medium can be chosen rather arbitrarily, e.g., as the same medium but with heterogeneity and roughness smoothed over scales comparable and smaller than the wavelength. In such a smoothed medium, with only large scale perturbations left, scattering occurs only in near forward directions and various small-angle approximations can be used. In this case, the Green function can be defined as a propagator to describe a one-way propagation process at given frequency. It can include all multiple forward scattering effects and, in particular, the field fluctuations in the direct path described by first term in Eq. (5). Reverberation itself appears as a field perturbation, or the second term in Eq. (5), due to difference between real and reference medium represented by a medium perturbation function, or, more generally, the perturbation operator, which can be of an arbitrary form and describe both volume, continuous or discrete (target-like), and roughness perturbations. In the case of rough interfaces, the volume integral Eq. (6) can be transformed to an integral over the reference interface, and the perturbation function describes the deviation of the real interface from the reference (or smoothed) one, see details in [1]. Effects of multiple forward scattering on reverberation are included, therefore, to the Green functions in Eq. (6).

In the case of a waveguide, the sound propagation is described through a summation of different signals (corresponding to different rays and modes). In this case, the Green function can be presented as a superposition of generalized rays or modes as follows

$$G(\omega, r, r') = \sum_n g_n(r, r' \mid \omega) \exp(i\omega T_n(r, r' \mid \omega)) \tag{7}$$

where g_n and T_n represent mainly geometrical factors in the amplitude and phase of the n-th ray/mode, but can also be slow functions of frequency ω to allow the ray/mode amplitude and phase frequency dispersion. In this paper, we consider, as a simple example, the reverberation in a plane waveguide in terms of normal modes. In this case, the Green function can be presented in the form

$$G(\omega, r, r') = \mid R - R' \mid^{-1/2} \sum_n \psi_n(\omega, z) \psi_n(\omega, z') \exp(i\xi_n(\omega) \mid R - R' \mid) \tag{8}$$

where ψ_n represent the modes with corresponding horizontal wave-numbers, $\xi_n(\omega) = \omega / C_n(\omega)$, and phase velocities, $C_n(\omega)$, at given frequency. Equation (8) gives, therefore, a particular example of Eq. (7) with

$$g_n(r, r' \mid \omega) = \mid R - R' \mid^{-1/2} \psi_n(\omega, z) \psi_n(\omega, z') \tag{9}$$

$$T_n(r, r' \mid \omega) = \mid R - R' \mid / C_n(\omega) \tag{10}$$

3 Narrow-band normal-mode reverberation

3.1 Narrow band

For the radiation signal, we assume

$$U(t) = u(t,\varphi)\exp(-i\omega_0 t) \tag{11}$$

where ω_0 is the carrier frequency, u is the signal envelope, $u = 0$ for $t < 0$ and $t > \tau$, with τ being the radiated pulse duration, which is long enough, so that $\tau >> 1/\omega_0$. A φ-parameter is introduced here for generality to allow a possibility of angular directivity of the source. For the radiated signal spectrum and its frequency band width, we have

$$\widetilde{U}(\omega) = \widetilde{u}(\omega - \omega_0) \tag{12}$$

$$|\omega - \omega_0| \approx 1/\tau << \omega_0 \tag{13}$$

The narrow band assumption allows the following approximation for the mode wave number within the radiation frequency band

$$\xi_n(\omega) \approx \xi_n(\omega_0) + c_n^{-1}(\omega_0)(\omega - \omega_0) + \ldots \tag{14}$$

with $c_n = (d\xi_n / d\omega)^{-1}$ being the group velocity of the mode.

3.2 Reverberation field

Using Eqs. (6) and (8), one obtains

$$p(t,r',r'') = \exp(-i\omega_0 t)\sum_{j,n} p_{jn}(t,r',r'') \tag{15}$$

where p_{jn} represents the envelope of the reverberation arrival corresponding to the $j-n$ channel of scattering in the waveguide, i.e., scattering from the j-th mode to the n-th one, and is described as follows

$$p_{jn} = A_{jn}(z',z'')\int v_{jn}(t,|R-R'|,|R-R''|,\varphi)J_{jn}(R)d^2R \tag{16}$$

$$A_{jn}(z',z'') = \psi_j(\omega_0,z')\psi_n(\omega_0,z'') \tag{17}$$

$$v_{jn}(t,x',x'') = (x'x'')^{-1/2} u(t - x'/c_j - x''/c_n, \varphi) \exp(i\xi_j x' + i\xi_n x'') \quad (18)$$

$$J_{jn}(R) = \sum_{\beta} \int \hat{\varepsilon}_{\beta}(R,z) A_{jn}(z,z) dz, \ \beta = \kappa, \rho, \zeta \quad (19)$$

Here $A_{jn}(z',z'')$ defines the excitation coefficient for the $j-n$ channel of scattering at given positions of the source and receiver, v_{jn} describes the sound propagation along this channel with corresponding time delay and complex phase (including attenuation) and also defines the scattering volume for this channel at given time, and J_{jn} defines the local scattering due to different types of perturbations, spatial fluctuations of compressibility and density, and the interface roughness, with corresponding indexes $\beta = \kappa, \rho, \zeta$, see details in [1,2].

3.3 *Bistatic reverberation intensity*

Using Eqs. (15) and (16), the ensemble-average intensity of reverberation in a general bistatic case can be obtained. Smoothing of inter-channel interference oscillations provides the following estimate for the intensity of reverberation as an incoherent summation over different channels

$$< | p(t,r',r'') |^2 > \approx \sum_{j,n} < | p_{jn}(t,r',r'') |^2 > \quad (20)$$

$$< | p_{jn} |^2 > = | A_{jn}(z',z'') |^2 \int | v_{jn}(t, | R - R' |, | R - R'' |, \varphi) |^2 \ M_{jn}(R) d^2 R \quad (21)$$

$$M_{jn}(R) = \int < J_{jn}(R - a/2) J^*_{jn}(R + a/2) > \exp(i\kappa_{jn} \cdot a) d^2 a \quad (22)$$

$$\kappa_{jn} = \mathrm{Re}\,\xi_j \frac{R - R'}{| R - R' |} + \mathrm{Re}\,\xi_n \frac{R - R''}{| R - R'' |} \quad (23)$$

where M_{jn} is the local scattering matrix coefficient describing the energy exchange between modes for each channel within the corresponding scattering volume, and κ_{jn} is the respective local scattering vector.

3.4 *Quasi-monostatic reverberation*

In the quasi-monostatic case, where $r' \approx r''$, assuming also that $t >> \tau$, one obtains

$$< | p |^2 > = \frac{E(\varphi)}{t} \sum_{j,n} | A_{jn}(z', z'') |^2 \; M_{jn}\left(R_{jn}(t), \varphi\right) \exp(-2\alpha_{jn} t) \quad (24)$$

$$E(\varphi) = \int | u(t, \varphi) |^2 \, dt \quad (25)$$

$$R_{jn}(t) = t / c_{jn}, \; c_{jn} = (c_j^{-1} + c_n^{-1})^{-1}, \; \alpha_{jn} = c_{jn} \, \mathrm{Im}(\xi_j + \xi_n) \quad (26)$$

where $E(\varphi)$ is radiation directivity of the source, or the total energy of the radiated signal in given direction, c_{jn} and α_{jn} are the speed of the signal return and attenuation coefficient for the $j-n$ reverberation channel, and R_{jn} is the corresponding horizontal range. Assuming that the parameters of shallow water waveguide are known, Eq. (24) can be used for inversion of the reverberation strength, given by the scattering matrix M_{jn}, from the range-direction measurements of reverberation, or the clutter maps.

4 Multiple scattering effects

4.1 Coherence functions

Recall now that the reference medium can be defined as the same medium but with smoothed parameters describing all heterogeneity and roughness with scales larger than the wavelength. The Green function of the reference medium takes into account all corresponding multiple scattering effects for near-forward directions of propagation and can be calculated using various small-angle approximations. For other directions (not near-forward), including backward, all the scattered waves are described by the perturbation field Eq. (6) and included to reverberation, which can be presented as follows

$$\tilde{p}(\omega, r', r'') = \tilde{U}(\omega) G_b(\omega, r', r'') \quad (27)$$

with

$$G_b(r', r'') = -\int \varepsilon(r) G(r, r') G(r, r'') d^3 r \quad (28)$$

In Eq. (28) and following equations, the frequency is omitted. For the intensity of the scattered field, one obtains

$$\left\langle | G_b(r', r'') |^2 \right\rangle = \int B(r_1, r_2) \Gamma_4(r_1, r_2 \mid r', r'') d^3 r_1 d^3 r_2 \quad (29)$$

$$B(r_1, r_2) = \left\langle \varepsilon(r_1) \varepsilon^*(r_2) \right\rangle \quad (30)$$

$$\Gamma_4(r_1, r_2 \mid r', r'') = \left\langle G(r_1, r')G(r_1, r'')G^*(r_2, r')G^*(r_2, r'') \right\rangle \tag{31}$$

where $B(r_1, r_2)$ is the spatial correlation function of the medium perturbations, and Γ_4 is the fourth statistical moment (or the fourth-order coherence function) of the propagation field. In particular, for calculation of the averaged backscattered intensity, or the monostatic reverberation, at $r' = r''$, the following coherence function is needed

$$\Gamma_4(r_1, r_2 \mid r', r') = \left\langle G^2(r_1, r')G^{*2}(r_2, r') \right\rangle \tag{32}$$

4.2 Backscattering enhancement

Consider now possible effects of multiple scattering. They are especially pronounced in the case of a strongly heterogeneous medium, where the propagating field is completely randomized, so that the mean field vanishes, i.e., $< G >= 0$. One can assume that in this case the two paths of propagation, that from the source to the scattering point, and that from the scattering point to the receiver, become mutually incoherent, or uncorrelated, and therefore the coherence function Eq. (32) can be presented in the form

$$\Gamma_4(r_1, r_2 \mid r', r'')_{uncor} = \Gamma_2(r_1, r_2 \mid r')\Gamma_2(r_1, r_2 \mid r'') \tag{33}$$

$$\Gamma_2(r_1, r_2 \mid r) = \left\langle G(r_1, r)G^*(r_2, r) \right\rangle \tag{34}$$

where Γ_2 is the second order coherence function of the propagation field. This function plays a fundamental role in description of the energy flux transfer. In particular, its spatial spectrum represents the angular distribution of the energy flux. Therefore, the reverberation models based on the energy flux theories actually assume that Eq. (33) holds in Eq. (29) for all source-receiver configurations, including monostatic, where Eq. (33) becomes

$$\Gamma_4(r_1, r_2 \mid r', r')_{uncor} = \left(\Gamma_2(r_1, r_2 \mid r')\right)^2 \tag{35}$$

It is known however that, in this case of strong fluctuations, the field obeys a Gaussian random distribution. As a result, from Eq. (31) one obtains

$$\Gamma_4(r_1, r_2 \mid r', r') = \left\langle G^2(r_1, r') \right\rangle \left\langle G^{*2}(r_2, r') \right\rangle + 2\left(\Gamma_2(r_1, r_2 \mid r')\right)^2 \tag{36}$$

Comparison of Eqs. (36) and (35), provides a simple explanation for the so-called effect of backscattering enhancement, or effect of the source localization in a strongly

heterogeneous medium. Indeed, the integration in Eq. (29) using Eqs. (35) and (36), results in inequality

$$\left\langle | G_b(r',r'') |^2 \right\rangle > \left\langle | G_b(r',r'') |^2 \right\rangle_{uncor} \tag{37}$$

which completes the demonstration of this effect.

Note that in the case of multi-paths reverberation in shallow water, the effect of backscattering enhancement should be clearly pronounced. As it was mentioned above, models of incoherent reverberation based on the energy flux theories are unable to describe this effect. Its demonstration however is possible if rays/modes models are used, but only if possible coherence of different channels of scattering are taken into account. This means that the summation of signals arriving through different rays or modes should consider their phases. This, in particular, would make possible an interesting numerical experiment. In the case of a homogeneous waveguide, this would result in a very complicated spatial "fine structure" of reverberation comprised of interferential maximums and minimums, which would completely mask the effects at near monostatic locations. However, if heterogeneity in the waveguide are taken into account, this fine structure vanishes except for the case where the receiver becomes close enough to the source and where, therefore, the effect of backscattering enhancement, or the source localization, becomes remarkable.

Acknowledgements

This work was partially supported by the US Office of Navel Research, Ocean Acoustics Program.

References

1. Ivakin A.N., A unified approach to volume and roughness scattering. *J. Acoust. Soc. Am.* **103**, 827-837 (1998).
2. Ivakin A.N., Reverberation in a plane randomly inhomogeneous waveguide under narrow-band probing. *Acoustical Physics* **40**, 426-428 (1994).
3. de Wolf D.A., Electromagnetic reflection from an extended turbulent medium: Cumulative forward-scatter single-backscatter approximation. *IEEE Trans. Antennas Propagat.*, **AP-19**, 254-262 (1971).

HIGH FREQUENCY SCATTERING FROM SANDY SEDIMENTS: ROUGHNESS VS DISCRETE INCLUSIONS

A. IVAKIN

Applied Physics Laboratory, University of Washington, 1013 NE 40th Street, Seattle WA 98105
E-mail: ivakin@apl.washington.edu

Environmental data obtained at SAX99 site, including the sediment particle size-depth distribution and the water-sediment interface roughness spectra, were used to compare contributions of volume and roughness components of the seafloor scattering. It is shown, in particular, that contribution of gravel and shell inclusions and coarse sand fraction in total scattering at SAX99 site can be dominating (over roughness) at very high frequencies (about 100 kHz and higher) and grazing angles above critical (about 30 degrees) while roughness is likely a dominating mechanism of bottom scattering at lower frequencies and grazing angles below critical.

1 Introduction

Models for seabed scattering based on realistic assumptions about scattering mechanisms in the sediment provide relationships between various seabed properties and characteristics of the scattered field and are required for solution of various practical problems such as prediction of bottom reverberation given seabed properties or/and inversion of various seabed parameters from acoustic scattering data. There are different mechanisms of seabed scattering which are due to different types of seabed medium irregularities: continuous volume fluctuations of the sediment acoustic parameters and discrete volume inclusions (rock, shell hash, etc), roughness of the seabed interfaces, as well as volume-roughness interactions. Testing various models and mechanisms of high frequency seabed scattering was one of primary goals of recent major experiments in sediment acoustics, SAX99 and SAX04 [1-4].

Analysis and model/data comparisons for SAX99 show that scattering from continuous volume fluctuations and their contribution to total scattering at SAX99 site is much lower than that of roughness and, therefore, can be neglected [3]. On the other hand, extensive measurements of roughness spectra allow estimation of the level of roughness scattering, which shows, within a reasonable uncertainty, that roughness scattering models provide a good description of bottom scattering at frequencies below 100 kHz [3]. However, at higher frequencies, there is a significant discrepancy between observed level of scattering and predicted by roughness scattering theories because the level of roughness spatial spectrum is too low at the corresponding spatial frequencies.

Preliminary analysis shows that SAX04 scattering is also very complicated and that there is a significant discrepancy, even in a more wide frequency range than for SAX99, between backscattering data and results predicted by models taking into account only

N.G.Pace and P Blondel, (Eds), Boundary Influences In High Frequency, Shallow Water Acoustics, Pages 185-192, University of Bath, UK 5th-9th September 2005

roughness scattering. Therefore, other mechanisms of scattering must be considered and other approaches are required for understanding SAX99 and SAX04 data.

In this paper, a model of volume scattering in the sediment is presented, generalizing results of previous models [5-9]. The model, in particular, considers the case of stratified discrete inclusions in the sediment. Environmental data set obtained at SAX99 site, including the sediment particle size-depth distribution and the water-sediment interface roughness spectra, is used to compare contributions of volume and roughness components of the seafloor scattering.

2 Seabed roughness scattering model/data comparison

Extensive measurements of roughness spectra and other sediment parameters at SAX99 allow, using various models of roughness scattering, prediction of frequency-angular dependencies of seabed roughness scattering strength and their comparisons with observed bottom scattering [3]. Results of such comparison are illustrated in Figure 1, where various symbols show frequency dependence of bottom backscattering strength at two fixed grazing angles, 35 and 20 degrees, representing angles above (a) and below (b) the critical grazing angle, which is about 30 degrees for sandy sediments considered here. Solid and dash-dot curves show roughness scattering prediction and bounds of uncertainty correspondingly. The comparison shows, within a reasonable uncertainty, that roughness scattering mechanism can be dominating at frequencies below 100 kHz. However, at higher frequencies, predicted roughness scattering is substantially lower than observed level of scattering because the level of roughness spatial spectrum was found to be too low at the corresponding spatial frequencies at SAX99 site [3].

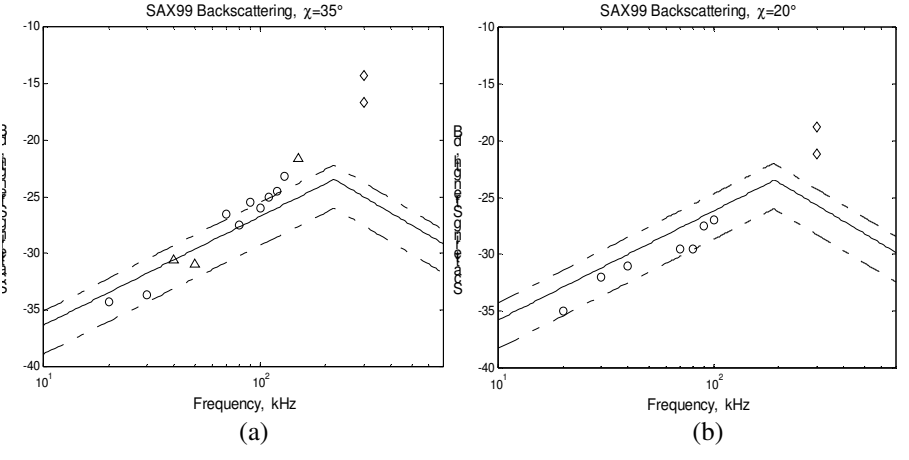

Figure 1: Roughness scattering model comparison with data for frequency dependence of SAX99 seabed backscattering strength at a fixed grazing angle above (a) and below (b) critical.

Preliminary analysis shows that SAX04 scattering is also very complicated and that there is a significant discrepancy, even in a more wide frequency range than for SAX99, between backscattering data and results predicted by models taking into account only roughness scattering. Therefore, other mechanisms of scattering must be considered and other approaches are required for understanding SAX99 and SAX04 data as well.

3 Seabed volume scattering

Let us assume that the seabed scattering is due to volume heterogeneity of the sediment layer with the average acoustical parameters, sound speed and density, independent from the depth. Between water and this heterogeneous scattering layer, an arbitrarily stratified transition layer is allowed. The volume backscattering coefficient in the sediment, or the cross section per unit sediment volume, m_v, can be treated generally as dependent on the depth. In this case, the seabed backscattering coefficient, or scattering cross section per unit area of seabed surface, m_s, can be presented in the form

$$m_s = |W|^4 \mu^{-2} \int_o^\infty m_v(z) \exp(-z/h_p) dz \cdot \tag{1}$$

Here, W is the sound transmission coefficient of the water-sediment transition layer (or interface), $\mu = \rho/\rho_w$ is the sediment/water density ratio; h_p is the depth of sound penetration into the sediment (see, e.g., [5,6]).

In a particular case, where the volume backscattering coefficient of the sediment, m_v, is depth independent, we have a well known result [5-9]

$$m_s = |W|^4 \mu^{-2} m_v h_p \tag{2}$$

For the transmission coefficient, in a particular case of a flat water-sediment interface, we have $W = 1 + V$, where V is the seabed reflection coefficient.

4 Incoherent discrete scattering model

Volume scattering in the sediment can be attributed to two different kinds of heterogeneity, continuous and discrete. Here, in this paper, we consider the case of scattering from discrete inclusions in an effective fluid sediment and assume incoherent summation of the scattered intensities for different scatterers [6,7]. Some considerations of possible coherent effects can be found in [10] and omitted here. In the frame of incoherent scattering model, the scattering cross section per unit sediment volume can be presented as follows [6]

$$m_v = \frac{3}{4\pi} \int F(k,a) a^{-2} \psi_v(a) da \cdot \tag{3}$$

where

$$\psi_v(a) = \frac{a \Delta v_a}{v \Delta a}, \tag{4}$$

is a dimensionless volume size distribution function, $\Delta v_a / v$ is the relative part of volume occupied by particles of the size (equivalent radius, a) within the correspondent interval Δa, k is the wave number in the sediment and F is a dimensionless individual scattering function related to the individual scattering cross section σ as follows

$$\sigma = a^2 F(k,a) \tag{5}$$

Equations (1)-(5) provide a solution for the seabed backscattering coefficient given an arbitrary depth-size distribution of arbitrary discrete inclusions in the sediment. In the calculations below, a simple case is considered. Assume that inclusions are spherical, homogeneous and have the same material properties. Also, here we ignore possible shear

effects within inclusions and surrounding sediments. The exact solution for the backscattering cross section and the scattering function in this case can be found, e.g., in [11]. A reasonable approximation represents a solution with smoothed interferential oscillations at $ka \geq 1$ [6] and used in the following sections for numerical calculations of the integral in Eq. (3).

5 Size distribution at SAX99

An environmental data set obtained at SAX99 site (near Walton Beach, Florida) [1] provides depth-size distribution histograms for a wide range of grain and inclusions sizes. Using the histograms (courtesy of K. Briggs) the volume size distribution function ψ_v defined by (4) was analyzed and results are presented in Figure 2.

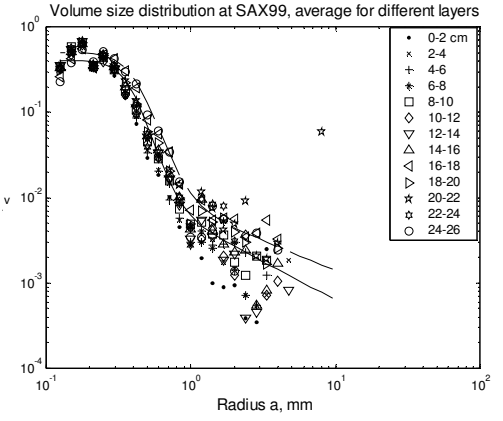

Figure 2. Volume size distribution for the SAX99 sediment at different depths (in-situ data). The solid line shows the best multi-power law fit to the environmental in-situ data. The dashed line shows the distribution that would provide the best fit for the acoustic scattering data.

Different symbols represent average within different layers of 2 cm thickness from the cores containing top 26 cm of the sediment. It is seen that shape of the size distribution is quite different for different depths and different size intervals. For example, concentration of shell fraction is low near the surface at 0-2 cm depth, while there is a remarkable shell layer at 20-22 cm depth. The solid line shows the best multi-power law fit to the environmental in-situ data [6]. The dashed line shows the distribution that will be used in model/data comparison below.

6 Volume scattering model/data comparison

Frequency dependence of the seabed backscattering strength, $10\log m_s$, obtained at SAX99 [3] is shown in Figure 3 at a fixed grazing angle, $\chi_w = 35°$, by various symbols. The curves show results of calculations for the model of discrete scattering described above, using Eqs. (1)-(5). Acoustic parameters of the sediment in the model correspond to environmental measurements at the SAX99 site [1]. The grain size distribution was taken as shown in Figure 2 (solid curve) and with changed location of the shell layer

(dashed curve) to demonstrate an effect of the size distribution stratification. Model/data comparison shows that prediction of volume scattering using real size distribution is a few dB lower than observed bottom scattering at SAX99 at frequencies below about 100 kHz. However, this difference can be easily compensated, if the shell layer is located near the sediment surface (dashed curve).

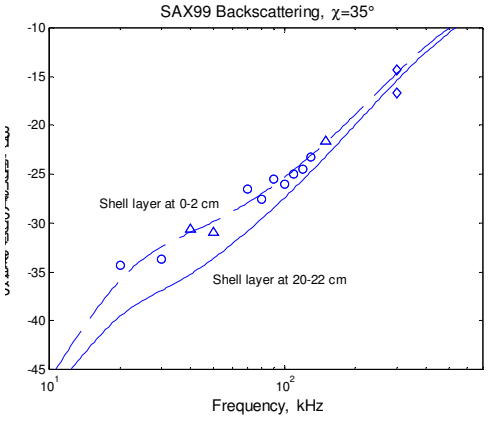

Figure 3. Frequency dependence of the bottom backscattering strength at SAX99 at a fixed grazing angle (35 degrees). The solid line shows model prediction using in-situ size distribution data (see Figure 1). Comparison of the solid and dashed lines shows effect of the shell layer location. The shell layer is placed at the 20-22 cm depth (solid) and 0-2 cm depth (dashed) respectively.

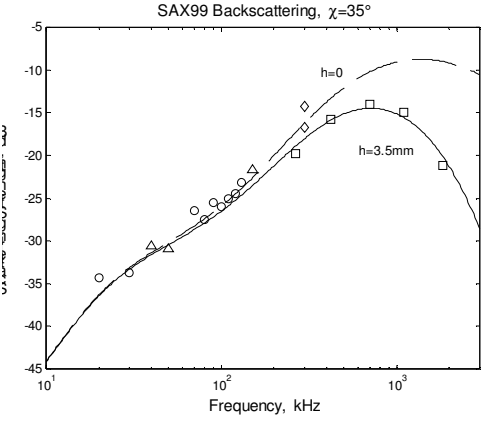

Figure 4. Effect of a thin (3.5 mm) top homogeneous (transition) layer at high frequencies. The frequency dependence of the bottom backscattering strength at SAX99 shows a remarkable roll-off above 1000 kHz. The solid and dashed lines show results for a model of discrete scattering respectively with and without the transition layer.

In Figures 4, another example of model/data comparison is demonstrated, showing that the model provides both qualitative and quantitative explanation of some interesting experimental results obtained at SAX99 site for higher frequencies range 265-1850 kHz, including backscattering data roll-off above 1000 kHz (see Figure 4), which has not been explained adequately [12]. The model takes into account the fact that concentration of shell fraction is low near the surface at 0-2 cm depth (see Figure 2) which allows to consider a thin (3.5 mm) top homogeneous (transition) layer placed on a sediment half-space with depth independent size distribution, which here is taken as shown by dashed curve in Figure 2. The result is shown in Figure 4 by solid curve. The dashed line corresponds to the case without the transition layer and perfectly agrees with data below 300 kHz but fails at higher frequencies.

7 Volume vs roughness scattering at SAX99

Thus, the results presented above show that the model of scattering from discrete inclusions in the sediment can be a good descriptor of seabed scattering at high frequency (above 100 kHz) and grazing angles above critical, at least at SAX99. Moreover, a simple summation of the two mechanisms, roughness and discrete volume scatterers, provides a good model/data comparison for backscattering for all frequencies used in SAX99 at grazing angles above critical. This result is illustrated in Figure 5.

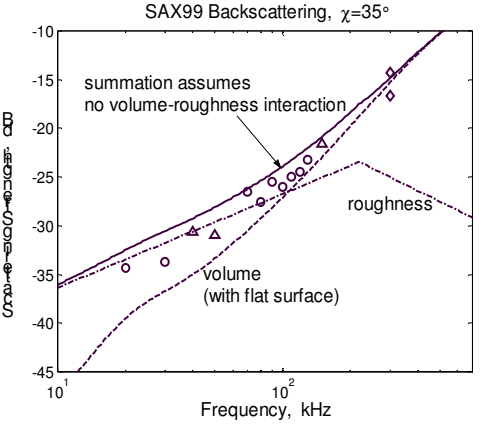

Figure 5: Model-data comparison for frequency dependence of SAX99 seabed backscattering strength at a fixed grazing angle above critical.

However, there is still a serious problem in understanding and modeling of backscattering for SAX99 at high frequencies (about 200 kHz and higher) at sub-critical grazing angles. This is demonstrated in Figure 6. Analogously to the case of grazing angles above critical, a simple summation of volume and roughness scattering was applied assuming no interaction between these two mechanisms. This means, that roughness scattering is being calculated for homogeneous sediment (with no inclusions) and discrete scattering is being considered assuming a flat sediment surface (no

roughness). This simplified approach, used successfully at higher grazing angles, as demonstrated in Figure 5, fails in attempts to explain high frequency data at sub-critical grazing angles (see Figure 6).

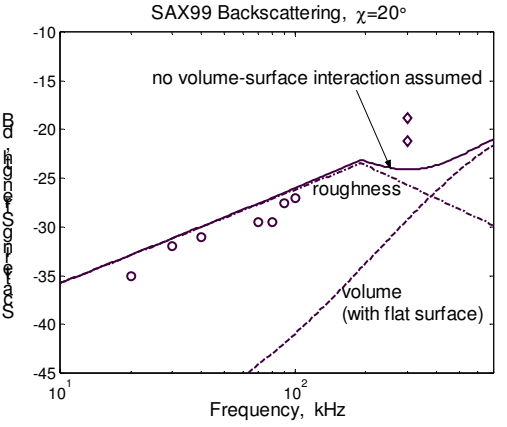

Figure 6: Model-data comparison for frequency dependence of SAX99 seabed backscattering strength at a fixed grazing angle below critical.

The discrepancy can be due to ignoring volume-roughness interaction. In the case of flat water-sediment interface, at grazing angles below critical, volume scattering is significantly reduced because of small depth of sound penetration into the sediment. In the case of randomly rough interface, there are always facets with local grazing angles above critical, which causes an enhancement of sound penetration and consequent enhancement of volume scattering in the sediment [13]. The effect can be very significant considering the fact that a slope of roughness at sub-cm scales at SAX99--SAX04 site is large and can be close to both angle of repose and critical angle (about 30 degrees).

8 Discussion

It is shown, in particular, that contribution of gravel and shell inclusions and coarse sand fraction in total scattering at SAX99 site can be dominating (over roughness) at very high frequencies (about 100 kHz and higher) and grazing angles above critical (about 30 degrees) while roughness is likely a dominating mechanism of bottom scattering at lower frequencies and grazing angles below critical. A simple summation of the two mechanisms, roughness and discrete volume scatterers, provides a good model/data comparison for backscattering for all frequencies used in SAX99 at grazing angles above critical.

However, there is a serious problem in modeling of backscattering for SAX99 at high frequencies (about 200 kHz and higher) at sub-critical grazing angles where there is a significant model/data discrepancy which can be due to ignoring volume-roughness

interaction. The effects of such interactions can be very significant and may require further theoretical considerations and other approaches.

One such approach, a unified approach to volume and roughness scattering [14,15], can be used to describe volume-roughness interactions in the sediments. It is exactly consistent with the small perturbation method, but it is not restricted by the smallness requirement for roughness height and slope, which makes it very appropriate tool for considering effects of non-small-slope roughness at SAX99-SAX04 conditions.

Acknowledgements

This work was supported by the US Office of Naval Research. The author thanks Dr. Kevin Briggs for providing SAX99 environmental data.

References

1. M.D. Richardson et al, Overview of SAX99: Environmental Considerations, *J.Oceanic Engr.,* **26**, 26-53 (2001).
2. E.I. Thorsos et al, Overview of SAX99: Acoustic Measurements, *J.Oceanic Engr.,* **26**, 4-25 (2001).
3. K.L. Williams et al, Acoustic Backscattering Experiments in a Well Characterized Sand Sediment: Data/Model Comparisons Using Sediment Fluid and Biot Models, *J.Oceanic Engr.,* **27**, 376-387 (2002).
4. Sediment Acoustics Experiment 2004 (SAX04) Workshop, Seattle, Washington, 4-5 May 2005.
5. A.N. Ivakin, Models of scattering for remote acoustic sensing of the seafloor, *Proc.Inst.Acoust.*, **23**: Part 2, 268-275 (2001).
6. A.N. Ivakin, Scattering from discrete inclusions in marine sediments, in *Proc. Seventh Europ. Conf. Underwater Acous., ECUA2004*, vol.1, 625-630 (Delft, The Netherlands, 2004).
7. A.N. Ivakin, High frequency scattering from heterogeneous seabeds, In *Proc. Fifth Europ. Conf. Underwater Acoust., ECUA2000,* vol.2, 1241-1246 (Lyon, France, 2000).
8. A.N. Ivakin, Sound scattering by random volume inhomogeneities and small surface roughness and of underwater ground, *Voprosy sudostroeniya, Akustika*, **17**, 20-25 (1983) (in Russian).
9. N.G. Pace, Low frequency acoustic backscatter from the sea bed, *Proc.Inst.Acoust.*, **16**, 181-188 (1994).
10. A.V. Bunchuk and A.N. Ivakin, Energy characteristics of an echo signal from discrete scatterers on the ocean bottom, *Sov.Phys.Acoust.,* **35**, 5-11 (1989).
11. P.M. Morse and K.U. Ingard, Theoretical acoustics, McGraw-Hill, pp. 927, 1968.
12. Greenlaw C.F., D.V. Holliday and D.E. McGehee, High-frequency scattering from saturated sand sediments, *J. Acoust. Soc. Am.*, **115**, 2818-2823 (2004).
13. Ivakin A.N. and Yu.P. Lysanov, Underwater sound scattering by volume inhomogeneities of a bottom medium bounded by a rough surface, *Sov.Phys.Acoust.*, **27**, 212-215 (1981).
14. A.N. Ivakin, A unified approach to volume and roughness scattering, *J.Acoust.Soc.Am.*, **103**, 827-837 (1998).
15. A.N. Ivakin, Effects of the top transition layer in marine sediments on seabed roughness and volume scattering, *J. Acoust. Soc. Am.*, **108**, 2616 (2000).

Proceedings of the Seventh European Conference on Underwater Acoustics, ECUA 2004
Delft, The Netherlands
5-8 July, 2004

SCATTERING FROM DISCRETE INCLUSIONS IN MARINE SEDIMENTS

Anatoliy N. Ivakin

Applied Physics Laboratory, University of Washington,
1013 NE 40th Street, Seattle WA 98105, USA
e-mail: ivakin@apl.washington.edu

A model of discrete scattering in marine sediments is developed which permits, using measurements of material parameters of inclusions and their size distribution, to provide prediction of bottom reverberation. An environmental data set obtained at SAX99 site (near Walton Beach, Florida), including the size distribution and sediment acoustic parameters, was used to calculate volume component of the seafloor scattering. Model/data comparison shows, in particular, that discrete scattering from gravel and shell inclusions and coarse sand fraction can be a dominating mechanism of high frequency reverberation at grazing angles above critical (about 30 degrees for sands). Possibilities for inversion of various sediment parameters from backscattering data are discussed.

1. INTRODUCTION

Acoustic scattering from marine sediments with discrete inclusions, such as shell fragments, gravel and rocks, can be described in terms of the individual scattering functions of discrete targets and statistical distributions of their parameters (size, shape, orientation, material, etc) [1,2]. An environmental data set obtained at SAX99 site (near Walton Beach, Florida) [3] provides the necessary data on the size distribution for a wide range of grain and inclusions sizes, as well as acoustic parameters of the sediments, the density, sound speed and attenuation, and parameters of bottom roughness. Acoustic measurements of the seabed backscattering strength made at SAX99 [4] along with environmental data provide a unique possibility for testing various models of scattering and for evaluating relative contributions of various mechanisms of scattering.

In this paper, the "inclusion scattering" model is demonstrated as a good descriptor of seabed backscattering measured at SAX99 experiment over a wide frequency range (30 kHz to 300 kHz) at grazing angles above critical (about 30 degrees for sands). Importantly, the model is quite simple and based solely on environmental measurements of a small number of understandable and measurable seabed parameters. Model/data comparisons and analysis show that the model can be used for solution of both forward and inverse problems, i.e.,

prediction of bottom reverberation given sediment properties are known and inversion of the sediment parameters from multi-frequency measurements of bottom backscattering.

2. SEABED BACKSCATTERING COEFFICIENT

Let us assume that the seabed scattering is due to volume heterogeneity of the sediment half-space with the average acoustical parameters, sound speed and density, independent from the depth. In this case, the seabed backscattering coefficient, or scattering cross section per unit area of seabed surface, m_s, is related to the volume backscattering coefficient of the sediment, or the cross section per unit sediment volume, m_v, as follows [1,5-7]

$$m_s = |W|^4 \mu^{-2} m_v h_p . \tag{1}$$

Here, W is the sound transmission coefficient of the water-sediment interface, $\mu = \rho / \rho_w$ is the sediment/water density ratio; h_p is the depth of sound penetration into the sediment at given frequency f and grazing angle in water χ_w,

$$h_p = \frac{n_o}{4k \operatorname{Im}\sqrt{n^2 - \cos^2 \chi_w}} = \frac{\operatorname{Re}\sqrt{n^2 - \cos^2 \chi_w}}{2\beta n_o}, \tag{2}$$

where $k = 2\pi f / c$, $\beta = 2k\delta$ and $n = n_o(1 + i\delta)$ are the wave number, attenuation coefficient and complex refraction index of the sediment, δ is the loss parameter, $n_o = c_w / c$ is the water/sediment sound speed ration (refraction coefficient), Re and Im denote real and imaginary parts of a complex value. For the transmission coefficient, in a particular case of a flat water-sediment interface, we have $W = 1 + V$, where V is the seabed reflection coefficient. More generally, the transmission coefficient can take into account the seabed roughness and/or presence of a stratified top transition layer in the sediment [8].

3. DISCRETE INCOHERENT SCATTERING MODEL

Volume scattering in the sediment can be attributed to two different kinds of heterogeneity, continuous and discrete. Here, in this paper, we consider the case of scattering from discrete inclusions in an effective fluid sediment and assume incoherent summation of the scattered intensities for different scatterers [1]. Some considerations of possible coherent effects can be found in [2] and omitted here. In the frame of incoherent scattering model, the scattering cross section per unit volume of sediment can be presented as follows

$$m_v = \frac{1}{V}\sum_{j=1}^{N} \sigma_j = \frac{N < \sigma >}{V} = \int \sigma(a) \psi_N(a) da , \tag{3}$$

where σ is the scattering cross section of an individual scatterer (inclusion) and $< \sigma >$ is its average, the ratio N / V is the average number of scatterers per unit sediment volume, a is a

parameter (or a set of parameters) characterizing individual scatterers, such as size, shape, material properties and others,

$$\psi_N(a) = \frac{\Delta N_a}{V \Delta a} \tag{4}$$

is the probability distribution function showing the number of scatterers per unit volume per unit interval of the parameter a. Here, we assume that inclusions have the same material properties, and a is considered as the randomly distributed equivalent radius of scatterers (radius of a sphere having the same volume as a non-spherical inclusion). In this case, relative measurements of volume and weight of grains are equivalent. Therefore, using a standard fractional weight analysis, so-called volume size distribution histograms can be obtained:

$$\psi_\eta(a) = \left.\frac{\Delta V_a}{\Delta V}\right|_{\frac{\Delta a}{a}=\eta}, \; \Delta V_a = \frac{4}{3}\pi a^3 \Delta N_a, \; \Delta V = (1-P)V, \tag{5}$$

where ΔV is the part of sediment volume occupied by inclusions themselves (grains), P is the sediment porosity. As ψ_η is proportional to η at small η, we will be using a normalized volume size distribution function

$$\psi_v(a) = (1-P)\psi_\eta / \eta = \frac{4}{3}\pi a^4 \psi_N(a) = \frac{a \Delta V_a}{V \Delta a}, \tag{6}$$

which is independent from the size interval used.

Consider a simple model for individual scatterer as a fluid sphere (representing inclusions) with acoustic parameters, sound speed and density, c_α and ρ_α, surrounded by a fluid medium (representing surrounding sediment) with respective parameters c and ρ. The exact solution for the backscattering cross section in this case can be found, e.g., in [9] and presented in the form

$$\sigma = a^2 F(ka), \tag{7}$$

where F is a dimensionless scattering function. We will use a smoothed function of the form

$$F(ka) = \frac{R_0^2}{4}(ka)^4 \left(1 + \frac{R_0^2}{R^2}(ka)^4\right)^{-1},$$

where

$$R_0 = \frac{2}{3}\left(1 - \frac{\rho c^2}{\rho_\alpha c_\alpha^2}\right) + \frac{\rho_\alpha - \rho}{\rho_\alpha + \rho/2}, \; R = \frac{\rho_\alpha c_\alpha - \rho c}{\rho_\alpha c_\alpha + \rho c}.$$

Using Eqs. (3,4) and (6,7), we obtain

$$m_v = \frac{3}{4\pi}\int F(ka)a^{-2}\psi_v(a)da\,. \tag{8}$$

Eqs. (1) and (8) provide a solution for the seabed backscattering coefficient given an arbitrary size distribution of discrete inclusions in the sediment and acoustic parameters of these inclusions and surrounding sediments.

4. SIZE DISTRIBUTION AT SAX99

An environmental data set obtained at SAX99 site (near Walton Beach, Florida) [1] provides the size distribution histograms for a wide range of grain and inclusions sizes. Using these histograms (courtesy of K. Briggs) the volume size distribution function defined by (6) was analyzed and results are presented in Figure 1. Different symbols represent average within different layers of 2 cm thickness from the cores containing top 26 cm of the sediment.

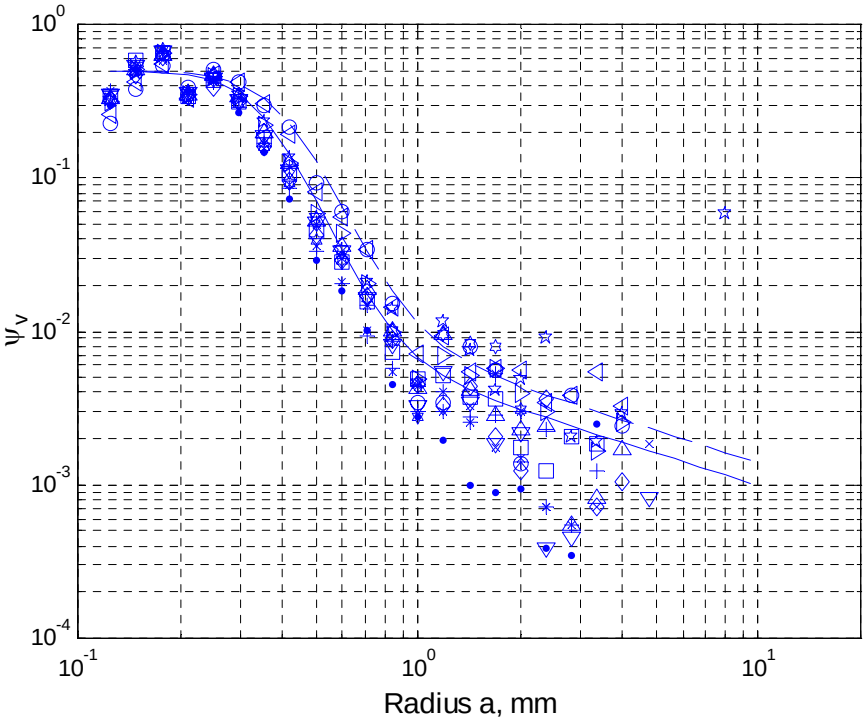

Fig.1: Volume size distribution of the sediment grains and inclusions at SAX99 site (medium and coarse sand and shell fractions). Solid and dashed curves correspond to a multi-power law approximation with slightly different parameters.

It is seen that shape of the size distribution is quite different for different size intervals. We use a theoretical approximation for the volume size distribution function of the form

$$\psi_v(a) = A\frac{(1+(a/a_2)^{\nu-\gamma})}{(1+(a/a_1)^{\nu})}\,. \tag{9}$$

This function is of a multi-power law type having different power exponents for three different intervals:

$$\begin{aligned} &\psi_v(a) \approx A, \quad a < a_1, \\ &\psi_v(a) \approx A(a/a_1)^{-\nu}, \quad a_1 < a < a_2, \\ &\psi_v(a) \approx A(a_2/a_1)^{-\nu}(a/a_2)^{-\gamma}, \quad a > a_2. \end{aligned} \tag{10}$$

The solid curve in Figure 1 represents the multi-power law function with the best fit to measured size distribution and was calculated using Eq. (9) with the following values of parameters: $A = 0.5$, $\gamma = 0.7$, $\nu = 5.873$, $a_1 = 0.35$mm, $a_2 = 0.8$mm. Corresponding values for the dashed curve are: $A = 0.5$, $\gamma = 0.7$, $\nu = 5.173$, $a_1 = 0.4$mm, $a_2 = 0.9$mm, and provide the best multi-power law fit to measured backscattering data shown in Figure 2.

5. BACKSCATTERING MODEL/DATA COMPARISON

Frequency dependence of the seabed backscattering strength, $10\log(m_s)$, obtained at SAX99 [2] is shown in Figure 2 at a fixed grazing angle, $\chi_w = 35°$, by various symbols.

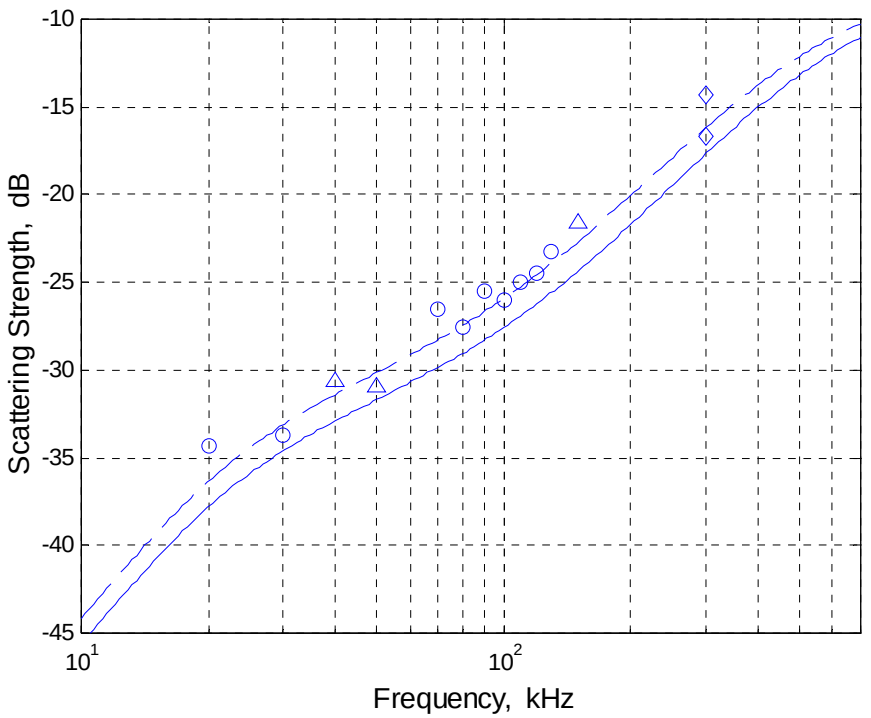

Fig.2: Frequency dependence of the seabed backscattering strength: comparison of the discrete scattering model and experimental data obtained at SAX99. The grazing angle is 35 degrees. Solid and dashed curves correspond to a multi-power law for the scatterers size distribution same as in Fig.1.

The curves show results of calculations for the model of discrete scattering described above, using Eqs. (1,8). The grain size distribution was taken as shown in Fig.1 by solid and

dashed curves. Acoustic parameters correspond to environmental measurements at the SAX99 site [1] and are taken as follows: $\rho = 2\text{g/cm}^3$, $c = 1.7\text{km/s}$, $\delta = 0.01$ (sediments); $\rho_\alpha = 2.7\text{g/cm}^3, c_\alpha = 5.7\text{km/s}, \delta = 0$ (individual grains); and $\rho_w = 1\text{g/cm}^3, c_w = 1.5\text{km/s}$ (water).

The model/data comparison represented in Figs. 1,2 and its analysis show that the "inclusion scattering" model is a good descriptor of seabed backscattering measured at SAX99 experiment over a wide frequency range (30 kHz to 300 kHz) at grazing angles above critical (about 30 degrees). The size distribution of discrete inclusions, such as shells and coarse sand particles, is the critical sediment characteristic in this model and an important factor determining level of seabed scattering. Also importantly, the model is quite simple and based solely on environmental measurements of a small number of understandable and measurable parameters. The model can be used for solution of both forward and inverse problems, i.e., prediction of bottom reverberation given sediment properties are known and inversion of the sediment parameters from multi-frequency measurements of bottom backscattering. For example, if acoustic parameters of the sediment, the density, sound speed and attenuation are known, remote acoustic measurements on frequency dependence of bottom reverberation can be used for data inversions with respect to size distribution of the sediment coarse fractions. From the other hand, the size distribution can be carefully analyzed in laboratory conditions, and, using multi-frequency measurements of bottom backscattering, other parameters of the sediment can be evaluated.

6. ACKNOWLEDGEMENTS

This work was supported by the US Office of Naval Research, Ocean Acoustics. The author thanks Dr. Kevin Briggs for providing SAX99 environmental data.

REFERENCES

[1] **A.N. Ivakin**, High frequency scattering from heterogeneous seabeds, *Proc. Fifth Europ. Conf. Underwater Acoust., ECUA2000*, vol.2, pp. 1241-1246, 2000.

[2] **A.V. Bunchuk, A.N. Ivakin**, Energy characteristics of an echo signal from discrete scatterers on the ocean bottom, *Sov.Phys.Acoust.*, vol.35, pp.5-11, 1989.

[3] **M.D. Richardson et al**, Overview of SAX99: Environmental Considerations, *J.Oceanic Engr.*, vol.26, pp.26-53, 2001.

[4] **E.I. Thorsos et al**, Overview of SAX99: Acoustic Measurements, *J.Oceanic Engr.*, vol.26, pp.4-25, 2001.

[5] **A.N. Ivakin**, Models of scattering for remote acoustic sensing of the seafloor, *Proc.Inst.Acoust.*, vol.23: Part 2, pp. 268-275, 2001.

[6] **A.N. Ivakin**, Sound scattering by random volume inhomogeneities and small surface roughness and of underwater ground, *Voprosy sudostroeniya, Akustika*, vol.17, pp.20-25, 1983 (in Russian).

[7] **N.G. Pace**, Low frequency acoustic backscatter from the sea bed, *Proc.Inst.Acoust.*, vol.16, pp.181-188, 1994.

[8] **A.N. Ivakin**, A unified approach to volume and roughness scattering, *J.Acoust.Soc.Amer.*, vol.103, pp.827-837, 1998.

[9] **P.M. Morse, K.U. Ingard**, *Theoretical acoustics*, McGraw-Hill, pp. 927, 1968.

NEAR-BOTTOM BISTATIC MEASUREMENT TECHNIQUE FOR ACOUSTIC CLASSIFICATION OF THE SEDIMENT AND BURIED OBJECTS

ANATOLIY N. IVAKIN AND DARRELL R. JACKSON

Applied Physics Laboratory, University of Washington
1013 NE 40th Street, Seattle, WA 98105, USA
E-mail: ivakin@apl.washington.edu

Bistatic acoustic measurements offer significant advantages in detection and remote classification of natural and man-made objects. They are non-intrusive, which is especially important for fragile archeological objects buried in the sediment. The results of such measurements are usually expressed through the scattering cross section as a function of frequency and directions of incident and scattered waves. While conventional bistatic techniques are performed in the far-field, with accompanying loss in resolution, we propose a new technique employing measurements of the near-bottom Green's function and its exact relationship to the scattering amplitude (T-matrix). Results of numerical experiments are presented to illustrate the new technique and its advantages.

1 Introduction

Bistatic acoustic measurements offer significant advantages in the remote characterization of the seabed, and in detection and remote classification of natural and man-made objects in marine sediments. They are non-intrusive, which is especially important for fragile archeological objects buried in the sediment. For remote acoustic characterization of the objects, in many cases, rather high resolution is needed to capture classification clues. But resolution is compromised in conventional techniques which require the measurements to be made far enough from the object so that the object is in the far-field region of the source and the receiver is in the far-field region of the object.

In this paper, a new technique is proposed employing near-bottom bistatic measurements. Ordinarily, bistatic measurements are extremely difficult, expensive and time consuming, requiring separate source and receiver platforms and accurate position and attitude information [1]. The method proposed here employs a single, highly portable platform to measure the near-bottom Green's function. Given this Green's function, several acoustically important quantities can be determined, e.g., the scattering cross section and the reflection coefficient, which usually are of the primary practical interest. The basis for all these relationships is the Fourier transform connection between the near-bottom Green's function and the so-called T-matrix. The T-matrix provides a complete description of scattering, giving the amplitude of the plane waves scattered in all directions for any given incident direction.

The near-bottom Green's function can be measured using a near-bottom array. The essential point is that the near-bottom array provides precise measurements that can be translated into practically useful estimates of scattering and reflection, overcoming the difficulties and uncertainties of previous techniques that employ transducers placed higher in the water column. In this paper, theory and computer simulations are used to account for the finite aperture and discrete spatial sampling of the actual device.

The numerical simulations illustrate the new technique, and its advantages in comparison to conventional approaches. In particular, the proposed technique can increase the accuracy and angular coverage of bistatic measurements, while providing a new tool for scientific measurements of acoustic bottom interaction based on principles of near-field acoustic holography.

Two simple examples are considered. The first example is a flat water-sediment interface for which the near-bottom Green's function was calculated via wave-number integration [2]. Then, using discrete samplings of the exact Green's function, an inversion with respect to the reflection coefficient is performed using the discrete Fourier transform. The result is compared with the exact expression for the reflection coefficient. This procedure allows determination of the required array size and the element spacing and aids in assessing the trade-off between measurement time and accuracy.

As another example, scattering from a target is considered using a point scatterer model. The main purpose of using this simple model is to provide a consistent exact calculation for the Greens function and scattering amplitude. Again, using discrete sampling of the exact Green's function, an inversion with respect to the scattering amplitude (T-matrix) is performed using the discrete Fourier transform. The result is compared with the exact expression for the T-matrix.

An important advantage of our approach is that the expressions used, in particular, for determining the reflection coefficient from the measured field, unlike traditional approaches, are exact and independent of any bottom model. Note that traditional approaches of measuring the reflection coefficient are based on asymptotic estimates of the above mentioned wave-number integral which are dependent on the chosen bottom model and measurement geometry and do not permit measurements with controlled accuracy. Our approach, in addition, will permit us to evaluate the accuracy and validity of traditional approaches simply by positioning virtual transducers at larger distance from the bottom and to compare traditional estimates with exact expressions for the reflection coefficient.

2 Green's function and Scattering Amplitude (T-matrix)

The Green's function of the fluid medium with a wave number k obeys the equation

$$\nabla^2 G(\mathrm{r},\mathrm{r}') + k^2 G(\mathrm{r},\mathrm{r}') = \delta(\mathrm{r},\mathrm{r}')$$

and can be presented in the form

$$G(\mathrm{r},\mathrm{r}') = G_0(\mathrm{r}-\mathrm{r}') + g(\mathrm{r},\mathrm{r}'),$$

where G_0 is the free-space Green's function describing the field radiated by a point source and g describes the medium response (scattered field), $\mathrm{r}=(\mathrm{R},z)$ and $\mathrm{r}'=(\mathrm{R}',z')$ are position vectors of the receiver and the source. In the 3D case, the free-space Green's function can be presented in the form

$$G_0(\mathrm{r}) = -\frac{e^{ik|\mathrm{r}|}}{4\pi|\mathrm{r}|}.$$

In the 2D case, the free space Green's function is

$$G_0(\mathrm{r}) = -\frac{i}{4}H_0^{(1)}(k|\mathrm{r}|),$$

where $H_0^{(1)}$ is the outgoing zero-order Hankel function.

Let all the scatterers be placed in a lower half-space, while the source and receivers are placed in the upper half-space, i.e., $z>0,\ z'>0$. Below the source, at $z<z'$, the free-space Green's function can be represented as a superposition of the incident (downward-going) plane waves as follows

$$2iG_0(\mathrm{r}-\mathrm{r}') = \frac{1}{(2\pi)^{n-1}}\int e^{i\mathrm{k}'\cdot(\mathrm{r}-\mathrm{r}')}\frac{d\mathrm{K}'}{\nu(K')},$$

where $\mathrm{k}'=(\mathrm{K}',-\nu(K'))$ is the wave vector of an incident plane wave, $\nu(K)=\sqrt{k^2-K^2}$, $n=2$ or $n=3$ in the 2D or 3D case respectively. The corresponding scattered component of the Green's function also can be presented in the form of a plane wave integral as follows

$$2ig(\mathrm{r},\mathrm{r}') = \frac{1}{(2\pi)^{n-1}}\iint e^{i\mathrm{k}\cdot\mathrm{r}-i\mathrm{k}'\cdot\mathrm{r}'}S(\mathrm{K},\mathrm{K}')\frac{d\mathrm{K}}{\nu(K)}\frac{d\mathrm{K}'}{\nu(K')}, \quad (1)$$

where $\mathrm{k}=(\mathrm{K},\nu(K))$ is the wave vector of a scattered going upward plane wave, $S(\mathrm{K},\mathrm{K}')$ is the so called scattering amplitude or T-matrix of the scattering medium.

The T-matrix provides a full description of the scattering from the half-space $z\le 0$ regardless of its complexity. When the T-matrix has been found, all the basic characteristics of the scattered field can be determined. For example, the reflection coefficient, $V(\mathrm{K})$, for an arbitrary plane-layered medium is defined by the following equation

$$S(\mathrm{K},\mathrm{K}') = \delta(\mathrm{K}-\mathrm{K}')\nu(K)V(\mathrm{K}).$$

The scattering cross section, $\sigma(\mathrm{K},\mathrm{K}')$, for an arbitrary 3D target placed in the lower half-space can be determined as follows

$$\sigma(\mathrm{K},\mathrm{K}') = 4\pi^2 \mid S(\mathrm{K},\mathrm{K}') \mid^2 .$$

In the 2D case, the corresponding equation is

$$\sigma(K,K') = 2\pi \mid S(K,K') \mid^2 / k .$$

Equation (1) allows determination of the T-matrix, if the Green's function is found, using an inverse Fourier transform

$$S(\mathrm{K},\mathrm{K}') = \frac{2i\nu(K)\nu(K')}{(2\pi)^{n-1}} \iint e^{-i\mathrm{k}\cdot\mathrm{r}+i\mathrm{k}'\cdot\mathrm{r}'} g(\mathrm{r},\mathrm{r}') d\mathrm{R} d\mathrm{R}' . \quad (2)$$

Equations (1, 2) are the main theoretical results of this paper.

In the case of a plane layered medium, the scattered (reflected) component of the Green's function can be represented as follows

$$g(\mathrm{r},\mathrm{r}') = g_0(\mathrm{R}-\mathrm{R}';z+z')$$

and expressed through the reflection coefficient

$$2ig_0(\mathrm{R},\mathrm{z}) = \frac{1}{(2\pi)^{n-1}} \int e^{i\mathrm{K}\cdot\mathrm{R}+i\nu(K)z} V(\mathrm{K}) \frac{d\mathrm{K}}{\nu(K)}, \quad (3)$$

The reflection coefficient for such a medium can be obtained as follows

$$V(\mathrm{K}) = 2i\nu(K) e^{-i\nu(K)z} \int e^{-i\mathrm{K}\cdot\mathrm{R}} g_0(\mathrm{R},z) d\mathrm{R} . \quad (4)$$

Equations (3, 4) were used in a numerical example of inversion of the reflection coefficient below.

3 Numerical examples

3.1 Reflection coefficient

As a simple numerical example, we consider a 2D problem of reflection from a flat interface between two fluids representing water and the sediment. The near-bottom Green's function was calculated via wave-number integration using Eq. (3) for a

sediment having density ratio 2 and refraction index 0.8+i0.01. In Figure 1, the Green's function and its direct-path and reflected components are shown.

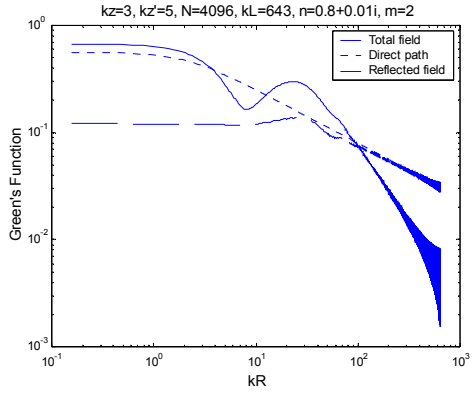

Figure 1. An example of the 2D Green's function and its components: incident field (direct path), reflected and total fields for a planar interface between water and a fluid having density ratio 2 and refraction index 0.8+i0.01. A discrete sampling of the total field was then used for inversion of the reflection coefficient.

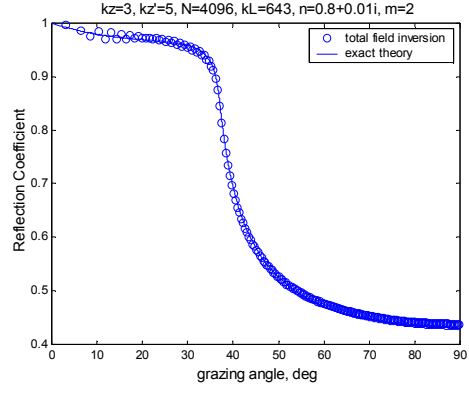

Figure 2. An example for inversion of the reflection coefficient.

If the Green's function is measured by a horizontal array., a discrete sampling of the exact Green's function is provided. Importantly, complex values of the Green function are required, including its magnitude and phase, which makes this procedure similar to that used in near-field holography. Then, inversions with respect to the plane-wave reflection coefficient can be made using the discrete Fourier transform and Eq.(4). The results of inversion for the magnitude of the reflection coefficient and its comparison with the exact expression are shown in Figure 2.

3.2 T-matrix for a target using a point scattering model

As another simple example, we use the point scatterer model to define scattering from a 2D target. This simple model provides a consistent exact calculation for the Green's function and scattering amplitude. This, again, yields a measured Green's function using discrete sampling, and then allows inversions with respect to the scattering amplitude (T-matrix) using the discrete Fourier transform and Eq. (4).

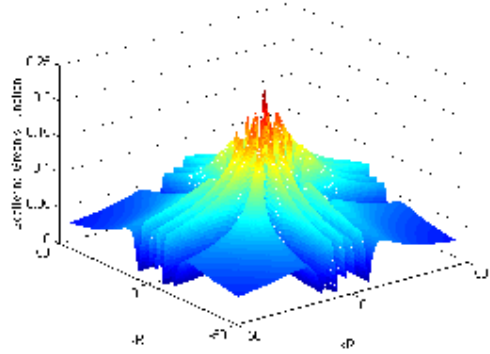

Figure 3. An example the Green's functions for a 2D target, discrete samplings of which, imitating the measurements, were used for inversion of the scattering amplitude.

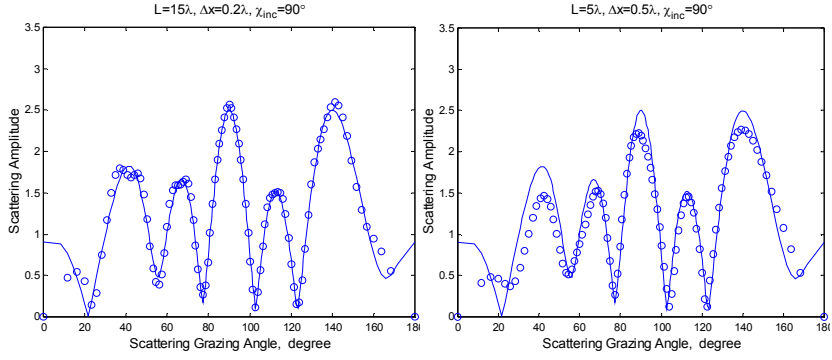

(a) (b)

Figure 4. An example for inversion of the bistatic scattering amplitude using a discrete sampling of the Green's function, corresponding to different array sizes, 15 (a) and 5 (b), and element spacing, 0.2 (a) and 0.5 (b), with all dimensions given in wavelengths. The solid line shows the exact solution.

An example of this procedure is illustrated in Figures 3 and 4. In Figure 3, an exact 2D Green's functions calculated for a target comprised of point 2D scatterers is shown. Its discrete sampling imitates the measurements with an array and then is used for inversion with respect to the scattering amplitude or T-matrix. The result of such an inversion and its comparison with the exact expression for the T-matrix is shown in Figure 4. This type of numerical procedure can be very useful, in particular, in determination of the required array size and the element spacing and can aid in assessing the trade-off between measurement time and accuracy.

4 Discussion

In this paper, a new technique for classification of the sediment and buried targets is proposed employing measurements of the near-bottom Green's function and its relationship to the scattering amplitude (T-matrix). Numerical experiments show the applicability of the new technique and its advantages in comparison to conventional approaches. In particular, the proposed technique can increase the accuracy and angular coverage of bistatic measurements, while providing a new tool for scientific measurements of acoustic bottom interaction based on principles of near-field acoustic holography.

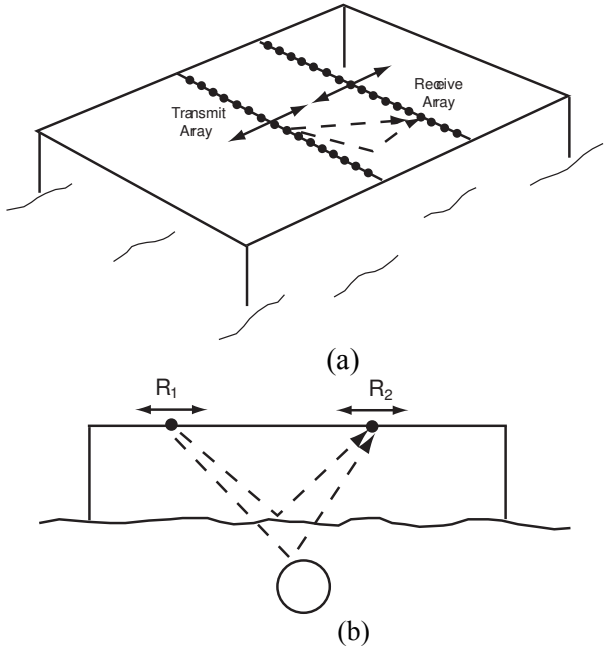

Figure 5. Sketch of near-bottom bistatic scattering measurements. The linear transmit and receive arrays are moved as shown by the arrows to provide 2-D synthetic apertures covering a region that is tens of wavelengths in dimension. The actual apparatus would have a drive mechanism, electronics, computer, and structure designed to reduce self-scattering.

Laboratory measurements with free-field and buried targets are the next logical step in the development of this technique. Figure 5 shows a conceptual picture of the near-bottom bistatic measurement apparatus (a) and a side view of near-bottom bistatic measurement of a buried target (b). Use of synthetic apertures for transmission and reception simplifies the apparatus and reduces the level of unwanted scattering by the array elements.

Acknowledgements

This work was supported by APL-UW.

References

Williams K.L. and Jackson D.R., Bistatic bottom scattering: Model, experiments, and model/data comparison, *J. Acoust. Soc. Am.* **103**, 169-181 (1998).

Schmidt H., OASES, Version 2.2, User Guide and Reference Manual, Massachusetts Institute of Technology, 1999.